

**SPONTANEOUS CP VIOLATION IN QUARK  
SCATTERING FROM QCD Z(3) DOMAINS  
AND ITS COSMOLOGICAL IMPLICATIONS**

*By*

**Abhishek Atreya**

**PHYS07200804003**

Institute of Physics, Bhubaneswar

*A thesis submitted to the  
Board of Studies in Physical Sciences*

*In partial fulfillment of requirements*

*For the Degree of*

**DOCTOR OF PHILOSOPHY**

*of*

**HOMI BHABHA NATIONAL INSTITUTE**



**March, 2015**

## STATEMENT BY AUTHOR

This dissertation has been submitted in partial fulfillment of requirements for an advanced degree at Homi Bhabha National Institute (HBNI) and is deposited in the Library to be made available to borrowers under rules of the HBNI. Brief quotations from this dissertation are allowable without special permission, provided that accurate acknowledgement of source is made. Requests for permission for extended quotation from or reproduction of this manuscript in whole or in part may be granted by the Competent Authority of HBNI when in his or her judgment the proposed use of the material is in the interests of scholarship. In all other instances, however, permission must be obtained from the author.

Date:-18<sup>th</sup> March 2015

(Abhishek Atreya)

## CERTIFICATE

This is to certify that the thesis entitled “**SPONTANEOUS CP VIOLATION IN QUARK SCATTERING FROM QCD Z(3) DOMAINS AND ITS COSMOLOGICAL IMPLICATIONS**”, which is being submitted by **Mr. Abhishek Atreya**, in partial fulfillment of the degree of **Doctor of Philosophy in Physics** of **Homi Bhabha National Institute** is a record of his own research work carried by him. He has carried out his investigations for the last six years on the subject matter of the thesis under my supervision at **Institute of Physics, Bhubaneswar**. To the best of our knowledge, the matter embodied in this thesis has not been submitted for the award of any other degree.

Signature of the Candidate

Signature of the Supervisor

Abhishek Atreya  
Institute of Physics  
Bhubaneswar

Dr. Ajit M. Srivastava  
Professor  
Institute of Physics  
Bhubaneswar

Date:- 18<sup>th</sup> March 2015.

## DECLARATION

I, Abhishek Atreya, hereby declare that the investigations presented in the thesis have been carried out by me. The matter embodied in the thesis is original and has not been submitted earlier as a whole or in part for a degree/diploma at this or any other Institution/University.

Date: 18<sup>th</sup> March 2015

(Abhishek Atreya)

*To My Beloved Mother*

---

# Contents

<b>Acknowledgement</b>	<b>ix</b>
<b>Synopsis</b>	<b>xii</b>
<b>List of Figures</b>	<b>xxv</b>
<b>List of Tables</b>	<b>xxvii</b>
<b>1 Introduction</b>	<b>1</b>
1.1 Isospin, SU(3) and Quark Model . . . . .	1
1.2 Quantum Chromo Dynamics . . . . .	5
1.2.1 The MIT Bag Model . . . . .	7
1.3 Statistical Mechanics and QCD . . . . .	9
1.3.1 Partition Function and Thermodynamic Quantities . . . . .	9
1.4 QCD Phase Diagram . . . . .	12
1.5 QGP in Lab . . . . .	16
1.5.1 Signatures of QGP . . . . .	18
1.6 Early Universe . . . . .	21
1.6.1 Pillars of Observational Cosmology . . . . .	21
1.6.2 Thermal History of Universe . . . . .	22
<b>2 Confinement-Deconfinement Transition</b>	<b>26</b>
2.1 Effective Potential and Spontaneous Symmetry Breaking . . . . .	26
2.1.1 Landau-Ginzburg Hamiltonian and Free Energy . . . . .	27
2.1.2 Spontaneous Symmetry Breaking . . . . .	30
2.1.3 Order Parameter Space as Coset Space . . . . .	32

2.2	Confinement-Deconfinement Phase Transition . . . . .	34
2.2.1	Polyakov Loop Order Parameter . . . . .	34
2.2.2	Spontaneous Breaking of $Z(3)$ Symmetry . . . . .	36
2.2.3	Results from Lattice QCD . . . . .	37
2.2.4	Effective Potential for Polyakov Loop . . . . .	41
2.3	Topological Defects . . . . .	44
2.3.1	Kibble Mechanism . . . . .	44
2.3.2	Types of Topological Defects . . . . .	45
2.4	Homotopy Groups . . . . .	47
<b>3</b>	<b>CP Violation from <math>Z(3)</math> Domains</b>	<b>50</b>
3.1	CP Odd Metastable Vacua in Standard Model . . . . .	51
3.2	Background Gauge Profile . . . . .	52
3.2.1	Calculating $A_0$ Profile . . . . .	53
3.2.2	Schematic Uncertainties . . . . .	55
3.3	Reflection of Quarks From $A_0$ Profile . . . . .	59
3.3.1	Dirac Equation . . . . .	59
3.3.2	Numerical Technique . . . . .	60
3.3.3	Results . . . . .	61
3.4	Discussion . . . . .	63
<b>4</b>	<b>Cosmological Implications of Spontaneous <math>CP</math> Violation</b>	<b>67</b>
4.1	Witten's Scenario . . . . .	68
4.1.1	Why an Alternate Scenario? . . . . .	69
4.2	$Z(3)$ Domains in Early Universe . . . . .	70
4.3	Nuggets Anti-Nuggets Formation . . . . .	74
4.3.1	Baryon Anti-Baryon Segregation . . . . .	75
4.4	Results . . . . .	77
4.5	Discussions and Conclusions . . . . .	82
<b>5</b>	<b>Effect of Quarks</b>	<b>83</b>
5.1	$Z(N)$ Symmetry and Dynamical Quarks . . . . .	83
5.1.1	Effective potential with Dynamical Quarks . . . . .	84

5.2	Profile of $Z(3)$ Interfaces with Dynamical Quarks . . . . .	85
5.3	Reflection and Transmission Coefficients with explicit symmetry breaking	90
5.4	Discussion . . . . .	91
<b>6</b>	<b>Summary</b>	<b>94</b>
	<b>Bibliography</b>	<b>99</b>

# Acknowledgement

Ph.D. tenure is a long time and supervisor plays the role in the life of a Ph.D student. In my case it was Ajit. I am deeply grateful to him, not because he has been my supervisor, but because of what he is. An excellent human being. I don't think I am qualified to comment on his physics and on his in depth understanding of a broad spectrum of topics in physics. I'll leave it to his contemporaries. I want to use this opportunity to acknowledge his role in my evolution as a person. He may not know this but I am a lot better person than what I was earlier because of his influence. I've learned a lot from him in all these years. People can testify that I was much worse as a person than I am today. I can write pages about his influence on my thinking but in short I'll say that he gave meaning to the term "Philosophy" in my degree.

Before I started my career in research it was my parents and my then girlfriend (now my wife) Isha, who played important role in my life and continued doing so during all these years. My parents loved me, raised me in the best possible way they thought. If there are certain values in life that I have, I owe it to them. If I've lost (some or all of) them it's all because of me, but they gave me the best they could. I think I am blessed to have parents like them. The person I miss at this moment is my mother. She would've been a proud mother today.

Isha has been another person who has been there for a decade in my life. If I am successful, she has been the woman behind me. It was her (and to some extent the strict HBNI guidelines about extensions) that pushed the lethargic me to get my thesis completed. In the last three and a half years or so another person who has become inseparable from me (at least in my thoughts) is my daughter, Ananya. I've not been able to spend as much time with her as I would've liked to, but even in that limited period the joy and the selfless love that she has given me is unparalleled.

Friends form an integral part of one's circle and when you are in an institute with handful of people around, their role is even more important. In my case it was Saumia who played this role with the help of my other friends. I am simply lucky to have such a beautiful human being as a friend. I cherish every tea we shared, movies we watched together. Memories of discussions in the mess over a vast spectrum of topics, late night walks in the campus always bring a smile on my face. If there is one thing I would like to keep for life, from these seven years of stay at IoP, it's the friendship

we have. I thank you with all my heart.

Vanaraj and Anshumaan have been two other people here about whom my social life used to revolve. The “male bonding” I shared with Anshumaan will always be a great memory of my IoP stay. Cooking, gym, outing all used to be a great fun with him around. Even irritating Vanaraj, which turned into our favorite shuggle. I don’t think Vanaraj will ever forget the tough time he faced because of me. Poor guy got respite only after I started visiting Delhi often after Ananya was born. From my IoP circle, these two, along with Ajit, make Isha’s favorite list which itself is an accomplishment on their part.

Pramita, Indrani, Shalik and Jaya were the other people who could tolerate my presence for more than 10 minutes. I’ve loved the time which I spent with them. I hope that they can say the same about me!. Except Jaya, I’ve cooked with all of them at one time or the other and this is one of the “tastiest” memory from my IoP stay. Jaya was different. She never made a simple Khichdi for me but she was always a game for a singing session. Herself being an excellent singer, she always encouraged me to sing and learn more. I’ve learned a lot from her in those interactions. Our work spaces were adjacent to each other and we shared some great moments together.

On the professional front, it was my collaborators Anjishnu, Partha and Arpan who made this thesis possible. I am lucky to have collaborators like you guys have been. Special thanks to Anjishnu, for his numerical expertise which I tried (unsuccessfully) to learn from him, and to Partha for the intense discussions we’ve had over the problems we worked on. The section of topological defects in this thesis was checked by Shreyansh initially and I am grateful to him for his valuable input. It is a pleasure to discuss physics with you. Ranjita, Saumia, Ananta and Uma Shankar were the other people with whom I discussed during my IoP stay. I thank them for their insights, especially Saumia for the extensive and seemingly never ending discussions over the lunch and dinner.

My initial one year at IoP was spent with the trio of Sandeep, Jaya and Souvik who were my batch-mates. Attending classes was fun with these people. I am grateful to our course work instructors, especially Prof. S. C. Phatak, Prof. Somendra Mohan Bhattacharjee, Prof. Sudipto Mukherjee and Prof. Biju Raja Shekhar for excellent courses they taught. Special thanks to Biju and Sudipto for making the interactions

informal. I am thankful to Ajit and Shikha for accepting my absence from their lectures without any problem, special thanks to Ajit for warning me before hand that I'll flip his course if I don't submit assignments.

I thank DAE for the financial support and the grant in terms of the fellowship and the contingency. I thank Prof. Pankaj Sharan for interactions during my visits at Jamia Millia Islamia University, Delhi. Special thanks to Prof. T. R. Seshadri for allowing me to use the IUCAA Resource Center (IRC) facility at University of Delhi, which I used extensively. I am also thankful to Prof. Debojyoti Choudhury and Prof. Patrick Dasgupta for useful physics discussions during my visit to physics department, University of Delhi. Special thanks to Atmjeet, Isha Pahwa and Sampooranand for making my visit to IRC an enjoyable one.

**Date:** 18<sup>th</sup> March 2015

**Abhishek Atreya**

# Synopsis

Ever since the discovery of the much celebrated asymptotic freedom of QCD in early 70's by Gross, Wilczek and Politzer [1,2], people working in this field have been living in what Chinese would call “interesting times”. The interesting times that saw the origin of Lattice Gauge Theory, String theory, supersymmetry etc. turned to full fledged excitement in the recent past with the advent of accelerators that could collide heavy ions, like gold (Au) and lead (Pb), at ultra relativistic energies at RHIC, BNL and recently at LHC, CERN. These Relativistic Heavy Ion Colliders have provided deep insights about the phase structure of QCD by experimentally establishing long expected theoretical results and by simultaneously posing new challenges. One of the most talked about result from these experiments has been the *discovery* of Quark Gluon Plasma as the most perfect fluid ever. Quark Gluon Plasma (QGP) is the plasma phase of QCD in which deconfined quarks and gluons (the elementary particles responsible for strong interactions) exist in thermal equilibrium. This phase is similar to the plasma phase of QED (where charged particles like electrons, positrons are in thermal equilibrium), but the similarity ends there. QED does not have any phase transition associated with the liberation of charged particles, while the phase structure of QCD is quite rich.

The bound states of strongly interacting particles (hadrons) are devoid of any color charge which is the charge associated with the strong interactions, just like atoms are devoid of electric charge which is associated with the electromagnetic interactions. However, unlike atoms it's not possible to add or remove a quark from a hadron and thus it's not possible to impart a color charge to hadrons. This property known as color confinement distinguishes QCD from QED in a major way, though not in the only way. The nature of transition associated with the liberation of color charge in the QGP plasma phase depends on various thermodynamical variables like the temperature, baryon number density of the system. With the experiments revealing various interesting properties of QGP, it is important to study various theoretical novelties that this system has to offer and look for their signals in the experiments.

These relativistic heavy ion collisions are at times referred to as *little bangs*, as the QGP system produced in these collision experiments is similar to what is expected to be present when the universe was just few micro-seconds old. This automatically

raises certain amount of curiosity about what implications these “novelties” will have in context of the early universe. This thesis is one small step towards understanding one of the various interesting phenomenon in QGP system, viz the structure of  $Z(3)$  domains, their properties and the implications these properties will have in the context of early universe. In the process we hope to address certain conceptual issues related to these structures, at least try to understand them if nothing more.

The  $Z(3)$  domain walls are the topological defects that are expected to be formed when a hadron gas undergoes a transition to from a thermal system of deconfined quarks and gluons. This transition, termed as the deconfinement transition, has an associated order parameter which is the the thermal expectation value of the Polyakov loop [3], which is defined as

$$l(x) = \text{Tr} \left\{ \mathbf{P} \left[ \exp \left( ig \int_0^\beta d\tau A_0(x) \right) \right] \right\}. \quad (0.1)$$

where,  $A_0(\vec{x}, \tau) = A_0^a(\vec{x}, \tau) T^a$ , ( $a = 1, \dots, N$ ) are the gauge fields and  $T^a$  are the generators of  $SU(N)$  in the fundamental representation.  $\mathbf{P}$  denotes the path ordering in the Euclidean time  $\tau$ ,  $\beta = T^{-1}$  and  $g$  is the gauge coupling.

Thermal expectation value of Polyakov loop ( $\langle l(x) \rangle$ ) has an interpretation in terms of the change in the free energy of the system when a static test quark is put in a pure gluonic system ( $\langle l(x) \rangle \propto e^{-\beta F}$ ). From now on we'll use  $l(x)$  in place of  $\langle l(x) \rangle$  for brevity. In the confined (hadron) phase the energy required to add a color charge (quark) is infinite hence  $l(x)$  is zero, while in the deconfined phase only a finite amount of energy is required and as a result  $l(x)$  is finite. The free energy of the system can be written in the spirit of Landau-Ginzburg free energy, knowing the symmetries of the order parameter. Since  $l(x)$  is the trace of a  $SU(3)$  matrix, it doesn't remain invariant under the action of  $Z(3)$  which is the centre of  $SU(N)$ . Under the action of  $Z(3)$ ,  $l(x) \rightarrow z l(x)$ , where  $z$  is an element of  $Z(3)$  ( $z = 1, e^{2\pi i/3}, e^{4\pi i/3}$ ).

In the confined phase,  $l(x) = 0$ , so it's invariant under the action of  $Z(3)$  but this is not the case in the deconfined phase. There Polyakov loop picks up an additional phase. As a result it has  $N$  distinct possible values in the deconfined phase. Thus  $Z(3)$  is not the symmetry of the order parameter, it's spontaneously broken in the deconfined phase. What it means is that within the QGP there are regions that can have different value of  $l(x)$ . Effective potentials that capture these properties

have been discussed in literature. We will use a specific form of potential given by Pisarski [4]. This potential captures the spontaneous breaking of  $Z(3)$  symmetry in the QGP phase.

One of the most interesting consequence of spontaneous symmetry breaking is the formation of topological defects. The type of topological defects formed depends upon the topology of the set of values order parameter is allowed to take in the ground state (vacuum manifold). In case of the Polyakov loop the vacuum manifold is a set of discrete values hence this system has domain walls as the topological defects. As one moves from one region of QGP (with some value of  $l(x)$  in it) to another region (where  $l(x)$  has some other value), there is a change in the value of  $l(x)$  away from the vacuum manifold. This small region where the order parameter changes, has a large amount of energy concentration. This is the domain wall between different  $Z(3)$  vacua.

There have been questions whether these  $Z(3)$  domains have some physical meaning or not [5,6]. The inclusion of quarks raises further issues as they do not respect the  $Z(3)$  symmetry. It has been argued that it is possible to interpret the effect of addition of quarks, as the explicit breaking of  $Z(3)$  symmetry and lifting of degeneracy of different  $Z(3)$  vacua [7]. There are recent lattice studies by Digal et al. [8] of QCD with quarks which have attempted to directly probe the existence of different  $Z(3)$  vacua. These results show strong possibility of the existence of non-trivial, metastable,  $Z(3)$  vacua for high temperatures. Though the exact value of the temperature, above which these metastable  $Z(3)$  vacua are seen is high ( $\sim 1$  GeV in ref [8]), what is important to realize is that these vacua seem to exist as metastable thermodynamics phases of QCD in the deconfining regime, and hence associated topological objects will necessarily arise in realistic transition from the confining phase to the QGP phase. These are the only example of topological defects in a relativistic quantum field theory which can be probed in present day laboratory conditions, namely, the relativistic heavy-ion collision experiments.

As the Polyakov loop varies across the domain wall, eq. (6.1) implies that there is an associated profile of  $A_0$  which interpolates between different  $Z(3)$  vacua. This background profile leads to the CP violation. This CP violation is spontaneous, arising due to the background configuration of the gauge field corresponding to the  $Z(3)$  wall,

and was first demonstrated by Altes et al. [9]. It was shown in ref. [9], in the context of the universe, that due to the non-trivial background field configuration for the standard model gauge fields, the localization of quarks and antiquarks on the wall is different. Its possible effects on the electroweak baryogenesis via sphalerons was discussed in [9]. Same possibility of spontaneous CP violation for the case of QCD was also discussed in [10]. The whole discussion in ref. [9, 10] was in the Euclidean formalism and detailed gauge field profile associated with the  $Z(3)$  interfaces was not determined.

In this thesis we calculate the detailed profile of  $A_0$  using the profile of  $l(x)$  between different  $Z(3)$  vacua and study the implications of spontaneous CP violation in quark scattering (due to this  $A_0$ ) in context of early universe. We also discuss its possible implications for relativistic heavy ion collision experiments. In the first study [11], we obtained the exact profile of  $A_0$  and calculated the reflection and transmission coefficients for the pure gauge case. The profile of  $l(x)$  was calculated by minimizing the energy of a trial configuration with appropriate boundary conditions. To calculate  $A_0$  from  $l(x)$ , we inverted eq (6.1). Working in the diagonal gauge we determined the profile of  $A_0$  and used it to calculate the reflection and transmission coefficients for quarks and anti-quarks. It was found that the CP violating effect was stronger for heavier quarks. In order to address the issue of uncertainties in the determination of the  $A_0$  profile depending on the choice of the specific form of the effective potential, we had repeated this calculation of  $A_0$  profile, in ref. [11], for another choice of effective potential of the Polyakov loop as provided by Fukushima [12]. It was found that even though the two effective potentials are of qualitatively different shapes, with polynomial type effective potential in ref. [4], and logarithmic effective potential in ref. [12], the resulting  $l(x)$  profile of the wall and the associated  $A_0$  profile were very similar. This gives us confidence that our conclusions arising from the calculations of scattering of quarks and antiquarks from  $Z(3)$  walls are not crucially dependent on the specific choice of the effective potential.

This CP violation will have interesting consequences in RHIC experiments and in the Universe as well. One important difference for the formation of  $Z(3)$  walls compared to the formation of other topological defects in the early universe arises from the fact that here symmetry is broken in the high temperature phase, and is

restored as the universe cools while expanding. Standard mechanism of formation of defects (the Kibble mechanism) [13] leads to the formation of defects during the transition to the symmetry broken phase. However we know that the universe was already in the broken phase of  $Z(3)$  symmetry in the early stages. One thus needs to discuss an appropriate scenario for the formation of these  $Z(3)$  domains in early universe where the system was in the hadronic (confined/low temperature) phase and then made a transition to the QGP (deconfined/high temperature) phase. Kibble mechanism can then be invoked to study the formation of these defects. Inflationary cosmology provides a natural resolution of this problem as was discussed by Layek et al [14].

During inflation, universe cools rapidly and temperature drops below the critical temperature for confinement-deconfined transition. After inflation, universe reheats and the temperature rises above the hadron-quark transition temperature. The  $Z(3)$  symmetry will then break spontaneously, and  $Z(3)$  walls and associated QGP string will form via the standard Kibble mechanism. However, in presence of quarks, there is an explicit breaking of  $Z(3)$  symmetry. Two of the vacua, with  $l(x) = z, z^2$ , become metastable leading to a pressure difference between the true vacuum and the metastable vacua. This leads to a preferential shrinking of metastable vacua. As a result, these domains are unlikely to survive until late times. However, there is a possibility that when effects of quarks scattering from the walls is taken into account their collapse may be slower due to the friction experienced by domain wall. For large friction, the walls may even remain almost frozen in the plasma. Even if the dynamics of the domain walls is not strongly friction dominated, it is still possible for these  $Z(3)$  domains to survive until the QCD scale, in certain low energy inflationary models. In these models the reheating temperature can be quite low ( $\sim 1 \text{ TeV}$ , or preferably, even lower). With inclusion of some friction in the dynamics of domain walls, it is then possible for the walls to survive until QCD transition. As argued by Layek et al [14], in such an optimistic scenario it may then be possible to ignore the effect of explicit symmetry breaking.

In our second study [15] of the thesis, we study the effects of such large domain walls in the universe, specifically the segregation of baryons and anti-baryons near the QCD phase transition epoch. After the domain walls have formed, the closed

domains start to collapse (the large domain walls with true vacuum inside may expand unless the pressure difference between the two vacua is dominated by the surface tension). The background  $A_0$  will then lead to different reflection and transmission coefficients for the quarks and antiquarks thus concentrating only quarks (or antiquarks, depending on the wall) within the collapsing domain. This will result in the segregation of baryons and anti-baryons in the early universe. These collapsing baryon (anti-baryon) rich regions can form quark (anti-quark) nuggets if the baryon concentration is sufficiently high in these regions. Such nuggets were first proposed by Witten [16]. He proposed that if the universe underwent a (strong) first order QCD phase transition, then localized regions of high temperature phase, trapped between expanding hadronic bubbles, will shrink, in the process trapping the baryons inside them. He also argued that resulting quark nuggets may be stable and survive upto the present epoch. His argument crucially depended on QCD phase transition being strong first order as it provides with an interface between two region of the universe in different phases. The baryon transport across the phase boundary then leads to the build up of baryon excess in the collapsing domains. Such an interface does not exist in a crossover or in a second order phase transition. Hence, with lattice QCD calculations ruling out the first order phase transition, the mechanism of formation of quark nuggets as proposed by Witten becomes inapplicable. However the  $Z(3)$  walls exist in the QGP phase as topological defects, forming irrespective of the order of the quark-hadron phase transition, even if it is a cross-over. Hence, the formation of quark nuggets in our model is via a very different mechanism than the originally proposed one.

We calculated the evolution of baryon density within a collapsing domain by studying the baryon transport across the wall [15]. We found that at  $T = 400 \text{ MeV}$ , the baryon concentration inside the domain wall is  $10^9$  times larger than the average quark number density of the universe. This gives us the net baryon number trapped inside to be of the order of  $10^{52}$  when the domain wall size is of the order  $1m$ . This is the upper limit where we do not consider any anti-quark to be present inside. Net baryon number to entropy ratio is about  $10^{-10}$ , hence it is safe to say that at least net baryon number of order  $10^{42}$  can be trapped inside collapsing domain walls. These quark nuggets may survive till now and may provide the dark matter candidates

within the standard model. It is usually stated that the data on Nucleosynthesis and CMBR does not allow baryonic dark matter. This indeed holds true for baryons in the form of gas (e.g. hydrogen, helium). Observational constraints from nucleosynthesis and CMBR are very strong on such forms of baryonic matter and restrict it to less than 20 % of all matter/radiation in the universe (excluding the dark energy). However, it is important to note that these constraints do not apply if baryons are in the form of heavy bodies, such as quark nuggets. Indeed, these were considered promising dark matter candidates after the work of Witten showing the possibility of formation of such objects in a strong first order quark-hadron transition in the universe. There were many investigations discussing the issues of stability of such objects. It was generally considered that quark nuggets (strangelets) having density above nuclear density, with baryon number ranging from few Thousand to  $\sim 10^{50}$  (sizes varying from fm to meters) may provide required dark matter. Such a candidate for dark matter will be extremely appealing as it does not require any physics beyond standard model.

Till now we confined our studies only to the pure gauge theory. In the third study, we extend our first work [11] by incorporating the effects of quarks in the effective potential and then studying the scattering of quarks and anti-quarks from the resulting  $Z(3)$  domains. The presence of quarks lifts the degeneracy of different  $Z(3)$  vacua with the two vacua ( $l(x) = z, z^2$ ) becoming metastable.  $Z(3)$  interfaces are no more solutions of time independent field equations as they move away from the region with the unique true vacuum. However, this does not mean that these domains do not survive as the topological structures. As the resulting profile of  $l(x)$  between the true vacuum and a metastable vacuum is no more symmetric it raises interesting possibilities for the generation of quark and antiquark inhomogeneities as a network of collapsing domain walls is considered, with different walls interpolating between different sets of  $Z(3)$  vacua. The effect of quarks is accounted for by adding a linear term in the Pisarski potential, which breaks the  $Z(3)$  symmetry explicitly [7]. The coefficient of the linear term measures the extent of symmetry breaking.

The coefficient of the linear term can be related to the estimates of explicit  $Z(3)$  symmetry breaking arising from quark effects which have been discussed in the literature. In the high temperature limit, the estimate of the difference in the potential

energies of the  $l = z$  vacuum, and the  $l = 1$  vacuum,  $\Delta V$ , is (as given in ref. [17])

$$\Delta V \sim \frac{2}{3}\pi^2 T^4 \frac{N_l}{N^3} (N^2 - 2) \quad (0.2)$$

where  $N_l$  is the number of massless quarks. If we take  $N_l = 2$  then  $\Delta V \simeq 3T^4$ . For  $T = 400$  MeV, this value of  $\Delta V$  is obtained if we take the value of the coefficient of the linear term to be 0.645. This is the largest value we consider for the explicit symmetry breaking. Strictly speaking the above expression is valid only for high temperature limit. However for temperatures of order  $T_c$ , it is not clear what should be the appropriate value of the coefficient of the linear term. It is entirely possible, that explicit symmetry breaking may be very small near  $T_c$ . In view of these uncertainties in the magnitude of explicit symmetry breaking for temperatures near  $T_c$ , we will consider a range of values of explicit symmetry breaking including the smallest value of the coefficient which gives a crossover (0.03), and determine the profile of  $l(x)$  and the associated  $A_0$  profile for these values.

On calculating the  $l(x)$  profile for the effective potential with the linear term [7], we found that explicit breaking of  $Z(3)$  symmetry leads to asymmetric profiles of  $l(x)$ . As expected, the extent of asymmetry depended on the extent of symmetry breaking i.e. on the coefficient of the linear term. Scattering of quarks from the Polyakov loop profile was discussed by Layek et al [14], by modeling the dependence of effective quark mass on the magnitude of the Polyakov loop order parameter  $l(x)$ . Spatially varying profile of  $l(x)$  leads to spatially varying effective mass, which behaves as potential in the Dirac equation for quarks/antiquarks leading to non-trivial scattering. In that case there was no explicit symmetry breaking and as a result the reflection of a quark coming from the right and from the left had the same reflection probability. Also, as the  $l(x)$  is a color singlet object, there was no CP violation. This immediately tells us that if we use the same modelling of quark mass here, then there will be a difference between the scattering of a quark coming from the right and that of the one coming from left *and* no CP violation.

As a next step we obtained the  $A_0$  profile from the asymmetric  $l(x)$  profile. We find that even though the profile of  $l(x)$  is asymmetric in this case (under reflection  $x \rightarrow -x$ ) quark-antiquark scattering from the gauge field configuration associated with it does not show any difference from the symmetric case when explicit  $Z(3)$

symmetry breaking is absent. The only difference is in the height of the potential which depends on the extent of symmetry breaking. Changing the coefficient of linear term by a factor of 20 produced a change of roughly 15% in the height of the potential. In short, the scattering of a quark from left on the wall is identical to the scattering of an antiquark from the right, as was the case in  $A_0$  profile obtained for the case with symmetric  $l(x)$  profile. This effect, when combined with the effective mass of the quark due to background  $l(x)$  profile leads to asymmetry in the scattering of quarks from one side and that of antiquarks from the other side of the domain wall. We find that the reflection coefficient of a quark coming from the left is roughly thousand times smaller than that of an anti-quark coming from the right. We also discuss the implications of these asymmetric reflection and transmission coefficients in context of early universe and also in the case of relativistic heavy ion collisions (like generation of event by event fluctuations in the heavy ion collisions due to  $Z(3)$  domains).

To summarize, in this thesis we have considered non-trivial scattering of quarks and anti-quarks from background gauge fields associated with the  $Z(3)$  walls. The spontaneous CP violation resulting from the background gauge field profile leads to the difference in the scattering of quarks and anti-quarks from the wall. We discuss the implications of this non-trivial scattering in the context of relativistic heavy ion collision experiments as well as in the case of early universe. We performed detailed calculations of the resulting baryon anti-baryon segregation and found that the collapsing  $Z(3)$  walls may lead to the formation of nuggets and anti nuggets. These nuggets and anti nuggets may provide us with a dark matter candidate within the standard model. We have incorporated the effects of dynamical quarks in these calculations in terms of explicit breaking of  $Z(3)$  symmetry. We argue that this can have interesting implications in context of heavy ion collisions and early universe.

# Bibliography

- [1] D. J. Gross and F. Wilczek, Phys. Rev. Lett. **30**, 1343 (1973).
- [2] H. D. Politzer, Phys. Rev. Lett. **30**, 1346 (1973).
- [3] A. M. Polyakov, Phys. Lett. B **72**, 477 (1978).
- [4] R. D. Pisarski, Phys. Rev. D **62**, 111501 (2000) [hep-ph/0006205].
- [5] A. V. Smilga, Annals Phys. **234**, 1 (1994).
- [6] V. M. Belyaev, I. I. Kogan, G. W. Semenoff and N. Weiss, Phys. Lett. B **277**, 331 (1992).
- [7] A. Dumitru, D. Roder and J. Ruppert, Phys. Rev. D **70**, 074001 (2004) [hep-ph/0311119].
- [8] M. Deka, S. Digal and A. P. Mishra, Phys. Rev. D **85**, 114505 (2012) [arXiv:1009.0739 [hep-lat]].
- [9] C. P. Korthals Altes and N. J. Watson, Phys. Rev. Lett. **75**, 2799 (1995) [hep-ph/9411304].
- [10] C. P. Korthals Altes, In \*Dallas 1992, Proceedings, High energy physics, vol. 2\* 1443-1447
- [11] A. Atreya, A. M. Srivastava and A. Sarkar, Phys. Rev. D **85**, 014009 (2012) [arXiv:1111.3027 [hep-ph]].
- [12] K. Fukushima, Phys. Lett. B **591**, 277 (2004) [hep-ph/0310121].
- [13] T. W. B. Kibble, J. Phys. A **9**, 1387 (1976).

- [14] B. Layek, A. P. Mishra, A. M. Srivastava and V. K. Tiwari, Phys. Rev. D **73**, 103514 (2006) [hep-ph/0512367].
- [15] A. Atreya, A. Sarkar and A. M. Srivastava, Phys. Rev. D **90**, no. 4, 045010 (2014) [arXiv:1405.6492 [hep-ph]].
- [16] E. Witten, Phys. Rev. D **30**, 272 (1984).
- [17] V. Dixit and M. C. Ogilvie, Phys. Lett. B **269**, 353 (1991).

# List of Publications

## 1. Published

- (a) *\*Spontaneous CP violation in quark scattering from QCD  $Z(3)$  interfaces*  
**Abhishek Atreya**, Anjishnu Sarkar, Ajit M. Srivastava  
Phys.Rev. D85 (2012) 014009; arXiv:1111.3027 [hep-ph]
- (b) *\*Reviving Quark Nuggets as a Candidate For Dark Matter*  
**Abhishek Atreya**, Anjishnu Sarkar, Ajit M. Srivastava  
Phys.Rev. D90 (2014) 4 045010; arXiv:1405.6492 [hep-ph]
- (c) *A Novel Mechanism for  $J/\psi$  Disintegration in Relativistic Heavy Ion Collisions*  
**Abhishek Atreya**, Partha Bagchi, Ajit M. Srivastava  
Phys. Rev. C90 (2014) 3 034912; arXiv:1404.5697 [hep-ph];
- (d) *\*Spontaneous CP Violating Quark Scattering From Asymmetric  $Z(3)$  Interfaces in QGP*  
**Abhishek Atreya**, Partha Bagchi, Arpan Das, Ajit M. Srivastava  
Phys. Rev. D90 (2014) 12, 125016; arXiv:1406.7411;

(\*) indicates the papers on which this thesis is based.

## 2. Conference Proceedings

(a) *Baryon inhomogeneities due to CP violating QCD Z(3) walls*

**Abhishek Atreya**, Anjishnu Sarkar, Ajit M. Srivastava

J.Phys.Conf.Ser. 484 (2014) 012053.

(b) *Nuggets Anti Nuggets formation from QCD Z(3) Domains*

**Abhishek Atreya**, Anjishnu Sarkar, Ajit M. Srivastava

To appear in Indian National Science Academy Proceedings.

(c) *A Novel Mechanism for J/ψ Disintegration in Relativistic Heavy Ion Collisions*

**Abhishek Atreya**, Partha Bagchi, Ajit M. Srivastava

To appear in Indian National Science Academy Proceedings.

# List of Figures

1.1	$(I_3, Y)$ plot of $0^-$ mesons. . . . .	3
1.2	A schematic plot of hardron-QGP phase transition form M.I.T. bag model . . . . .	13
1.3	Current understanding of QCD phase diagram (see ref. [15]). . . . .	14
1.4	A schematic diagram showing various stages of evolution in Heavy Ion Collisions . . . . .	17
1.5	Schematic representation of various stages in the thermal history of the universe. . . . .	23
2.1	Free energy plot for real scalar field. . . . .	30
2.2	Free energy plot for complex scalar field. . . . .	31
2.3	Lattice results showing the variation of Polyakov Loop (for a pure glue theory) and the Chiral order parameter [50]. . . . .	38
2.4	Lattice results for QCD with quarks. (a): Variation of Polyakov Loop susceptibility as a function of $\beta$ for 3 different quark mass. (b): Chiral susceptibility as function of $\beta$ for 3 different quark mass [51]. . . . .	39
2.5	(a): Lattice results showing the variation of energy density for pure QCD. [52] (b): Results for QCD with quarks. [53] . . . . .	40
2.6	The domain wall configuration. . . . .	45
2.7	Magnetization in real space. . . . .	46
2.8	Right: Magnetization in real space. Left: Mapping to order parameter space. From [48] . . . . .	48
2.9	(a):Profile of Domain Wall between two $Z(3)$ domains. (b): QGP String at the junction of three interfaces. . . . .	49

3.1	Variation of $ L(\vec{x}) $ between different $Z(3)$ vacua for $T = 400$ . . . . .	53
3.2	On left: Plot of calculated $ L $ and the one obtained from minimizing the energy. The inset figure shows the deviation between the two profiles. On right: Variation of $a$ and $b$ between the regions $L(\vec{x}) = 1$ and $L(\vec{x}) = e^{i2\pi/3}$ . Initial point is $(-1.5, -1.0)$ . . . . .	54
3.3	Plot of calculated $A_0$ and the fitted profile ( $A_0(x) = p \tanh(qx+r) + s$ ). The parameters have values $p = -378.27$ , $q = 7.95001$ , $r = -49.7141$ , $s = -1692.48$ . Only $(1, 1)$ component of $A_0$ is plotted. The other components also have similar fit. . . . .	55
3.4	(a) Plot of the profile of $ L $ corresponding to the effective potential in Eq.(3.4). (b) Comparison of the profiles of $ L $ for different choices of $T_d$ in Eq.(3.4). . . . .	57
3.5	(a) Plot of calculated values of $a$ and $b$ for the $ L $ profile of Fig. 3.4a. (b) corresponding plot of $A_0$ . . . . .	58
3.6	Potential ( $V(z)$ ) approximated by $n$ step potentials, each of width $w$ , in series. . . . .	60
4.1	The background $A_0$ profile calculated from the $l(x)$ profile. The profile is fitted to a tanh curve. . . . .	77
4.2	Number density evolution with step function profile: (a)For Red, green and anti-blue charm quark. (b)For anti-red, anti-green and blue charm quark. . . . .	79
4.3	Number density evolution with smooth profile: (a)For Red, green and anti-blue charm quark. (b)For anti-red, anti-green and blue charm quark. . . . .	79
4.4	Evolution of baryon density profile . . . . .	81
5.1	Plot of $ l(x) $ obtained from energy minimization for $b_1 = 0.645$ (solid curve). On the left is the initial trial configuration. The final configuration is on right. . . . .	87
5.2	Plot of calculated $A_0$ and the fitted profile ( $A_0(x) = p \tanh(qx+r) + s$ ) for $b_1 = 0.03$ and $0.645$ . . . . .	87

# List of Tables

3.1	Table for the reflection coefficients for various quarks. Reflection is higher for heavier quarks. . . . .	62
3.2	Table for the reflection coefficients when the profile is shrunk. Results approach the step potential as the profile gets narrower. . . . .	63
4.1	Table for the transmission coefficients for charm quarks and anti-quarks, moving parallel to the wall, from the $l = z^2$ wall. . . . .	78
5.1	Table for the reflection coefficients for charm quark and antiquark for smooth profiles of $A_0$ and $m(x)$ . . . . .	92

# Chapter 1

## Introduction

Since the time immemorial, the curiosity of *homo sapiens* has set them apart from the other species around. The curiosity which led to the discovery of new phenomenon, like fire, is the driving force behind the entire scientific endeavor. For more than two millennia, the understanding of the world around us has improved slowly and gradually. One of the questions which has plagued the scientist and philosophers over the time, is to understand the basic constituents that form matter. As in any other field, our understanding has evolved from the days of the ancient civilizations when *atoms* were the fundamental particles. It was the much celebrated backscattering experiment by Rutherford in early 20th century which proved that atoms have sub-structure. The central heavy mass was called the nucleus while the electrons were supposed to go around it in orbits. The advent of quantum mechanics saw to it that this picture becomes more and more refined, while the independent theoretical and experimental investigations of the nuclear properties revealed that the nucleus is composed of protons and neutrons.

### 1.1 Isospin, SU(3) and Quark Model

That was the situation till the middle of 20th century. But by that time there was a plethora of experimental data and numerous “fundamental” particles were discovered. With no underlying theoretical framework to study these particle, there was a growing unease about the fundamental nature of these particles. The situation was akin to

that faced by Mendeleev when he formed the periodic table. A categorization was desperately needed. These particles belonged to two categories. Particles with integer spins or bosons, of which  $\pi$ -mesons are the lightest and the particles with half integer spins of which protons and neutrons are the lowest lying states. Proton and neutron have roughly the same mass but while the charge of proton is unity (in the units of electronic charge), the neutron is neutral. It was realized that the nuclear interactions are insensitive to the electric charge to a good approximation. In other words, under the exchange of proton and neutron, the strong interactions remained invariant. This led to the idea that proton and neutron form a isospin (spin like) doublet under the  $SU(2)$  isospin symmetry. If this symmetry is an exact symmetry then

$$\left[ I_i, H \right] = 0, \quad i = 1, 2, 3 \quad (1.1)$$

where  $I_i$  are the are the generators of  $SU(2)$  isospin and  $H$  is the total Hamiltonian of the system. This would mean that the proton and neutron are strictly degenerate in mass. However, as we know that is not the case. Hence, Isospin is a good symmetry albeit an approximate one. This concept can be extended to various other hadrons like pions, rho mesons, sigma baryons etc.

Strong interaction time scale is very small. However, some particles like  $\Lambda$  and  $\Sigma$  baryons have lifetime much larger than the strong interaction time scale. These particles would readily decay via weak interactions. It was postulated by Gell-Mann [1] and independently by Nishijima [2] that this can be explained if these particle carry another quantum number called “strangeness” which is conserved in the strong and electromagnetic interactions but is violated in the weak interactions. With various experiments confirming this proposal in the properties of other strange particles, the search for higher symmetry that can incorporate both the isospin and strangeness intensified. However, what that higher symmetry group could be remained unanswered. It was Gell-Mann [3] and Ne’eman [4] who showed that all the baryons and mesons of the same spin and parity can be grouped together on  $(I_3, Y)$  plot, where  $Y$  is the hypercharge, (fig. 1.1 )and it looked very much like the representation of  $SU(3)$  group.

Based on these arguments, Gell-Mann [5] predicted the existence of  $\Omega^-$  baryon. Its experimental discovery in 1964 with all the predicted quantum number established

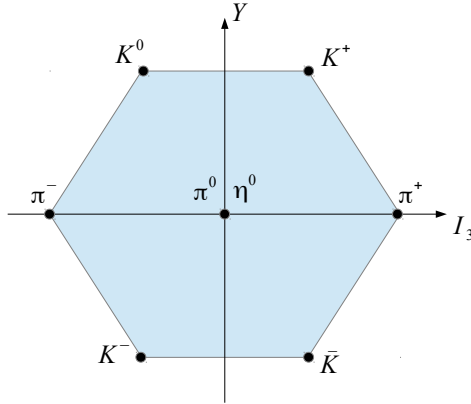


Figure 1.1:  $(I_3, Y)$  plot of  $0^-$  mesons.

$SU(3)$  as the most suited symmetry group for describing the strongly interacting particles. However like  $SU(2)$ ,  $SU(3)$  is an approximate symmetry. Actually it is a worse approximation than  $SU(2)$  symmetry due to the large mass splitting in the case of strange hadrons. Nonetheless, it provides a very accurate categorization scheme for the hadrons. This classification strongly suggests an underlying structure in these particles. The quark model was proposed as a model for the underlying structure of these particles. It was independently proposed by Gell-Mann [6] and Zweig [7, 8]. In this model the basic constituents are quarks which are point like fermionic particles. They come in three variants (or flavors)  $u$  (up),  $d$  (down) and  $s$  (strange) and form a  $SU(3)$  triplet. These quarks are assigned various quantum numbers like hypercharge, spin, color etc. The hadrons are combinations of quarks and their anti particles. However, there was a problem with the model. The  $\Delta^{++}$  baryon, according to quark model, should have three  $u$  quarks, all with spin up (as it has spin  $3/2$ ) and with zero angular momentum. This means that the wavefunction is symmetric under the exchange of the quarks. This is forbidden by Pauli's exclusion principle. To make the wavefunction anti-symmetric it was postulated that the quarks carry an additional quantum number called color [9, 10]. Each quark comes in three colors viz red, green and blue. It was the color part of the wavefunction which was anti-symmetric. The quarks form hadrons in such a manner that the color quantum number is zero i.e it is

a singlet under color transformations. Since then, various experiments have provided the indirect evidence for the existence of quarks and anti-quarks.

With lots of interest getting aroused in the type of interactions involved in the exchange of color charges, it was soon realized that the underlying theory of the color charges is a gauge theory similar to quantum electrodynamics, which is the theory governing the interactions between electrically charged particles. This theory, known as quantum chromodynamics (QCD), has some very interesting properties like asymptotic freedom and color confinement. It has been argued that under certain extreme conditions (like high density and/or high temperature), quark can be liberated from the hadrons and can exist in the form of plasma known as quark gluon plasma (QGP). New high energy accelerators that can collide heavy ions at ultra relativistic energies have provided a never before realised opportunity to experimentally study these new phases under laboratory conditions. Study of these phases will also be important in context of cosmology. It has been established that universe has an extremely intricate thermal history. When universe was just few micro seconds old, it witnessed QCD phase transition. Around that epoch, the free quarks and gluons combined to form hadrons. This thesis is based on the studies of certain interesting objects that can be present in the QGP phase, namely  $Z(3)$  domains and the cosmological implications that these domains can have.

The thesis is structured in the following manner: This chapter will give a brief overview of QCD, the theory of color (or strong) forces. We argue that QCD has a very rich phase structure and discuss it. The chapter concludes with a discussion of the heavy ion experiments and early universe. In chapter 2 we'll focus on the confinement-deconfinement transition. This is of interest to us as this is of relevance in context of early universe. We'll look at the order parameter and write down the effective potential to study the confinement-deconfinement phase transition. We'll see how topological defects can arise in QGP medium as a result of spontaneous symmetry breaking of the center symmetry of  $SU(3)$ .

In the next three chapters we present our original research work. In chapter 3 we look at the spontaneous CP violation in the scattering of quarks from the QCD  $Z(3)$  domain walls. Confining our discussion to pure gauge theory, we argue that with these  $Z(3)$  domain walls there is an associated  $A_0$  profile which differentiates between

quarks and anti-quarks leading to different reflection and transmission coefficients for quarks and anti-quarks. We also discuss the consequences of this CP violation in relativistic heavy ion collisions and in case of early universe. We use this result in chapter 4, where we discuss, in detail, the consequence of this CP violation in context of early universe. We show that this CP violation can lead to the segregation of baryons and anti-baryons and one can form quarks nuggets as well as anti-nuggets around QCD phase transition epoch. In chapter 5, we discuss the effect of quarks on these  $Z(3)$  domains. Arguing that the inclusion of dynamical quarks in the discussion leads to the explicit breaking of  $Z(3)$  symmetry, we show that in this case there is a certain asymmetric scattering of quarks and anti-quarks from the  $Z(3)$  domains which can lead to different distributions of nuggets and anti-nuggets for a generic domain wall network.

## 1.2 Quantum Chromo Dynamics

In this section we'll do a quick overview of QCD and argue that liberation of color degrees of freedom is expected at high temperature and/or high baryon density.

The fundamental particles in this theory are quarks and gluons. Quarks are fermionic particles that carry the gauge charge, also known as the *color* charge. It is an internal quantum number, in addition to the spin, weak hypercharge and electric charge. The color charge is of three types and is designated as red, green and blue. Quarks transform under the fundamental representation of  $SU(3)$ . The color interactions between quarks are facilitated by gluons, which are the gauge bosons in this theory. Gluons come in eight variants and they transform under the adjoint representation of  $SU(3)$ . Unlike photons, which are the gauge particle for QED, gluons carry the gauge charge i.e. the color charge. This necessarily implies that gluons can interact among themselves (unlike photons). This is the *non-abelian* property of QCD. The QCD Lagrangian is written as

$$\mathcal{L} = -\frac{1}{4}G_{\alpha\beta}^a G_a^{\alpha\beta} + \bar{\psi} (i\gamma^\mu D_\mu - m) \psi, \quad (1.2)$$

where  $D_\mu$  is called the covariant derivative and is given by

$$D_\mu = \partial_\mu - igT_a A_\mu^a. \quad (1.3)$$

where  $T_a$  are the generators of  $SU(3)$  in the fundamental representation.  $G_{\alpha\beta}$  is the gluonic field strength tensor. It is defined as

$$\left[ D_\alpha, D_\beta \right] = igG_{\alpha\beta} \equiv igT_a G_{\alpha\beta}^a, \quad (1.4a)$$

$$\text{where } G_{\alpha\beta}^a = \partial_\alpha A_\beta^a - \partial_\beta A_\alpha^a + gf^{abc} A_\alpha^b A_\beta^c \quad (1.4b)$$

The transformation of fields under  $SU(3)$  rotations  $U$ , are given by

$$\psi \rightarrow \psi' = U\psi, \quad (1.5a)$$

$$\text{and } T_a A_\mu^a \rightarrow T_a A_\mu^{a'} = UT_a A_\mu^a U^{-1} - i(\partial_\mu U)U^{-1}. \quad (1.5b)$$

Like any sensible quantum field theory, QCD is also a renormalizable theory. One of the consequences of the renormalizability is that various parameters in the theory (like mass, coupling constant) are dependent on the energy scale at which the theory is being studied. In case of QCD, it turns out that gauge coupling decreases with the increase in energy. The strong coupling constant  $\alpha_s$  is

$$\alpha_s(Q^2) = \frac{4\pi}{(11 - 2n_f/3) \ln(Q^2/\Lambda^2)} \quad (1.6)$$

where  $\Lambda \sim 200 \text{ MeV}$  is known as the  $QCD$  scale and  $n_f$  is the number of fermions in the theory. Since  $n_f = 6$ , the coupling decreases with the increase in the momentum transfer  $Q^2$ . This is the much celebrated asymptotic freedom of QCD [11, 12].

The above expression for the strong coupling constant also dictates that at low energies the interactions between quarks and gluons is very strong. In other words, at large distances the coupling increases. This along with the fact that gluons self interact, leads to quark confinement. So it is not possible to remove quarks from the proton. They are *confined* within the protons. It is an experimental fact that all the low energy hadrons fit the scheme in which constituent quarks combine to form a color singlet state. There is no experimental evidence of an isolated quark or a gluon or in general of any particle in a color non-singlet state. Thus one can give a heuristic definition of confinement as

There are no isolated particles in nature with non-vanishing color charge.

### 1.2.1 The MIT Bag Model

A phenomenological model which takes into account both the asymptotic freedom and color confinement is M.I.T. bag model. In this model a hadron has an internal structure associated with quark and gluon fields. The fields are localized in a space-time region. This region is called a bag, hence the name of the model. The particle quarks are viewed as the quantum excitation of the corresponding fields. These constituent particles exist only in the interior of the hadron. As we shall see, this ansatz captures the confinement part. In what follows we follow the discussion as given in [13].

The quark field is given by  $\psi_a(x)$ . The index  $a$  is the  $SU(3)$  color index of the field. If there are  $n_f$  flavors of quarks, then there are  $n_f$  such fields. These fields are zero outside the hadron by definition. The quark flux in the interior is then given by

$$j_{ab}^\mu(x) = \bar{\psi}(x)_a \gamma^\mu \psi(x)_b \quad (1.7)$$

The quark confinement then requires that the flux through the surface of the hadron is zero. This implies that

$$n_\mu j_{ab}^\mu(x) = \bar{\psi}_a(x) n_\mu \gamma^\mu \psi(x)_b = 0 \quad (1.8)$$

where  $n_\mu$  is the unit space like vector normal to the surface of hadrons. In the instantaneous rest frame,  $n_i$  is the ordinary space normal, and  $n_0$  is zero. It is then trivial to show that the ansatz

$$i\gamma_\mu n^\mu \psi_a(x) = \psi_a(x) \quad (1.9)$$

on the surface satisfies eq. (1.8). This also implies that  $\bar{\psi}_a(x)\psi_b(x) = 0$ . Since the quark fields are Dirac fields, their stress energy momentum is given by

$$T_q^{\mu\nu} = \sum_a \frac{i}{2} \left[ \partial^\nu \bar{\psi}_a \gamma^\mu \psi_a - \bar{\psi}_a \gamma^\mu \partial^\nu \psi_a \right] \quad (1.10)$$

and is conserved i.e  $\partial_\mu T_q^{\mu\nu} = 0$ . The flow of total energy and momentum of the hadron through the surface is given by (using eq. 1.9 and 1.10).

$$n_\mu T_q^{\mu\nu} = \frac{1}{2} \partial^\nu \left( \sum_a \bar{\psi}_a \psi_a \right). \quad (1.11)$$

Since  $\bar{\psi}_a\psi_a$  is zero on the surface, it's derivative lies along the normal. Thus

$$\frac{1}{2}\partial^\nu\left(\sum_a\bar{\psi}_a\psi_a\right)=n^\nu P_q \quad (1.12a)$$

$$n_\mu T_q^{\mu\nu}=n^\nu P_q. \quad (1.12b)$$

where  $P_q$  is identified with the pressure exerted on the bag due to quarks. If the momentum flows out of the bag,  $T^{\mu\nu}$  will not be conserved inside the hadron. So one must put an external pressure on the bag from the outside. Thus the total energy momentum tensor of a hadron is given as

$$\begin{aligned} T_H^{\mu\nu} &= T_q^{\mu\nu} - g^{\mu\nu} B \quad (\text{Inside}) \\ &= 0 \quad (\text{Outside}), \end{aligned} \quad (1.13)$$

where  $B$  is called the bag pressure which is a constant. It has the dimensions same as that of energy density. Eq. (1.13) can be redefined using the 2-D  $\theta$  function as

$$T_H^{\mu\nu} = \theta(x) (T_q^{\mu\nu} - g^{\mu\nu} B) \quad (1.14)$$

The conservation of energy momentum tensor for hadron requires  $\partial_\mu T_H^{\mu\nu} = 0$ , which yields  $P_q = B$ . We have used eq. (1.14) along with identity  $\partial_\mu\theta(x) = n_\mu\delta^{(2)}(x)$  to get the condition.  $\delta^{(2)}(x)$  is the surface delta function. If  $P_q = B$ , then energy momentum tensor is conserved and the energy momentum 4-vector,  $P^\mu$ , is a constant given by

$$\begin{aligned} P^\mu &= \int d^3x T_H^{0\mu} \\ &= \int_{Bag} d^3x (T_q^{0\mu} - g^{0\mu} B). \end{aligned} \quad (1.15)$$

We note that the bag pressure contributes to the energy ( $P^0$ ) of the hadron and not to the momentum ( $P^i$ ). The quark contribution to the hadron energy can be calculated by solving Dirac equation for the quark fields. We assume that hadron is spherical in it's rest frame. We also assume the quarks to be free and massless. The problem then reduces to finding the normal modes of the quark field in a spherical cavity of radius  $R$ , subject to the boundary condition given by eq. (1.9) at  $r = R$ . One can then proceed with quantization by quantizing the amplitudes of these normal

modes. The solution for the ground state mode is  $E_q = 2.04/R$ . Thus the energy of the lowest lying hadron is given by (using eq. (1.15))

$$E = \frac{2.04N}{R} + \frac{4\pi}{3}R^3B. \quad (1.16)$$

where  $N$  is the number of quarks in the hadron. The equilibrium radius of the hadron is given by  $dE/dR = 0$ . This gives

$$R = \left( \frac{2.04N}{4\pi B} \right)^{1/4}. \quad (1.17)$$

For a 3 quark system of baryons (say proton), if we assume the size to be  $0.8fm$ , then we get the bag pressure to be  $206 MeV$ .

Till now we have only concerned ourselves with quarks. However, there are gluons which mediate the interaction between the quarks. So to get the total pressure being exerted on the bag we should add the pressure contribution of the gluons too. So the bag pressure is just the sum of pressure of the gluons and that of quarks. One then expects that as the pressure of the quarks and gluons exceeds the bag pressure, the equilibrium is lost and the quark and gluons are no more confined inside the hadronic “bag”. We’ll now use this model to study the situations under which a gas of hadrons changes to a plasma of quarks and gluons.

## 1.3 Statistical Mechanics and QCD

The discussion of a gas of quarks and gluons requires a statistical description of quantum fields. In this section we’ll look at the thermal aspects of QCD. We’ll see that there is a critical value of temperature and chemical potential beyond which the quarks are deconfined and are free.

### 1.3.1 Partition Function and Thermodynamic Quantities

We’ll start with the transition amplitude in a relativistic quantum field theory. Let the system be in state  $|\phi\rangle$  at time  $t = t_0$ . After time  $\Delta t$  the state evolves to  $e^{-iH\Delta t}|\phi\rangle$ . Then the amplitude for transition from state  $|\phi\rangle$  to  $|\phi'\rangle$  after time  $\Delta t$  is given by

$$\mathcal{M} = \langle\phi'|e^{-iH\Delta t}|\phi\rangle \quad (1.18)$$

where  $H = \int d^3x \mathcal{H}(\hat{\phi}, \hat{\pi})$  is the (time independent) Hamiltonian of the system.  $\hat{\pi}(\vec{x})$  and  $\hat{\phi}(\vec{x})$  are field operators with eigen states  $|\pi\rangle$  and  $|\phi\rangle$  and eigen values  $\phi(\vec{x})$  and  $\pi(\vec{x})$  respectively, i.e

$$\hat{\phi}(\vec{x})|\phi\rangle = \phi(\vec{x})|\phi\rangle \quad \text{and} \quad \hat{\pi}(\vec{x})|\pi\rangle = \pi(\vec{x})|\pi\rangle. \quad (1.19)$$

One can then write a path integral expression for the transition amplitude as:

$$\begin{aligned} \mathcal{M} &= \langle \phi_b | e^{-iH\Delta t} | \phi_a \rangle \\ &= \int \mathcal{D}\pi \int \mathcal{D}\phi \exp \left[ i \int_0^t dt \int d^3x \left( \pi(\vec{x}, t) \dot{\phi}(\vec{x}, t) - \mathcal{H}(\pi, \phi) \right) \right], \end{aligned} \quad (1.20)$$

where in the above expression we have chosen  $t_0 = 0$  and  $\Delta t = t$ .

Now, the partition function of the system is defined as

$$\begin{aligned} \mathcal{Z} &= Tr \left( e^{-\beta \hat{H}} \right) \\ &= \sum_{|\phi(\vec{x}, 0)\rangle} \langle \phi(\vec{x}, 0) | e^{-\beta \hat{H}} | \phi(\vec{x}, 0) \rangle. \end{aligned} \quad (1.21)$$

Comparing with eq. (1.20) we notice that we can express the partition function in terms of transition amplitude, if we make the following connections

- map  $it \rightarrow \tau$ ;  $\tau \in [0, \beta]$ .  $\tau$  is *Imaginary time parameter*.
- Apply boundary conditions  $\phi(x, 0) = \phi(x, \beta) = \phi$ .

This leads us to the path integral expression for the partition function as

$$\mathcal{Z} = \int \mathcal{D}\pi \int_{\text{periodic}} \mathcal{D}\phi \exp \left[ \int_0^\beta d\tau \int d^3x \left( \pi(\vec{x}, \tau) \dot{\phi}(\vec{x}, \tau) - \mathcal{H}(\pi, \phi) \right) \right]. \quad (1.22)$$

Note that there is no constraint over  $\pi$  integral.

In the special cases where the  $\dot{\phi}$  is the conjugate momenta  $\pi$  (which is the case in most of the situations), one can perform the integration over  $\pi$  fields to get the partition function in the form

$$\mathcal{Z} = N \int_{\text{periodic}} \mathcal{D}\phi e^{\mathcal{S}_E}, \quad (1.23)$$

where  $\mathcal{S}_E = \int dt \int d^3x \mathcal{L}_E$  is the Euclidean action and  $\mathcal{L}_E$  is the Euclidean Lagrangian density.  $N$  is an overall normalization constant.

The above case was for the scalar field. For the case of gauge fields, the situation is a bit tricky. The gauge fields have only two independent degrees of freedom (the polarizations of  $\vec{E}$  for example in the case of photon). However, the Lagrangian involves four degrees of freedom. Thus, naively, the partition function will not be given by the  $\text{Tre}^{-\beta\hat{H}}$  as the unphysical degrees of freedom need to be taken care of. The way out is to work either in a specific gauge where one has only two degrees of freedom or to work with the gauge fields as well as the ghost fields. In the latter case the contribution of the unphysical degrees of freedom is cancelled by the ghost fields.

The above discussion was confined to the situation where the system had no net charge. If there is a net conserved charge associated with the system then we make the replacement  $\mathcal{H} \rightarrow \mathcal{H} - \mu\mathcal{N}$ , where  $\mathcal{N}$  is the conserved charge density.

With the partition function in hand, one can then, in principle evaluate all the thermodynamic variables corresponding to the underlying theory. For the case of QCD, the Lagrangian is given by eq. (1.2). One can then use the above discussed techniques to calculate the partition function and various other quantities from it. The pressure, entropy density, number density and the energy density of the system in the ideal gas approximation then turn out to be [14]

$$P = \left(g_b + \frac{7}{8}g_f\right) \frac{\pi^2 T^4}{90} + \frac{g_f}{24} \left(\mu^2 T^2 + \frac{\mu^4}{2\pi^2}\right) \quad (1.24a)$$

$$S = 2 \left(g_b + \frac{7}{8}g_f\right) \frac{\pi^2 T^3}{45} + \frac{g_f}{12} \mu^2 T \quad (1.24b)$$

$$n = \frac{g_f}{12} \left(\mu T^2 + \frac{\mu^3}{\pi^2}\right) \quad (1.24c)$$

$$\mathcal{E} = \left(g_b + \frac{7}{8}g_f\right) \frac{\pi^2 T^4}{30} + \frac{g_f}{8} \left(\mu^2 T^2 + \frac{\mu^4}{2\pi^2}\right) \quad (1.24d)$$

We will now study the system under two extreme limits: at very high temperatures and at very high density.

### A. At High temperatures, $\mu = 0$

For  $\mu = 0$  and two quarks ( $u$  and  $d$ ) degrees of freedom we get the pressure exerted due to quarks and gluons, using eq. (1.24a), to be

$$P = 37 \frac{\pi^2}{90} T^4. \quad (1.25)$$

Under equilibrium conditions, this pressure is balanced by the bag pressure. The critical value of temperature beyond which this pressure exceeds the bag pressure is

given by

$$37 \frac{\pi^2}{90} T_c^4 = B. \quad (1.26)$$

Using the value of  $B = 206 \text{ MeV}$ , which we calculated in previous section, we get  $T_c \sim 144 \text{ MeV}$ . Beyond this value of temperature, the quarks do not remain confined in the bag and are free. This is the case in the early universe, where in the early stages the temperature is extremely high and the net baryon content is almost zero (excess of roughly one quark in 10 billion anti-quarks). Baryon content is also small in the central rapidity region of ongoing relativistic heavy ion collision experiments at BNL and LHC (CERN). We'll discuss these experiments in a bit more detail later.

### B. At High Densities

Let us consider another extreme. For  $T = 0$  and non-zero  $\mu$ , we again calculate the pressure due to ( $u$  and  $d$ ) quarks and gluons. From eq. (1.24a) we get

$$P = \frac{g_f}{24\pi^2} \mu_q^4, \quad (1.27)$$

which gives the critical value of chemical potential to be

$$\mu_c = \left( \frac{24\pi^2}{g_f} \right)^{\frac{1}{4}} B^{\frac{1}{4}}. \quad (1.28)$$

For  $B = 206 \text{ MeV}$ , we get  $\mu_c = 434 \text{ MeV}$ . This gives, the baryon number density to be, from eq. (1.24c), to be  $n_b^{\text{critical}} = 0.72/fm^3$  which is roughly 5 times the density of normal nuclear matter. Such high densities can occur in the core of certain astrophysical objects like neutron stars.

For intermediate values of  $T$  and  $\mu$ , we'll have to use the relation  $P_{QGP} = P_{Hadron}$ , where  $P_{Hadron} = P_\pi + P_{Nucleon}$ , to get the equilibrium curve on a  $T - \mu$  plot (fig. 1.2). The phase transition thus constructed is a first order phase transition except for the  $T = 0$  case, where the order of the transition depends on the value of the bag constant. For the value of  $B$  we are assuming the transition is second order [14]. In the next section we'll look at the current status of the QCD phase diagram in a bit detail.

## 1.4 QCD Phase Diagram

In this section we summarize our current understanding of the phase structure of QCD matter. At present, somewhat concrete statements can be made only in the

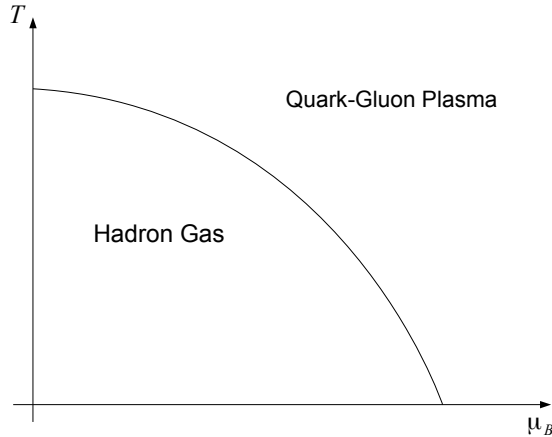


Figure 1.2: A schematic plot of hardron-QGP phase transition from M.I.T. bag model

case of finite  $T$  with a small baryon density ( $\mu_B \ll T$ ) and at an asymptotically high density ( $\mu_B \gg \Lambda_{QCD}$ ). The phase diagram of QCD is divided into three regions (fig. 1.3), see [15].

**A. Along  $\mu_B = 0$ :** The QCD phase transition at finite temperature with zero chemical potential has been studied extensively in the numerical simulation on the lattice. The results depend on the number of colors and flavors. For three colors, in the pure gauge case (no fermions), Lattice calculations have established a first-order deconfinement transition [16]. The critical temperature is found to be  $T_c = 270 \text{ MeV}$ . Recent calculations which take into account the effect of fermions, indicate a crossover from the hadronic phase to the quark-gluon plasma for realistic  $u$ ,  $d$  and  $s$  quark masses [17,18]. The crossover temperature, is likely to be in the range  $150 - 200 \text{ MeV}$ .

**B. Along  $T = 0$ :** Along the  $\mu_B$  axis, various features are present.

1. Liquid-gas phase transition of nuclear matter:- As we move along the  $T = 0$  axis we approach the nuclear matter density. Since the nuclear mass is  $\sim 940 \text{ MeV}$  and the binding energy in nucleon matter is  $16 \text{ MeV}$ , nuclear matter starts appearing around  $924 \text{ MeV}$ . For  $924 \text{ MeV} < \mu_B < 940 \text{ MeV}$ , the nuclear matter appears in the form of droplets. This is a typical first-order phase transition of the liquid-gas type. The first-order transition weakens as

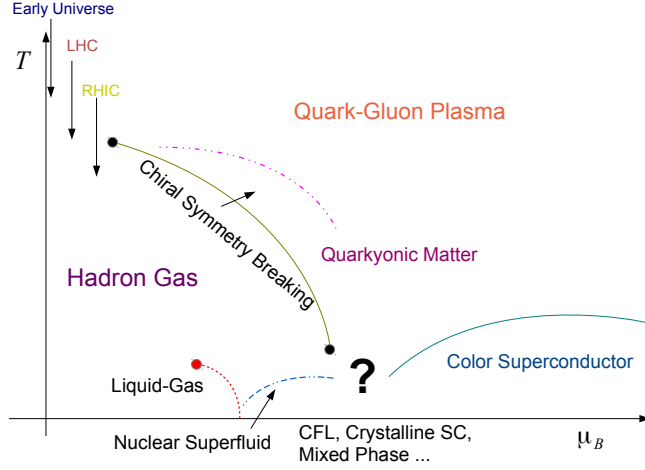


Figure 1.3: Current understanding of QCD phase diagram (see ref. [15]).

$T$  grows and eventually ends up with a second-order critical point (red dot) as indicated in fig. 1.3. Low-energy HIC experiments indicate that  $\mu_G \sim \mu_{NM}$  and  $T_G = 15 - 20 \text{ MeV}$ .

2.  $\mu_B \gg \Lambda_{QCD}$ : At asymptotically large values of  $\mu_B$  one can use perturbative methods in QCD to study the ground state properties of QCD matter. It has been argued that at high baryon density, the fundamental degrees of freedom (for QCD with three colors and three flavors) are diquarks. This provides an analogue between the electrons in superconductors and the quarks in quark matter. This leads to an expectation that the ground state of QCD matter at low  $T$  and large  $\mu_B$  could be in the form of Cooper pairs of quarks leading to color superconductivity (similar to what happens in the case of superconductivity in condensed matter system). What is the exact nature of this true ground state remains an unsettled issue. There are many patterns of Cooper pairing and thus many different color superconducting states. For a review see ref. [19]. At the intermediate values of  $\mu_B$  and along  $T = 0$  axis, the situation is quite complicated. The main issue is the large mass of strange quark. For different quark flavors, there is a mismatch in their Fermi surface. As  $u$  and  $d$  quarks are almost degenerate, one can neglect the mismatch of their Fermi surface.

However for strange quark, that is not the case and mismatch is quite large. This can lead to the inhomogeneous phases in the intermediate  $\mu$  region. Possibilities of the exotic phases like the Color Flavor Locked (CFL) phase, or the crystalline color superconductor have been discussed in the literature [15].

**C. Finite  $T$  and Finite  $\mu_B$** :- At finite  $T$  and  $\mu_B$ , most of the information comes from the effective models. All of them indicate a first order phase transition associated with the restoration of chiral symmetry in the deconfined phase. The lattice calculations indicate that the chiral restoration is a crossover at non zero but small  $\mu_B$ . The effective models predict a first order phase transition at large  $\mu_B$  and high  $T$ . Another interesting possibility is the existence of quarkyonic matter at finite  $T$  and  $\mu_B$  [20]. Such a phase is suggested from the large  $N_c$  limit of QCD. There is also a suggestive result that supports the idea of quarkyonic matter in  $N_c = 2$  from lattice simulations. Whether the remnant of quarkyonic matter remains in the QCD phase diagram at  $N_c = 3$  is an open question [21].

Other than the above three discussed regimes, QCD phase diagram also features certain critical points.

**D. QCD critical point**:- The lattice calculations show that for the small chemical potential, chiral transition is a crossover for realistic  $u$ ,  $d$  and  $s$  quark masses. While the effective chiral models suggest that the chiral transition becomes first order at large  $\mu_B$  and high  $T$ . This means that there is a QCD critical point located at an intermediate value ( $\mu_B = \mu_c, T = T_c$ ). Above  $\mu_c$ , the chiral phase transition is first order, while below this value it is a crossover. A lot of experimental effort is now being put to locate the critical point.

There is also a possibility that the first-order chiral phase boundary ends at another critical point in the lower  $T$  and higher  $\mu_B$  region. It has been argued in literature that the cold dense QCD matter with three degenerate flavors may have no clear border between superfluid nuclear matter and superconducting quark matter due to the effects of  $U(1)_A$  anomaly. In reality, the fate of the above critical points depends strongly on the relative magnitude of the strange quark mass and the typical values of  $T$  and  $\mu_B$  at the phase boundary.

As discussed above, quarkyonic matter is predicted by the large  $N_c$  limit of QCD. In these theories, the phase diagram consists of three regions separated by first-order

phase transitions, i.e. the confined, deconfined and quarkyonic phases. The meeting point of these three lines is the Quarkyonic Triple Point.

With this brief look at the QCD phase diagram, we now discuss the experimental efforts that are being made to probe this phase diagram in the laboratory.

## 1.5 QGP in Lab

The relativistic heavy ion collision experiments are designed to study the properties of the QGP phase. In these experiments, the heavy nuclei (like gold or lead) are accelerated to ultra relativistic energies and are then collided with each other. The center of mass energies are of the order of few hundred  $GeV$ s per nucleon (in case of LHC they are of the order of  $TeV$ ). At these energies various interesting things happen to nuclei. The nuclei get Lorentz contracted in the direction of the boost. The contraction factor is roughly 100 for RHIC at BNL (even more for LHC). So the nuclei looks like a thin pancake in the laboratory frame. With the nuclear radius being  $\sim 15 fm$ , the transverse extent of the nucleus is same, but in the longitudinal direction the thickness of nuclei is  $\sim 1 fm$ . This should be much less but due to the sea quark anti-quark pairs that surround the nucleus at such high energies, the effective thickness remain of the order of  $1 fm$ . The various stages that the system undergoes from the collision to the final particle production are as follows (see fig. 1.4):

### A. Initial Conditions and Thermalization

At such high energies, the asymptotic freedom makes all the quarks and gluons inside the nucleons essentially free. As a result when the nucleus collide, they pass through each other as if they are transparent. However, the coupling is not exactly zero. This leads to the secondary particle productions and it means that some of the partons and the energy of the incoming nuclei gets *stopped* in the overlapping region of the nuclei as they pass through. This gives the initial conditions for the formation of QGP in lab. The modeling of these initial conditions is itself a very intricate problem. Generally there are two types of initial conditions used: The Color Glass Condensate (CGC) or the Glauber initial conditions. The other models used to study the initial conditions are string decays, parton cascade etc. However these

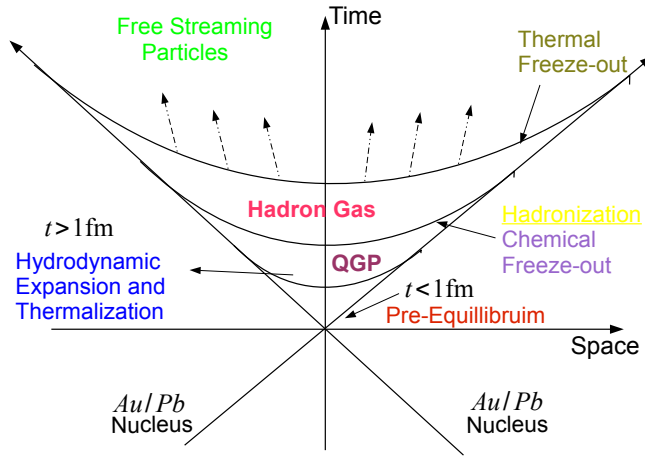


Figure 1.4: A schematic diagram showing various stages of evolution in Heavy Ion Collisions

have their own limitations. A lot of research is being carried out to get a detailed understanding of these initial conditions. The particles in the central region interact and soon attain thermal equilibrium. The successful reproduction of experimental data requires that the thermalization time is very small, roughly a fraction of a  $fm$ . However, till now we do not have a theory or a model that can successfully give us such small thermalization time.

### B. Hydrodynamic Expansion and Thermalization

As the initial system fills up the region in between the two receding nuclei it expands longitudinally. Faster in the longitudinal direction than the transverse direction initially, but becoming more or less uniform in all directions at later stages. As the system expands it cools. Finally when the temperature of the system falls below the quark hadron transition temperature, it hadronize. The system from this time onwards evolves as a hadron gas. Since the system reaches thermalization very fast, the evolution of the system is described by relativistic hydrodynamics. The hydrodynamic modelling of the system and comparing it's predictions with data provide deep insights about the QGP. An example is the much celebrated low  $\eta/s$  value of the QGP, establishing it as the most perfect fluid ever.

### C. Chemical Freeze-out

Initially the hadrons produced have high enough scattering cross-section to undergo inelastic collisions. This changes the chemical composition of the hadron gas. However with expansion, the temperature and density of the hadron gas and consequently the inelastic scattering cross-section of the hadrons decreases. After sometime the inelastic collisions stop. This is the chemical freeze-out. Beyond this, the chemical composition of the system doesn't change (other than the weak decays which happen at much later times) After the chemical freeze-out, the elastic collision and the strong decays of the heavier hadrons take place. One can then use the statistical approach to describe the data.

#### **D. Thermal Freeze-out**

After the inelastic collisions have stopped, the elastic collisions also cease after sometime. This is because the expansion of matter leads to the increases in the mean free path of the particles. As a result the collision time between the particles is much larger than the expansion time scale. This essentially means that the momentum distribution of the particles does not change and they freely reach the detector. This itself is not as simple as it sounds. Different particles have different mean free paths and as a result, they will decouple at different times.

### **1.5.1 Signatures of QGP**

What is finally observed in the detectors is the hadron spectrum. To infer whether there has been any QGP phase formed during these heavy ion collisions or not, there are certain signatures (predicted by using the above mentioned theoretical understanding which assumes the existence of QGP) that one needs to look for while analyzing the data. We briefly discuss some of the important signatures here.

#### **1. Direct Photon Production**

During the pre-equilibrium stage of creating QGP, the quarks, anti-quarks and gluons interact with each other either by various processes like bremsstrahlung, pair-annihilation or by Compton process etc. As quarks carry electric charge, they also lose energy via electromagnetic interactions and in the process photons are produced. The cross-section of these photons is proportional to the square of the fine structure constant which is very small. So they are produced in small numbers but they also don't interact with the system due to their small cross-section. These photons thus

largely escape from the initial system and carry pristine information about the initial momentum distribution of the quarks and anti-quarks. This signal however, suffer from the huge backgrounds which is due to the decays of pions and other decays in the hadronic phase.

## 2. Dilepton Production

The quark and anti quarks can also produce a lepton and an anti-lepton via a virtual photon. Again, these particles interact with the medium through the electromagnetic interaction, which is suppressed, and hence they carry very important information about the initial conditions. Again this signal suffers from huge background coming from various decays.

For both the above signals an enhancement was observed in SPS and RHIC experiments [22–24]. A complete understanding of these results requires an improved theoretical understanding of the underlying process.

## 3. Strangeness Enhancement

As the incoming nuclei have only  $u$  and  $d$  quarks, the strange particle production will not be substantial owing to the high mass of strange hadron. However, if there is a QGP medium then the strange quarks and anti-quarks will be thermally produced by the gluons in the medium. This will lead to the enhancement of the strangeness content in the final hadron distribution [25, 26]. The first observation of such an enhancement was made by NA57 collaboration of SPS at 158  $GeV/A$  energies [27]. Similar observation was made by STAR collaboration at RHIC [28, 29].

## 4. $J/\psi$ Suppression

The  $J/\psi$  is the bound state of charm quark and its anti particle. With a plasma there is an associated characteristic “Debye length” which limits the range of interaction of charged particles. For the distances much larger than the Debye length, the charged particles cannot interact with each other. As a result, the  $c$  and the  $\bar{c}$  of the  $J/\psi$  will not be able to form bound states in the plasma and it “melts” in the medium [30]. These  $c$  the  $\bar{c}$  form open charms during the subsequent hadronization process. Thus  $J/\psi$  suppression is a signal for the presence of QGP. It was observed at SPS in central Pb-Pb collisions [31, 32]. At RHIC the suppression was observed but it was stronger for forward rapidity than on the mid rapidity [33, 34]. Similar trend was noticed at LHC too [35]. This type of suppression does not go well with

the screening picture because the Debye length is inversely promotional to the temperature of the medium and hence decreases with the increase in temperature,. Since the temperature is large at central rapidity one would expect that the suppression would be more in the central rapidity region. Attempts have been made to explain this observation by arguing that  $J/\psi$  gets regenerated in the medium [36–39].

### 5. Elliptic Flow

This is one of the most important signal of QGP. It was proposed that the non central collisions will give rise to the momentum anisotropy of final state particles. In particular the second Fourier coefficient of the azimuthal distribution of particles will be non-zero. This happens because in the case of non central collisions, there is an initial spatial anisotropy. This leads to the different pressure gradients in different azimuthal directions in the transverse plane. Due to the hydrodynamical evolution of the system, it leads to the momentum anisotropy in the hadron spectrum. This has been experimentally observed in RHIC and LHC experiments [40]. Hydrodynamical simulations show that the observed anisotropy can be explained only when there is a QGP medium, with thermalization time smaller than 1  $fm$  and with a small value of  $\eta/s$  [41].

### 6. Jet Quenching

Jets are very high momentum particles produced due to hard scattering of partons at the initial stages of collision. It was argued that while travelling in the medium jets will lose their energies due to strong interactions. The jet near the boundary escapes easily with all the energy, but the jet travelling in the opposite direction loses its energy due to scattering with partons in the QGP. This effect is known as jet quenching. A strong suppression of high transverse momentum was first observed at RHIC energies [42, 43]. It has also been seen at LHC [44]. The jet energy loss also gives important information about the dynamical properties of the medium it is passing through.

All these signatures have been analyzed and it is a general consensus that the QGP has been created in lab. Studying various properties of QGP will also provide us important insights in the evolution of early universe. In the next section we provide a brief discussion on the evolution of early universe and our understanding of it.

## 1.6 Early Universe

The most universal query that every person has had at some stage in their lifetime is probably about the stars, galaxies as we see at the night time. Just like our current understanding of the fundamental particles, our current understanding of the universe around us also finds its origin in early 20<sup>th</sup> century. In this section, we'll give a brief overview of our present understanding of the history of early universe [45, 46].

### 1.6.1 Pillars of Observational Cosmology

Though the foundation work in understanding the gravitational force was laid by the likes of Kepler, Newton and Einstein, the field of cosmology started getting its long overdue attention after Edwin Hubble reported his results (in 1929) on the observation of the galaxies which suggested that the universe is expanding. Assuming that the universe is homogeneous and isotropic (the famous Friedman Robertson Walker space time), it was argued that our observed universe was much smaller, denser and hotter at earlier times. This was the standard hot big bang picture of the evolution of our universe. This theory had some serious contenders, for example the steady state theory of Hoyle and Narlikar, till 1960's.

It was the discovery of Cosmic Microwave Background Radiation (CMBR), by Penzias and Wilson in 1965 that completely tilted the worldview in the favor of hot big bang. It was predicted by Gamow and his collaborators on the basis of the hot big bang scenario. The homogeneous and isotropic nature of this background radiation dictates the homogeneous and isotropic nature of the universe at very early times. The temperature of the universe was around 1 eV when the electrons and protons combined to form Hydrogen atom. The photons free stream after this time and thus carry pristine information about the early stages of the universe. It was also argued that if the universe was in thermal equilibrium till  $\sim 200000$  years after the big bang then this should have a perfect black body spectrum. Since a perfectly homogeneous and isotropic universe cannot have structure formation, it was clear that the CMBR must have anisotropies of the order of  $10^{-5}$  in order to explain the structure formation. Both of these expectations were verified in 1992 by COBE satellite. Since then, it has been one of the most active field of research. With the WMAP data and more

recently PLANCK data coming in, CMBR observations have now moved towards what is called an era of “precision cosmology”.

At even earlier stages, the universe was in the form of a hot electromagnetic plasma of protons and electrons. The formation of nuclei, including helium and others like lithium etc. took place few minutes after big bang. This is called the big bang nucleosynthesis. There are strong observational constraints on the relative abundances on the nuclei from the big bang nucleosynthesis. It was during the subsequent expansion and the cooling of the universe that the first stars were formed and then galaxies and finally we got our present universe.

The Hubble expansion, CMBR and Big Bang Nucleosynthesis together form the three pillars of observational cosmology.

## 1.6.2 Thermal History of Universe

Around the same time when CMBR was discovered, the particle physics was going through a revolution in terms of uncovering various phenomenon in the fundamental interactions. It was then possible to address the questions relating to the first three minutes of the origin of the universe. With the symmetry unification arguments being successfully applied in the particle physics, it was soon realized that universe might have had a much more intricate thermal history than envisaged (see fig. 1.5).

As discussed above, it became clearer that the nucleons also have a substructure and free quarks and gluons exist above a critical value of temperature and chemical potential. Thus in the earlier times, before the formation of nucleons, universe too must have been in such a phase. This is expected to happen up-to a few micro seconds after the big bang. The temperature of the universe was around  $200 \text{ MeV}$  at that time. That was the epoch of Quark Hadron transition.

With the electro-weak symmetry breaking appearing at the energies of  $\sim 100 \text{ GeV}$ , it is expected that the universe witnessed a electro-weak phase transition when the temperature of the universe was around  $100 \text{ GeV}$ . It is characterized by the breaking of  $SU(2) \times U(1)$  symmetry group to  $U(1)$  symmetry. The electro-weak phase transition at finite temperature has been extensively studied and is expected to be of first order. It was soon realized that various non-perturbative effects will play a major role

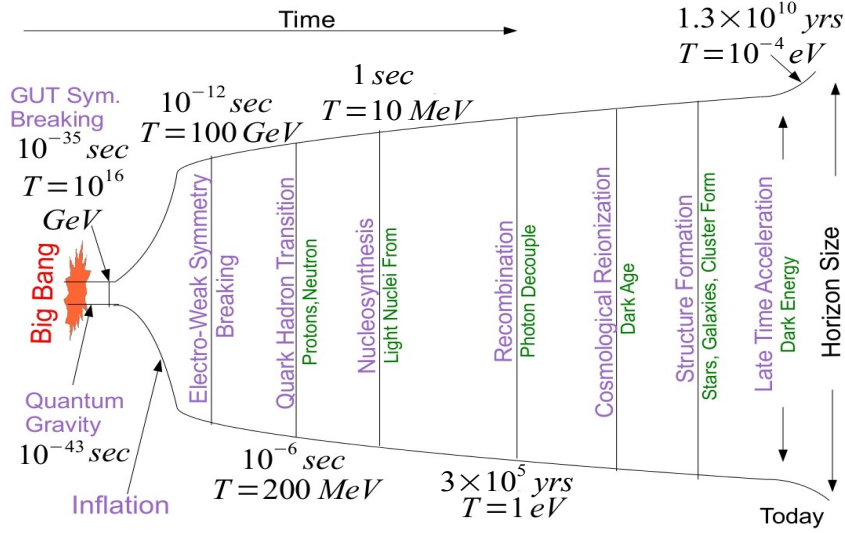


Figure 1.5: Schematic representation of various stages in the thermal history of the universe.

during the phase transition. One of the most interesting phenomenon to have happened around this epoch is baryogenesis, which may provide an answer to one of the puzzles: Why the present universe is matter dominated? The age of the universe was roughly  $10^{-12}$  sec at that time. Due to the lack of direct experimental observations (the present day accelerators have been able to reach only till  $T < 1$  GeV scales) a direct probing of these scales have not yet been possible.

As one increases the energies, the coupling constants of electro-weak and the strong interactions approach each other. The general expectation is that all the couplings meet at the energies of  $\sim 10^{15}$  GeV (including supersymmetry). This is the Grand Unification (GUT) scale in particle physics. In early universe, this situation occurs in the initial  $10^{-35}$  sec. If some symmetry group  $\mathcal{G}$  describes the GUT symmetry for  $T > 10^{15}$  GeV, then at lower temperatures it breaks to the standard model which is  $SU(3)_c \times SU(2)_L \times U(1)_Y$ . This is the GUT phase transition and it posses very rich features which have been discussed in quite detail in literature. At present there are a number of GUT models but again, no direct or indirect experimental test is possible (apart from the constraints coming from the proton decay experiments).

A spontaneous symmetry breaking phase transition can lead to the formation of

topological defects e.g monopoles, cosmic strings and domain walls. All the GUT models predict the abundance of monopoles during GUT transition. The abundance is large enough to close the universe and make it collapse on to itself soon after the big bang. This was one of the problem that led Guth to propose the idea of inflation. During inflation which supposedly took place after GUT transition, the universe expanded exponentially during a very short period of time. The inflationary expansion of the Universe dilutes the density of monopoles drastically. So, the monopole problem is neatly solved by the idea of inflation. The theory of inflation also solves the so called horizon and flatness problem of cosmology. Another prediction of inflation is the acoustic peaks in the CMBR spectrum. This has been verified experimentally by WMAP data. The origin of these peaks is the fluctuations produced at early times in the otherwise homogeneous and isotropic universe. These fluctuations act as the seed for structure formation. Before inflation it was the topological defects, namely cosmic strings, produced during the GUT transition that were the favored source of these fluctuations. However, the perturbations produced by these topological defects are not coherent and hence they can't account for the acoustic peaks in the CMBR spectrum. What inflation naturally does is to explain these peaks in an elegant framework. The quantum fluctuations in the inflaton field provide the seed for the formation of galaxies, clusters that we see around us today. Inflation is now an integral part of the the standard model of Cosmology. However, there are various models of inflation and it's only the more refined cosmological observations or high energy experiments that can select the right model.

The particle physics inspired GUT models allow us to extrapolate the thermal history of the universe till  $10^{-43}$  sec after the big bang. The temperature of the universe at that time is expected to be  $\sim 10^{19}$  GeV. At such high energies, the quantum effects of gravitational interactions become important. A self consistent quantum theory of gravity is needed to understand the physics beyond those time and energy scales.

With heavy ion collision experiments providing us a unique window to look at the QGP phase transition which happened when the universe was just micro seconds old, it is worth every penny to revisit the QCD phase transition in early universe. The study of QCD phase transitions and the associated experimental efforts not

only provide useful insights on the fundamental interactions but they also help us in understanding an important part of the history of our universe. In the next chapter we'll discuss the confinement deconfinement transition in more detail.

# Chapter 2

## Confinement-Deconfinement Transition

In this chapter, we'll look at the symmetry breaking phase transitions in a bit more detail with special focus on confinement-deconfinement phase transition. We start by looking at the phenomenon of spontaneous symmetry breaking in section 2.1. We follow it with the discussion of spontaneous symmetry breaking in the context of confinement deconfinement phase transition in section 2.2. The topological defects are the subject of discussion in section 2.3.

### 2.1 Effective Potential and Spontaneous Symmetry Breaking

Consider liquid-gas transition. The two phases can be distinguished by their respective densities  $\rho_l$  and  $\rho_g$ . So one can use  $\rho - \rho_g$  to label whether system is in liquid phase or in gaseous phase. It vanishes in gaseous phase while it's non-zero in the liquid phase. Similarly in a ferromagnetic system one can use magnetization  $m$  to label distinct phases. It is interesting to note that the quantities mentioned above are not microscopic quantities. For example, the water molecule is not the relevant quantity when we discuss water-steam transition or individual spins are not relevant if we are to discuss the ferromagnetic system. The density and magnetization are averages defined over certain length scales.

A thermodynamic quantity which is different in each phase and hence can be used to distinguish between them is called the *order parameter*.

We should appreciate here that with this averaging we have moved from a particle description to a field description of the problem. This process of averaging is known as *coarse graining*. It is important to note that after coarse graining the order parameter has no variations over the length scales over which the averaging is done, this implies that there is an upper cutoff in the energy scales ( $\lambda \sim 1/a$ , where  $a$  is the length scale over which averages are done).

### 2.1.1 Landau-Ginzburg Hamiltonian and Free Energy

The construction of the Landau-Ginzburg Hamiltonian is a standard procedure in studying phase transitions. We present a brief outline of the underlying steps involved in the construction of the effective Hamiltonian following the book by Kardar [47]. In the original description, the degrees of freedom were microscopic quantities (like water molecule or spin). Going over to the order parameter is a change of variables and the mapping is non-invertible as averaging involves loss of information. In principle, we can get the corresponding probabilities of order parameter field configurations from the microscopic probabilities ( $e^{-\beta\mathcal{H}_{mic}}$ ). Since the change of variables doesn't alter any physical properties of the system, its partition function remains preserved in this process and can be written as:

$$\mathcal{Z} = \text{tr} \left[ e^{-\beta\mathcal{H}_{mic}} \right] \equiv \int \mathcal{D}\phi(\vec{x}) \mathcal{P}[\phi(\vec{x})], \quad (2.1)$$

where  $\mathcal{P}[\phi(\vec{x})]$  is the probability of finding a configuration  $\phi(\vec{x})$ . The problem is to find these probability distribution. This issue was first addressed by Landau for the case of *He* superfluidity. Using the coarse grained probability weights of eq. 2.1, one can define an effective Hamiltonian  $\mathcal{H}[\phi(\vec{x})]$  which gives the probabilities of the order parameter configuration by a Boltzmann factor

$$-\ln \mathcal{P}[\phi(\vec{x})] \equiv \beta\mathcal{H}[\phi(\vec{x})] \quad (2.2)$$

The problem then reduces to the construction of effective Hamiltonian. If  $\mathcal{E}[\phi(\vec{x}), \vec{x}]$  is the effective energy density then one can write

$$\mathcal{H} = \int d\vec{x} \int \mathcal{E}[\phi(\vec{x}), \vec{x}] \quad (2.3)$$

One writes the effective Hamiltonian in a phenomenological manner. As an example, we look at a real scalar field as the order parameter (like density). Order parameter can be complex or a vector too (like in superconductivity or magnetism) but the generalization is straight forward. The entire exercise can be carried out in a  $d$  dimensional space, but we confine ourselves to the case of 3 dimensional space. The most general form for energy density is

$$\mathcal{E} = \mathcal{E} \left[ \vec{x}, \phi(\vec{x}), \vec{\nabla} \phi(\vec{x}), \vec{\nabla}^2 \phi(\vec{x}), \dots \right]. \quad (2.4)$$

One then constrains the form by the following considerations:-

- **Locality and uniformity**:- If the system is homogeneous then  $\mathcal{E}$  is independent of  $\vec{x}$  and we can treat the order parameter field to be independent of  $\vec{x}$  as well. However, this is not the case in general. So we include gradients of the order parameter field too. One would like to restrict to only a few terms in the derivatives where one can get a good understanding of the system by local interactions, like in the case of short range interactions. However, non-local interactions can also be accounted for by including various terms in the derivative.
- **Symmetry**:- For an isotropic system (full  $3 - D$  rotation), there is no preferred direction. This means that gradients can only have the form  $(\vec{\nabla} \phi)^2$  and higher order terms along with the terms like  $\vec{\nabla}^2 \phi$  and higher powers. If the field has  $\phi \rightarrow -\phi$  symmetry, then only terms like  $\phi^2, \phi^4$  are allowed. Thus various terms in  $\mathcal{E}$  should respect the expected symmetries of the system.
- **Analyticity**:- Since we have coarse grained over certain distances, the singularities due to the microscopic description are not present. So,  $\mathcal{E}$  should be an analytic function, hence it can be expressed as the power series of its arguments.
- **Stability**:- The energy density given by eq. (2.4) should be bounded below and it should also not lead to divergences in the probabilities of eq. 2.2 for infinitely large values of the field. This implies the coefficient of the highest order power of field should be positive. The signs of gradient terms are also constrained to avoid instabilities, for eg. the coefficient of the  $(\nabla \phi)^2$  should be positive.

**Saddle Point Approximation:-** The partition function corresponding to the Landau-Ginzburg Hamiltonian is

$$\mathcal{Z} = \int \mathcal{D}\phi(\vec{x}) \exp\{-\beta\mathcal{H}[\phi(\vec{x})]\} \quad (2.5)$$

where  $\mathcal{H}[\phi(\vec{x})]$  is given by eq. (2.3) and eq. (2.4). To obtain thermodynamic quantities from this partition function, we make the *saddle point approximation*, i.e replace the field by the its most probable configuration. The most probable configuration is the uniform field configuration and in that approximation, all the gradient terms can be neglected as they cost energy. This approximation is valid as long as we are not in a region close to  $T_c$ , where the fluctuations are large. Thus, the partition function in this approximation is

$$\mathcal{Z} \approx \mathcal{Z}_{sp} = C \int d\phi \exp\left[-V (A\phi^2 + B\phi^4 + \dots)\right] \quad (2.6)$$

where  $V$  is the volume of the system and  $C$  is a constant. The corresponding saddle point free energy (ignoring the constant) is then given by

$$\beta F_{sp} = -\ln \mathcal{Z}_{sp} \approx V \min\{\mathcal{E}[\phi]\}_\phi \quad (2.7)$$

It is customary to call the function  $\mathcal{E}[\phi]$  as the Landau-Ginzburg free energy. An important point to note is that the free energy of the system, in eq. (2.7), is given by the minimum of the Landau-Ginzburg free energy. The convexity constraints apply to the free energy of the system and in turn to the minimum of the Landau-Ginzburg free energy. In general, the Landau-Ginzburg free energy doesn't follow convexity constraints. Another important point to note is that while the Landau-Ginzburg free energy is analytic, the saddle point free energy given by eq. (2.7) may be non-analytic as the minimization is a non-analytic operation. So, we finally write the saddle point Landau-Ginzburg free energy as

$$V = b\phi^2 + c\phi^4 + \dots \quad (2.8)$$

In the above equation, we have used  $V$  instead of  $\mathcal{E}$  as it only represents the potential part of the otherwise complete energy density of eq. (2.4). Further studies like renormalisation group analysis can restrict the above expansion to the first few terms only. Coefficients  $b, c, \dots$  are analytic function of temperature and can be

expanded around  $T_c$ . The expansion coefficients are phenomenological parameters that are fixed by experiments.

### 2.1.2 Spontaneous Symmetry Breaking

Let us look at the free energy given by eq. (2.8). Keeping ourselves to the first two terms we note that the stability criteria dictates that  $c$  should be positive, while  $b$  can be negative or positive.

**Real Scalar Field:-** This is the case for the Ising system. In the Ising system, one can identify  $\phi$  with the magnetization  $m$ , which is the order parameter. The

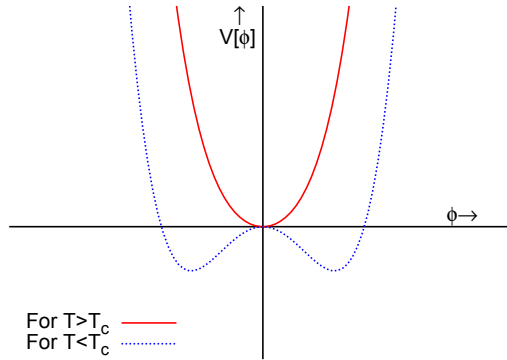


Figure 2.1: Free energy plot for real scalar field.

extrema of the potential are  $\phi = 0$  and  $\phi = \pm(-b/c)^{1/2}$ . Since  $m$  vanishes above the critical temperature  $T_c$ ,  $\phi = 0$  is the true minima of the potential. Hence  $b > 0$  for  $T > T_c$ . Below  $T_c$ , the magnetization or  $\phi$  is non-zero. So, the potential should have at least one minima at  $\phi \neq 0$  (fig. 2.1). That is possible if  $b$  is negative. Thus  $b$  should change sign as  $T$  varies from  $T_c^+$  to  $T_c^-$ . This is achieved in the simplest manner by choosing  $b = b_0(T - T_c)$  with  $b_0 > 0$ . The potential for the  $1 - D$  Ising system then takes the form

$$V = b_0(T - T_c)\phi^2 + c\phi^4. \quad (2.9)$$

Note that the Hamiltonian of the system has  $\phi \rightarrow -\phi$  symmetry. But below  $T_c$  system finds itself in one of the minima and the symmetry is lost. This is called *spontaneous symmetry breaking* and the phase transition is termed as spontaneous

symmetry breaking phase transition. In the Ising model, the order parameter has discrete symmetry.

**Complex Scalar:-** Let's take the case when the order parameter is a complex scalar field. A very well known example is that of superconductivity. In this case the order parameter is related to the wavefunction of cooper pairs which vanishes above the critical temperature and is non-zero below the critical temperature. The potential is of the form

$$V = b(\phi^* \phi) + c(\phi^* \phi)^2. \quad (2.10)$$

Again one asks for the minima of the potential and finds that  $|\phi| = 0$  and  $|\phi| =$

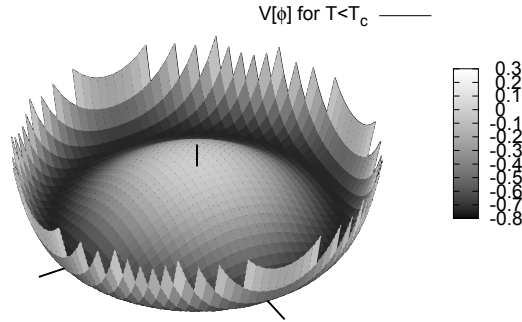


Figure 2.2: Free energy plot for complex scalar field.

$(-b/c)^{1/2}$ . With the same reasoning as above we conclude that above  $T_c$ ,  $b > 0$  with minima at  $|\phi| = 0$  while below  $T_c$  the minimum of the potential is  $|\phi| = (-b/c)^{1/2}$  with  $b < 0$ . The parameter  $b$  is then phenomenologically fixed to be  $b_0(T - T_c)$  as in the case above. Again in the low temperature phase, the symmetry is spontaneously broken but now only the magnitude of order parameter is fixed. The phase of the order parameter can be arbitrary (full  $2\pi$  rotations are allowed). This is an example of order parameter having continuous symmetry. Fig. 2.2 gives the free energy plot for the complex scalar field. Another example of order parameter enjoying continuous symmetry would be the Heisenberg magnet where the magnetization has  $3 - D$  rotational symmetry as it is a vector in a  $3 - D$  space. With the above examples in place, we are set to define the order parameter space as follows:

*An order parameter space is a set of all the allowed values of the order parameter in a given phase of the system.*

The Ising magnetization is an example of the discrete order parameter space, where order parameter space is  $S = \{-m_0, +m_0\}$ . In case of superconductivity the phase of the wavefunction can have full  $2\pi$  rotation hence the order parameter space is circle  $S^1$ . For the Heisenberg magnet the order parameter space is the surface of 2- sphere.

In particle physics, the role of order parameter and order parameter space is played by some scalar field (like Higgs field for the electro-weak phase transition) and the vacuum manifold respectively. The celebrated examples of spontaneous symmetry breaking in particle physics are Chiral symmetry breaking (where the Chiral symmetry of QCD is broken spontaneously), Electro-weak symmetry breaking and GUT symmetry breaking. A very important feature of the continuous symmetry breaking phase transition is the existence of Goldstone modes. However, we are interested in the confinement deconfinement phase transition which, as we shall see in section 2.2, is also associated with a spontaneous symmetry breaking pattern albeit a discrete one. Goldstone modes (or bosons as they are termed in particle physics) are not present in the discrete symmetry breaking, so we'll avoid a discussion of this aspect of symmetry breaking here.

However before we move ahead and look at the confinement-deconfinement transition, we'll define a very useful notion of the order parameter space in terms of the coset space.

### **2.1.3 Order Parameter Space as Coset Space**

As we discussed in section 2.1.2, a phase transition is generally accompanied by a change in the symmetry properties of the ground state. The symmetry of the system, or more specifically Hamiltonian, are captured by a suitable symmetry group  $G$ . In most of the cases,  $G$  is a Lie group. After the phase transition, the symmetry of the ground state or equivalently that of the order parameter are described by a smaller group  $H \subset G$ . The order parameter is invariant under the action of  $H$ . This is called the *isotropy subgroup* of order parameter. Consider a special case where  $H$  is just identity. Then each element of  $G$  will take the order parameter to a new point

in the order parameter space. Then,  $G$  can be completely identified with the order parameter space. However if there is some symmetry operation which leaves the order parameter invariant i.e.  $H$  is not identity, then order parameter will remain invariant under the action of  $H \subset G$ . Under the action of any other element  $g \in G$ , which is not in  $H$ , the order parameter will go to some other point in the order parameter space. The set  $gH$  is called the coset of  $H$ . For a given  $g \in G$  it gives a unique value of the order parameter. If we make a collection of all such sets it will form a space of all possible values of the order parameter. Such a space is called Coset space,  $G/H$ , of  $H$  which is the order parameter space or the vacuum manifold of the system. Hence,

If  $G$  is the symmetry group of the Hamiltonian and  $H$  is the isotropy subgroup of order parameter, then the order parameter space is given by the coset space  $G/H$ .

The above correspondence can be proved in full mathematical rigor [48]. However, we'll refrain from any such exercise and will now discuss some examples to illustrate the concept of coset space as the order parameter space.

**Examples:-**

- **2-D Spins:-** The order parameter is a vector in a plane. The symmetry group is therefore  $SO(2)$ , which is the rotation group in  $2 - D$ . In a plane, the vector is left invariant under the operation of identity only. Hence, the order parameter space is  $S = S^1$ .
- **3-D Spins:-**The order parameter is a vector in  $3 - D$ . Then the full rotation group  $SO(3)$  is the symmetry group. Now the vector can be left invariant by the rotation with the direction of vector as the axis. Hence,  $H = SO(2)$ . The order parameter space is then  $S = SO(3)/SO(2)$  which is a 2 sphere ( $S^2$ ).
- **Superfluidity of  $^4He$ :-** The order parameter is the wavefunction which is a complex scalar field. The symmetry group is the phase rotation which is  $U(1)$ . Since the isotropy subgroup is identity, the order parameter space is  $S = U(1) \equiv S^1$ .
- **Quark Gluon Plasma:-** As we shall see in the subsequent sections, the order parameter associated with the confinement deconfinement transition has  $Z(3)$  as

the symmetry group which spontaneously breaks in the QGP phase. The order parameter space is also  $Z(3)$  since, the symmetry group of order parameter space consists of only identity element. This is an example of disconnected order parameter space.

## 2.2 Confinement-Deconfinement Phase Transition

In this section we'll discuss confinement-deconfinement phase transition in a bit detail. We start by writing the order parameter (which is known as the Polyakov Loop) to label the confined and deconfined phases of QCD. By looking at its symmetry we then argue that the change in the phase of the system is associated with the change in the symmetry transformation property of the order parameter. We then look at the effective potential constructed for this order parameter. In the present discussion we keep ourselves confined to only the pure gauge theory. The effect of quarks is discussed in chapter 5. We follow ref. [49] in the following discussion.

### 2.2.1 Polyakov Loop Order Parameter

Consider  $SU(N)$  theory at finite temperature *without* dynamical quarks. Let us denote the states by  $|s_G\rangle$ . The partition function of the system is then written as

$$\mathcal{Z} = e^{-\beta F} = \sum_{s_G} \langle s_G | e^{-\beta H} | s_G \rangle \quad (2.11)$$

To figure out if the system is in confined phase or not we use an infinitely heavy test quark, placed at position  $\vec{x}_0$ , as a probe. The test quark is considered to be infinitely heavy and hence it's static. As a result there is no back-reaction of this quark on the system. In the presence of test quark the state of the system is not  $|s_G\rangle$  anymore. We denote it by  $|s\rangle = \psi_a^\dagger(\vec{x}_0, 0)|s_G\rangle$ . Here we have introduced the field operators  $\psi_a^\dagger(\vec{x}_0, t)$  which create a quark with color  $a$  at position  $\vec{x}_0$  and time  $t$ . These operator fields satisfy the anti commutation relations

$$\{\psi_a(\vec{x}_1, t), \psi_b^\dagger(\vec{x}_2, t)\} = \delta_{ab} \delta^3(\vec{x}_1 - \vec{x}_2) \quad (2.12)$$

Then the partition function is

$$\begin{aligned}\mathcal{Z}_q &= e^{-\beta F(\vec{x}_0)} = \frac{1}{N} \sum_s \langle s | e^{-\beta H} | s \rangle \\ &= \frac{1}{N} \sum_{s_G} \langle s_G | \sum_a \psi_a(\vec{x}_0, 0) e^{-\beta H} \psi_a^\dagger(\vec{x}_0, 0) | s_G \rangle,\end{aligned}\tag{2.13}$$

where  $N$  is the number of colors.  $N = 3$  for QCD. Thus the sum over  $N$  is on the all possible color states. Now just like the operator  $e^{-iHt}$  generated the time translation in Minkowski time,  $e^{-\beta H}$  generates the time translation in Euclidean space. Thus

$$e^{\beta H} \psi_a(\vec{x}_0, 0) e^{-\beta H} = \psi_a(\vec{x}_0, \beta),\tag{2.14a}$$

$$\Rightarrow \mathcal{Z}_q = \frac{1}{N} \sum_{s_G} \langle s_G | \sum_a e^{-\beta H} \psi_a(\vec{x}_0, \beta) \psi_a^\dagger(\vec{x}_0, 0) | s_G \rangle\tag{2.14b}$$

The (Euclidean) time evolution of the wavefunction is given by Dirac eq in Euclidean space.

$$(-i\partial_0 \delta^{ab} - g A_0^{ab}(\vec{x}_0, \tau)) \psi_b(\vec{x}_0, \tau) = 0\tag{2.15}$$

where  $A_0 = A_0^i \lambda_i$ , with  $\lambda_i$  being the Gell-Mann matrices. This gives the solution as

$$\psi_a(\vec{x}_0, \beta) = \mathbf{P} \left[ \exp \left( ig \int_0^{\tau=\beta} d\tau A_0(\vec{x}_0, \tau) \right) \right]_{ab} \psi_b(\vec{x}_0, 0)\tag{2.16}$$

where  $\mathbf{P}$  denotes path ordering. We see that the time evolved field is related to the initial field by an overall phase. This overall phase is the non-abelian analogue of Bohm-Arhanov phase and is called the Wilson line. In the Euclidean space, due to the periodicity in time direction, it is a loop. The trace of this quantity over all color degree of freedom is known as Polyakov Loop. It is defined as

$$L(\vec{x}) = \frac{1}{N} \text{Tr} \left\{ \mathbf{P} \left[ \exp \left( ig \int_0^{\tau=\beta} d\tau A_0(\vec{x}_0, \tau) \right) \right] \right\}\tag{2.17}$$

Using eq. (2.16) and eq. (2.17) in eq. (2.14) we get

$$\mathcal{Z}_q = \sum_{s_G} \langle s_G | e^{-\beta H} L(\vec{x}) | s_G \rangle.\tag{2.18}$$

On dividing by the partition function of the pure glue system, we get the change in the free energy of the system as

$$\frac{\mathcal{Z}_q}{\mathcal{Z}} \equiv e^{-\beta \Delta F} = \langle L(\vec{x}) \rangle\tag{2.19}$$

Since the test quark is static and infinitely heavy, the free energy of a single quark doesn't make much sense. However, if we consider a quark and an anti-quark at positions  $\vec{x}$  and  $\vec{y}$  respectively, then one can look at the free energy of the system as the function of the distance between the quark and the anti-quark. Thus,

$$\langle L^\dagger(\vec{y})L(\vec{x}) \rangle \propto e^{-\beta F_{q\bar{q}}}. \quad (2.20)$$

Far away from the critical region, the fields are uncorrelated at the distance larger than the correlation length. Thus  $\langle L^\dagger(\vec{y})L(\vec{x}) \rangle \longrightarrow \langle L^\dagger(\vec{y}) \rangle \langle L(\vec{x}) \rangle = |\langle L(\vec{x}) \rangle|^2$ . Eq. (2.20) then becomes

$$\langle L^\dagger(\vec{y})L(\vec{x}) \rangle = |\langle L(\vec{x}) \rangle|^2 \propto e^{-\beta F_{q\bar{q}}}. \quad (2.21)$$

Now in the confining phase, the free energy required to separate a quark from an anti quark is infinite. Thus  $F_{q\bar{q}} \rightarrow \infty$ , implying that  $\langle L(x) \rangle = 0$  in the confining phase. In the deconfined phase,  $F_{q\bar{q}}$  is finite, hence  $\langle L(x) \rangle$  is finite in the deconfined phase. Thus Polyakov loop is an order parameter and can be used to distinguish between different phases of the system. In the high temperature limit eq. (2.21) tells us that  $|\langle L(\vec{x}) \rangle| \rightarrow 1$ .

## 2.2.2 Spontaneous Breaking of $Z(3)$ Symmetry

Let's now look at the symmetry properties of the order parameter. By construction, the Lagrangian (and hence the action) of QCD (with or without quarks) is invariant under any arbitrary  $SU(3)$  transformation. Let  $U(x, \tau) \in SU(3)$  be the transformation. Then the gauge fields transform as

$$A_\mu(x, \tau) \longrightarrow A'_\mu(x, \tau) = U(x, \tau)A_\mu(x, \tau)U(x, \tau)^{-1} + iU(x, \tau)\partial_\mu U(x, \tau)^{-1} \quad (2.22)$$

and the Polyakov Loop transforms as

$$L(\vec{x}) \longrightarrow L(\vec{x})' = \frac{1}{N} \text{Tr} \left\{ U(x, \beta) \mathbf{P} \left[ \exp \left( ig \int_0^{\tau=\beta} d\tau A_0(\vec{x}_0, \tau) \right) \right] U(x, 0) \right\} \quad (2.23)$$

As discussed in section 1.3.1, the gauge fields should be periodic in the direction of Euclidean time. Thus, only those transformation are allowed that conserve the periodic boundary conditions of the gauge fields. Thus with  $A_\mu(x, 0) = A_\mu(x, \beta)$ , if  $U(x, \beta) = U(x, 0)$ , then eq. (2.22) tells us that  $A'_\mu(x, \beta) = A'_\mu(x, 0)$ . Under these

transformations, eq. (2.23) tells us that the Polyakov Loop remains invariant due to the cyclic property of the trace. However, a more general set of transformations remain. If we consider  $U(x, \beta) = ZU(x, 0)$  such that  $Z \in SU(N)$ , commutes with all the  $SU(N)$  matrices and is space-time independent, then also the periodicity condition on the gauge fields is satisfied. By definition, the set of all such elements  $Z$ , is called the center group of  $SU(N)$  denoted by  $Z(N)$ . The elements of  $Z(N)$  are

$$Z = e^{i\phi} \mathbf{1}; \quad \phi = 2\pi m/N; \quad m = 0, 1 \dots (N - 1) \quad (2.24)$$

Under the  $Z(N)$  transformations, the fields remain periodic and the action is also invariant. However, the Polyakov loop picks up an extra phase and is no longer invariant under these transformations. Using  $U(x, \beta) = ZU(x, 0)$  in eq. (2.23) we get

$$L(\vec{x}) \longrightarrow ZL(\vec{x}). \quad (2.25)$$

For the case of QCD,  $N = 3$  and hence the Polyakov loop transforms in eq. (2.25) under  $Z(3)$ . Thus  $\langle L(\vec{x}) \rangle \longrightarrow Z\langle L(\vec{x}) \rangle$ . In the confining phase,  $\langle L(\vec{x}) \rangle$  doesn't change (since  $\langle L(\vec{x}) \rangle = 0$  in that phase). However, in the deconfined phase  $\langle L(\vec{x}) \rangle \neq 0$ , thus it is *not* invariant under  $Z(3)$  transformations. Thus there are 3 equivalent phases in the high temperature phase, or the deconfined (QGP) phase viz  $\langle L(\vec{x}) \rangle$ ,  $Z\langle L(\vec{x}) \rangle$  and  $Z^2\langle L(\vec{x}) \rangle$ . Thus the  $Z(3)$  symmetry is spontaneously broken in the QGP or the high temperature phase but it's restored in the low temperature or the confined phase. This is in contrast to usual situations where the symmetry is restored in the high temperature phase.

### 2.2.3 Results from Lattice QCD

As discussed in section 1.3.1, once we know the partition function various thermodynamic quantities can be calculated. The thermal expectation value of Polyakov loop can then also be calculated, in principle. In general, if  $\hat{\mathcal{O}}$  is an operator, the its thermal expectation value,  $\langle \hat{\mathcal{O}} \rangle$ , is

$$\langle \hat{\mathcal{O}} \rangle = \frac{\int \mathcal{D}A_\mu(x, \tau) \mathcal{D}\psi(x, \tau) \mathcal{D}\bar{\psi}(x, \tau) \hat{\mathcal{O}}[A_\mu, \psi, \bar{\psi}] e^{-\mathcal{S}_E}}{\int \mathcal{D}A_\mu(x, \tau) \mathcal{D}\psi(x, \tau) \mathcal{D}\bar{\psi}(x, \tau) e^{-\mathcal{S}_E}}, \quad (2.26)$$

where  $\mathcal{S}_E$  is the Euclidean Action. The path integral over the fermionic fields can be exactly evaluated and it results in an infinite dimensional determinant over all space-time points.

However, the calculation involves path integral calculation of interacting fields and it is not possible to carry out analytically. *Lattice QCD* refers to an algorithm to numerically evaluate this path integral. It requires discretizing space and time into  $N_s^3$  space lattice points and  $N_\tau$  lattice points in time direction. One then evaluate the  $N_s^3 \times N_\tau$  dimensional fermion determinant (which appears in the path integral) and then integrates all the gluons. The integrals are performed by Monte Carlo integration. This method works well as long as the fermion determinant is positive. This is the case for the system with zero chemical potential. It describes a quark-gluon plasma with vanishing net baryon density, which is the situation in the Early Universe. Heavy-ion collisions experiments, where heavy nuclei are brought into the collisions, involve systems with non-zero net baryon number. This requires a non-zero baryon chemical potential which enters into the fermion determinant with a factor  $i$ .

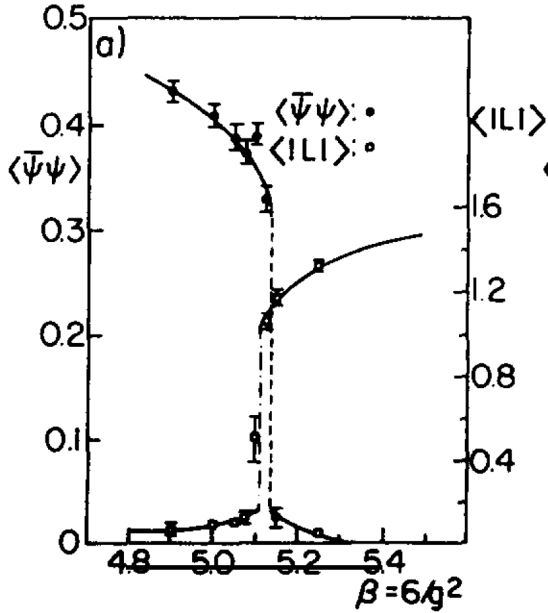


Figure 2.3: Lattice results showing the variation of Polyakov Loop (for a pure glue theory) and the Chiral order parameter [50].

The resulting “sign problem” has been a major block for lattice QCD at finite net baryon density, and only recently significant progress was made, resulting in first lattice QCD results for the hadronization phase transition in a quark-gluon plasma with nonzero baryon chemical potential, see [18] and references therein. The quantities which are generally of interest while studying the QCD phase transition on lattice are the expectation values of energy density, Polyakov Loop and the Chiral condensate. Chiral condensate is the order parameter for the Chiral phase transition. We’ll not discuss the Chiral phase transition in detail here and our focus here will be on the confinement deconfinement transition. An important factor is the mass of quarks.

In the infinite quark mass limit (used in the definition of Polyakov Loop), QCD has

a first order deconfining phase transition, while in the limit of quark masses going to zero there is a first order Chiral phase transition. Figure 2.3 shows the variation of Polyakov Loop and that of the Chiral condensate as function of temperature [50]. The sudden change in the value of order parameters indicates a first order phase transition. It is interesting to note that the Chiral order parameter and the Polyakov loop order parameter experience the sudden jump around the same value of  $\beta$ , indicating that both the confinement-deconfinement and the Chiral phase transition happen almost simultaneously. This is not surprising, as in the QGP phase quarks are free and are no more confined within the hadrons. Thus it looks natural that they lose their constituent mass and become light in the QGP phase, thus restoring the Chiral symmetry.

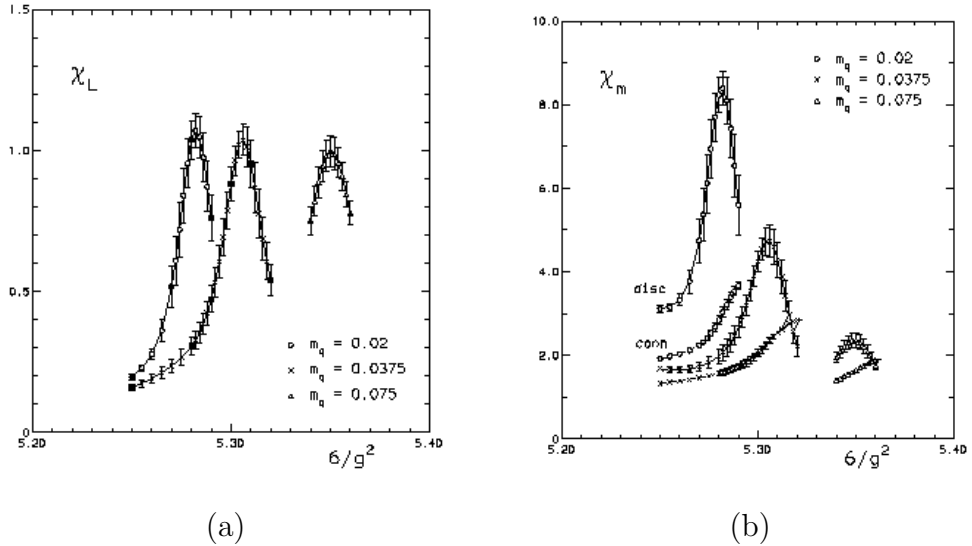


Figure 2.4: Lattice results for QCD with quarks. (a): Variation of Polyakov Loop susceptibility as a function of  $\beta$  for 3 different quark mass. (b): Chiral susceptibility as function of  $\beta$  for 3 different quark mass [51].

Another important thing is that for QCD with quarks having physical mass, the Polyakov loop and Chiral condensate are not exact order parameters. They are mere indicators of phase transitions, if any. Figure 2.4 gives the lattice results for the order parameters and associated susceptibilities [51]. As the calculations with realistic masses of light quarks ( $u, d$ ) are not yet available, the calculations are repeated for several unrealistically large masses. They are then extrapolated to zero mass. The

perfect coincidence of the peaks in the chiral and Polyakov loop susceptibilities is seen for all quark masses and thus expected to survive in the chiral limit [51]. In fig. (2.4),  $m_q$  denotes the quark mass in the units of lattice spacing  $a$ .

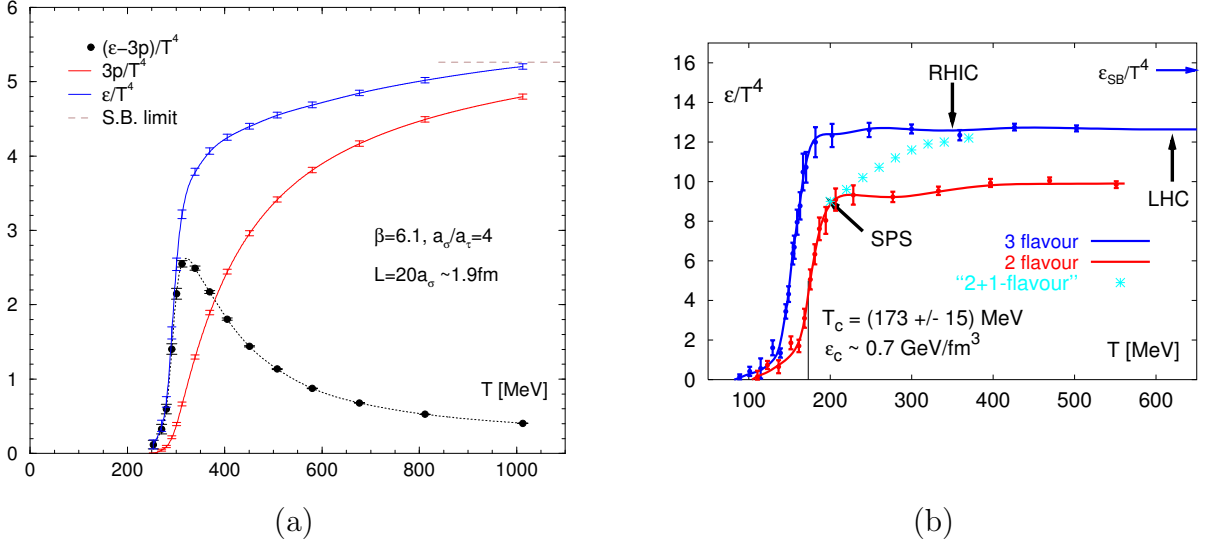


Figure 2.5: (a): Lattice results showing the variation of energy density for pure QCD. [52] (b): Results for QCD with quarks. [53]

The first order phase transition is associated with latent heat. Figure (2.5a) shows the energy density plot along with the pressure and the interaction measure (in the units of  $T^4$ ) for the pure QCD [52]. The sharp increase in the energy density around the critical temperature indicates the first order phase transition. For the case of QCD with quarks, the variation is smoother and depends on the number of massless quarks, fig. (2.5b) [53]. For the case of 3 massless quarks the energy density is higher than the case of 2 massless quarks as expected. For the case with 2 light flavors and one heavy flavor, the energy density has the same value as in the case of the two light flavors for  $T < T_c$ , then goes to the values as in the case three light flavors for  $T > T_c$ . The explanation of this can be found in the liberation of a large number of gluons during the deconfinement transition. These gluons can produce extra quark-antiquark pairs and drive the system towards chemical equilibrium among quarks, antiquarks and gluons. The restoration of chiral symmetry above the critical temperature makes the quarks light and lowers the quark anti-quark pair production threshold. Now as the strange quark has a very high constituent mass but low current mass ( $m_s \sim T_c$ ), the

thermal processes will most probably lead to the large production of strange quarks and the system has the energy density as for the case of three light quarks above  $T_c$ .

As it is clear from the above figures, inclusion of quarks with physical masses makes the variation of the order parameter and the energy density smoother. It is now believed that the confinement-deconfinement transition is a crossover at physical quark masses. The same is true for the Chiral transition at low chemical potential and small quark masses (see [18] and references therein).

## 2.2.4 Effective Potential for Polyakov Loop

Once we have the order parameter and certain expectations from the lattice calculations, we can now try to construct the effective potential using the order parameter. The form of the effective potential is dictated by the symmetries of order parameter. At high temperature, the Polyakov Loop is almost unity and thus, it can be expanded in the power series of  $A_0$ . In that case, one can trade off Polyakov loop with  $A_0$  and construct an effective potential for  $A_0$ . However, this is not the case at low temperatures. Again, we begin with the discussion with the pure glue theory and later on discuss the case with the inclusion of quarks. The discussion here is along the lines of [54, 55].

Before we start, let's set out the notations in order. First we'll suppress the vector indices on  $\vec{x}$ . From now on we'll reserve  $L(x)$  for the quantity given by eq. (2.17). For the thermal expectation of Polyakov loop, we'll use the symbol  $l(x)$ , while the thermal Wilson Loop (the trace of which gives Polyakov loop) will be denoted by  $\mathbf{L}(x)$ . Since the Wilson line is a  $SU(N)$  matrix, it satisfies the following constraints

$$\mathbf{L}(x)^\dagger \mathbf{L}(x) = \mathbf{1}, \quad \det(\mathbf{L}(x)) = 1. \quad (2.27)$$

Let's start by looking at the mass terms of the effective potential. The above constraints imply that there are many more terms other than the  $\text{tr}\mathbf{L}(x)$ , like  $\text{tr}\mathbf{L}^p(x)$ , where  $p = 1, \dots, (N - 1)$ . Mathematically, these terms are related to the Polyakov loop in higher representations. Following [55], we define the traceless part of  $\mathbf{L}(x)$  as:

$$\tilde{\mathbf{L}}(x) = \mathbf{L}(x) - L(x)\mathbf{1}. \quad (2.28)$$

Then under  $Z(N)$  transformations,  $\text{tr}\tilde{\mathbf{L}}^p(x)$  transforms as  $e^{ip\phi}\tilde{\mathbf{L}}^p(x)$ . We denote it by  $L_p(x)$ . This is termed as the Polyakov loop of charge  $p$ . Now the mass terms in

the effective Lagrangian are:

$$\mathcal{L}_1^{eff} = m_1^2 |L(x)|^2 + m_2^2 |L_2(x)|^2 + \dots \quad (2.29)$$

The simplest assumption is that for  $T > T_c$ ,  $m_1 < 0$ , while  $m_1 > 0$  for  $T < T_c$  and rest of the  $m_i > 0$  at all temperatures. As a result, it's the Polyakov loop of charge 1 which controls the critical behavior, as discussed in section 2.1.2. In that case the vacuum after symmetry breaking is given by the maximum of  $|\text{tr}\mathbf{L}(x)|^2$ . This is possible if  $\langle \mathbf{L}(\mathbf{x}) \rangle$  is a constant times the identity matrix. This choice is readily available by the use of global  $SU(N)$  rotations. The constant is the center of  $SU(N)$ . Thus,

$$\langle \mathbf{L}(\mathbf{x}) \rangle = Z l(x) \mathbf{1}, \quad (2.30)$$

where  $Z$  is the element of the center of the  $SU(N)$  group, given by eq. (2.24). For this expectation value, the vacuum respects the (global)  $SU(N)$  above  $T_c$ . The negative  $m_1$  for  $T > T_c$  also finds support from the perturbative calculations (valid at very high temperatures). As discussed above, at high temperatures one can use the effective potential for  $A_0$ . This has been calculated up-to fourth order at one loop. Comparing the effective potential for  $\mathbf{L}(x)$  by expanding in terms of  $A_0$  one finds that the coefficient of  $|\text{tr}\mathbf{L}(x)|^2$  is negative (since  $\mathbf{L}(x) \sim -g^2 A_0^2$ , a positive mass term in  $A_0$  effective potential will correspond to a negative mass of the Polyakov loop) [54].

Since it's the condensation of  $L(x)$  which governs the phase transition, we will not consider the operators of the form  $\text{tr}\mathbf{L}^p(x)$  with  $p > 1$ . Other than the mass term various other terms can be added to the potential, the simplest being (for  $N = 3$ ):

$$(\text{tr}\mathbf{L}(x))^3 + c.c.; \text{ and } |(\text{tr}\mathbf{L}(x))|^4 \quad (2.31)$$

We now discuss the possible form of the kinetic terms. We start by coupling the static vector gauge potentials  $A_i(x)$ 's to the Wilson line. In the continuum limit of the lattice model as given by Banks and Ukawa [56], the kinetic term can be written as

$$\mathcal{L}_{kin} = \frac{1}{2} (G_{ij}^2) + c \text{tr}|D_i\mathbf{L}(x)|T^2, \quad c = \frac{1}{g^2} + \dots \quad (2.32)$$

The first term is the standard gauge potential Lagrangian. The second term gives the coupling of gauge potential to the Wilson line. An important thing to note is

the factor of  $T^2$ . Since Wilson line is just a phase factor, the dimensions can only be made up by the powers of  $T$ . Other than these terms there are other terms available too, but we keep ourselves confined to the simplest possible terms.

To construct the effective theory (as in section 2.1.1) we need to define a mean field obtained by averaging over some region of space. This can be done by introducing a “spin”  $\mathbf{W}(x)$  at point  $x$  by performing a gauge covariant sum of Wilson line  $\mathbf{L}(x)$  over some region of space around point  $x$  [54]. Since the sum of two unitary matrix need not be unitary, this average  $\mathbf{W}(x)$  is just a complex  $N \times N$  matrix. Writing the  $\mathbf{W}(x)$  as sum of its diagonal and non diagonal components we get

$$\mathbf{W}(x) = l(x)\mathbf{1} + 2i\tilde{l}_a(x)t^a, \quad (2.33)$$

where  $t^a$  are the generators of  $SU(N)$  and  $l(x)$ ,  $\tilde{l}_a(x)$  are complex valued fields. The color singlet field,  $l(x)$ , is called the  $Z(N)$  spin while the color adjoint field,  $\tilde{l}_a(x)$ , is called the  $SU(N)$  spin. It can be argued that whatever be the order of the deconfining phase transition, one can write a mean field theory in which the deconfinement transition is controlled by a potential for  $Z(N)$  spins [54]. For  $N = 3$  the Lagrangian is:

$$\mathcal{L} = \frac{c}{g^2}|\partial_i l|^2 T^2 + (-b_2|l|^2 + b_3(l^3 + (l^*)^3) + |l|^4) b_4 T^4. \quad (2.34)$$

The kinetic term is just the  $Z(N)$  spin part obtained by using eq. (2.33) in eq. (2.32). The potential is novel in the sense that the dimensions are made up by the factor  $T^4$ . In the mean field theory,  $b_4$  is taken as constant and  $b_2$  varies with temperature. For  $b_3 \neq 0$ , the  $Z(3)$  symmetry is broken. These parameters are fitted in ref. [57–59] such that that the effective potential reproduces the thermodynamics of pure  $SU(3)$  gauge theory on lattice [60, 61]. The coefficients are  $b_2 = (1 - 1.11/x)(1 + 0.265/x)^2(1 + 0.300/x)^3 - 0.478$ , (with  $x = T/T_c$  and  $T_c \sim 182$  MeV),  $b_3 = 2.0$  and  $b_4 = 0.6061 \times 47.5/16$ . With these values,  $l(x) \rightarrow y = b_3/2 + \frac{1}{2} \times \sqrt{b_3^2 + 4b_2(T = \infty)}$  as  $T \rightarrow \infty$ . Various quantities are then rescaled such that  $l(x) \rightarrow 1$  as  $T \rightarrow \infty$ . The scaling are

$$l(x) \rightarrow \frac{l(x)}{y}, \quad b_2 \rightarrow \frac{b_2}{y^2}, \quad b_3 \rightarrow \frac{b_3}{y}, \quad b_4 \rightarrow b_4 y^4. \quad (2.35)$$

At low temperature where  $l = 0$ , the potential has only one minimum. For temperatures higher than  $T_c$ ,  $l(x)$  develops a non vanishing vacuum expectation value  $l_0$ ,

and the cubic term above leads to  $Z(3)$  degenerate vacua. In the above discussion we have assumed that it's possible to extract renormalized Polyakov loop from the bare loop. A detailed discussion on this important issue can be found in [62].

## 2.3 Topological Defects

The above discussion of free energy and the symmetry of order parameter is in “field space”. How does this correspond to the order parameter configurations in the real space? To understand this correspondence it's instructive to first understand the process of symmetry breaking during a phase transition. Kibble [63] first proposed that the formation of various non-trivial field configurations, in context of early universe, can be understood as the consequence of formation of domain structures during phase transitions. We'll now look at this argument in a bit more detail. Kibble mechanism has been verified in certain condensed matter systems.

### 2.3.1 Kibble Mechanism

The crux of Kibble's argument is that the order parameter field can only be correlated over the correlation length of the system. In case of early universe, the correlation length has the upper limit of horizon size of the universe at a given time. As the length scales above the horizon size are causally disconnected, there cannot be any correlation between the order parameter field over those length scales. In case of condensed matter systems with first order phase transition, the horizon size is replaced by the average bubble size of ordered phase nucleated in the background of disordered phase. In systems with second order phase transition the average domains size is again the correlation length. Within a domain the order parameter takes one of the values from the order parameter space. In a different domain the order parameter can take some other value.

In between two such domains, the order parameter varies, so system tends to lower it's free energy as a result the gradients of the order parameter are minimized. The variation of the order parameter in the intermediate region is governed by the geodesic rule which states that the order parameter traces the shortest path on the vacuum manifold to minimize the gradients. For example, in case of planar spins

the orientation of the spin  $\theta$  can take different values in different domains. Near the interface of domains the system does minimize the gradients in the local region such that the variation of order parameter at the interface is governed by geodesic rule.

Sometimes at the intersection of these domains, a non trivial configuration of order parameter can exist. A typical example would be the interface between the domains with magnetization  $m_0$  and  $-m_0$ , in a  $1 - D$  Ising model. It is not possible to remove this *defect* by locally changing the spin orientations. One needs to modify the entire system to get rid of the interface. Such configurations are called *topological defects*. These are different from the “normal” defects in the sense that the normal defects can be removed by the local modifications in the systems We’ll discuss some examples of these configurations next and discuss the formal aspects of such non-trivial field configurations afterwards.

### 2.3.2 Types of Topological Defects

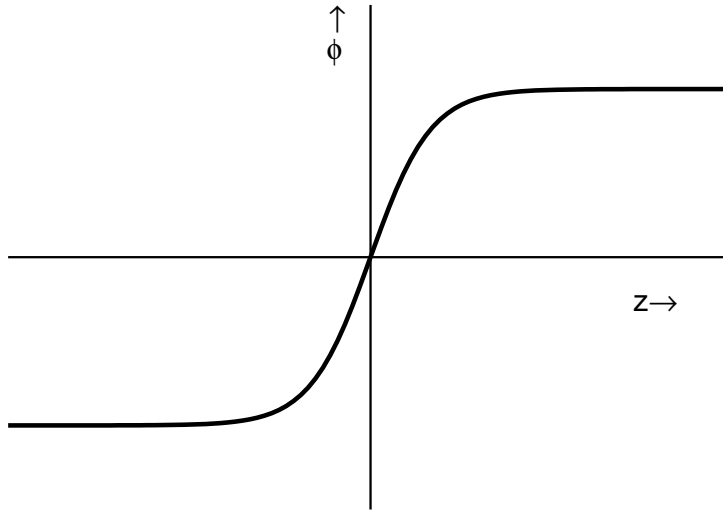


Figure 2.6: The domain wall configuration.

- **Kink and Domain Walls:-** Let’s look at the example of  $1 - D$  Ising model once again. In the  $\phi - z$  plot, the magnetization is  $-m_0$  on the far left, while  $+m_0$  on the far right. Also  $\phi$  needs to vary continuously from  $-m_0$  to  $+m_0$ ,

else the free energy will be infinite. This would mean that  $\phi$  must pass through zero as it goes from far left to far right. This is called a kink (fig. 2.6).

In 3 dimensions, this leads to a domain wall. These defects occur in the systems where order parameter space has disconnected sectors (eg. a point set). It is interesting to note that at  $m = 0$  the free energy is maximum. Thus the system has an energetically unstable region even below  $T_c$ . However this configuration is topologically stable i.e. it cannot be removed by local fluctuations.

- Vortices or Point Defects:-** Now we take the example of  $2 - D$  planar spins. The order parameter space is all orientations ( $\theta$ ) of the planar spin, hence it is  $(S^1)$ . Let's take a point  $P$  (fig. 2.7) and traverse a circle, centered at  $P$ , at some large  $r$ . Then as order parameter changes on the circle,  $\theta$  varies in order parameter space. Then if  $\theta = 2\pi n$  where  $n$  is a non zero integer then the spin must rotate by the angle  $2\pi n$  in the real space. If we shrink the circle continuously and approach point  $P$ , then we find that  $\theta$  is singular at point  $P$ . Only possibility is that the order parameter is zero at the center. It

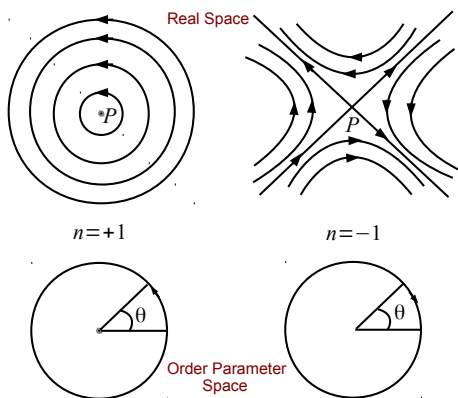


Figure 2.7: Magnetization in real space.

is important to note that the peculiar nature of the order parameter at point  $P$  could be determined at arbitrary large distance from  $P$ . Hence, we can not remove the singularity by local modifications. Again the only condition was that of the continuity of the order parameter. This type of defect is known as Point defect (Vortex) of winding number  $n$ . In fig. 2.7, there are two defects, one

with winding number  $+1$  signifying counter-clockwise rotation (called defect) while  $n = -1$  signifies clockwise rotation and it called an anti-defect.

- **Line Defects or Strings:-** A 3-D space can be viewed as an infinite stack of plane sheets. Then as one goes from one planar sheet to another, the singularity discussed above is an extended object in 3-D space. This is the line defect or the string defect. The string are characterized in the same manner as the Vortices, except that they are in 3 dimension. They are also labeled by their winding number which is calculated by encircling the line along a closed path. An example is strings in superfluid helium.

## 2.4 Homotopy Groups

Let's again go back to our favorite example of  $2 - D$  planar spins. Consider a field configuration on a circle in a real space. There is nothing particular about a circle, any closed curve in  $2 - D$  will be fine. Both are topologically equivalent. The allowed orientations of spin are from zero to  $2\pi$ , so the order parameter space is also a circle. Consider mapping of the spin orientation in  $2 - D$  plane to the order parameter space. The mapping is defined in the following manner. Let's choose a reference direction in the  $2 - D$  plane (say x-axis). Measure the angle  $\theta$  which spin vector makes with respect to the reference direction. The corresponding point on the order parameter space is the point on the circle which makes the angle  $\theta$  with the x-axis.

Fig. (2.8) shows the configurations of field in the real space on the left while the corresponding loop in the order parameter space, using the map defined above, is shown on the right. The top figure in (2.8) is a uniform field configuration and it corresponds to a point in the order parameter space. The second figure has a non uniform field configuration in real space on right. The corresponding loop in the order parameter space is shown on the left. The loop in the order parameter space doesn't complete the full  $2\pi$  rotation and it can be continuously shrunk to a point. Hence, the top two configurations actually correspond to only one point in the order parameter. In other words, we have continuously deformed the two mappings into each other. These configurations have winding number zero and hence they don't correspond to any topological defect (vortices).

Two mappings of a given space to another space are said to be *homotopic* if they can be continuously deformed to one another. The deformation is called *Homotopy*.

In the third figure we note that as we complete two loops in the real space, we complete two loops in the order parameter space. This is an example of a vortex with winding number 2. It is clear that this loop cannot be shrunk continuously to a point. Hence,  $n = 0$  and  $n = 2$  are not topologically equivalent configuration or they are not homotopic. It can be shown that all the configuration of same winding number are homotopic to each other i.e. one configuration can be continuously deformed to obtain the other configuration.

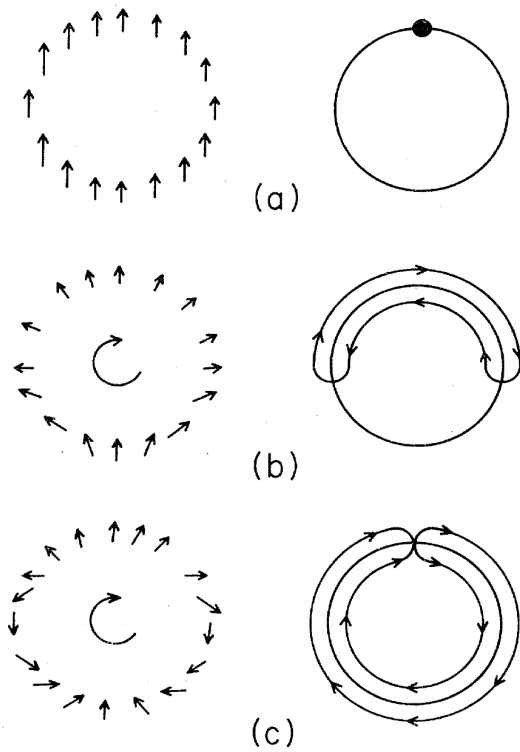


Figure 2.8: Right: Magnetization in real space. Left: Mapping to order parameter space. From [48]

From the above discussion we conclude that we can separate the singularities in separate classes labeled by their winding number. These *Homotopy classes* form a group known as the *fundamental group* or the *first Homotopy group* and is denoted by  $\pi_1(S)$ . One can take this notion of Homotopy group and generalize it to a mapping of the  $n$ -dimensional sphere to the order parameter space. The Homotopy group thus obtained is known as  $n^{th}$  Homotopy group, denoted by  $\pi_n(S)$ . For the classification of topological defects one needs to calculate various Homotopy groups for a given order parameter space. For the existence of topological defects it is necessary that the  $n^{th}$  Homotopy group is non-trivial. We will skip that discussion as it requires a pretty detailed discussion on Homotopy theory.

**Examples:-** Below are  $\pi_n(S)$  for the examples discussed in 2.1.3

- **2-D Spins:-** The order parameter space is  $S = S^1$ . The fundamental group is  $\pi_1(S) = Z$ , the set of integers. Hence, there are point like defects or vortices.
- **3-D Spins:-** The order parameter space is  $S = SO(3)/SO(2)$  which is a 2 sphere ( $S^2$ ). The fundamental group is trivial i.e.  $\pi_1(S^2) = 1$ , so there are no string defects. The second Homotopy group  $\pi_2(S^2) = Z$ , hence there are point like defects in 3 –  $D$  known as monopoles.
- **Superfluidity of  $^4He$ :-** The order parameter space is  $S = U(1) \equiv S^1$ . The fundamental Homotopy group is  $\pi_1(S^1) = Z$ . Hence, there are string defects.
- **Quark Gluon Plasma:-** The order parameter space is a set of disconnected points (as with Ising model), hence domain wall appear as the topological defects. At the junction of three domain walls one will have a string defect too [64]. Figure 2.9 shows the  $Z(3)$  interface and the associated string.

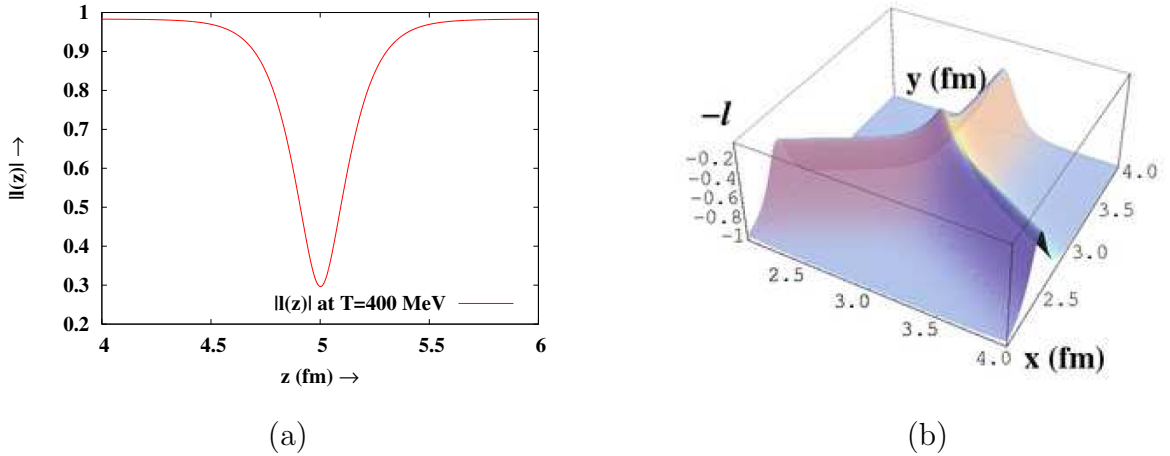


Figure 2.9: (a):Profile of Domain Wall between two  $Z(3)$  domains. (b): QGP String at the junction of three interfaces.

With this discussion of the topological defects we conclude this chapter. In the next chapter we focus our attention on to these  $Z(3)$  interfaces and look a the possibility of spontaneous CP violation from these  $Z(3)$  structures.

# Chapter 3

## CP Violation from $Z(3)$ Domains

As we discussed in chapter 2, the effective theory for the confinement deconfinement transition is associated with the spontaneous breaking of  $Z(3)$  symmetry in the QGP phase. This allows for domain walls and strings as the topological defects in the QGP phase. This assumes significance in the light of heavy ion collisions as these are then the only topological objects in the particle physics theories that can be probed by the present day accelerators. There are lattice results [65] that suggest that these domains start appearing around the temperatures  $\sim 700 \text{ MeV}$ . It would be interesting to see if the proposed upgrade of Large Hadron collider at CERN can attain such temperatures. Detailed simulations have been performed to study the evolution of these domain walls in the context of heavy ion collisions [66,67].

In this chapter we discuss an interesting property of these  $Z(3)$  domains which is the spontaneous  $CP$  violation. First we start by looking at the earlier studies of this  $CP$  violation [68,69], in section 3.1. These studies were conducted in the context of electro-weak phase transition in early universe. We present our work on the  $CP$  violation from  $Z(3)$  domains [70] in the following sections. Since the region of our interest is the confinement deconfinement transition in QCD, we will calculate the background gauge field profile using the effective potential given by eq. (2.34). This is the central theme of section 3.2.1. In sec 3.2.2 we will use another effective potential as given by Fukushima [71] to calculate the wall profile and check the schematic uncertainties. We will also discuss various conceptual issues related to our calculation of the background profile. In section 3.3, we will then calculate the

reflection of quarks and anti quarks and show that there is a  $CP$  violation in the quark scattering. We conclude this chapter with discussion in section 3.4.

### 3.1 CP Odd Metastable Vacua in Standard Model

In particle physics  $CP$  symmetry stands for Charge conjugation and Parity symmetry. It postulates that if a particle is replaced by its anti-particle ( $C$ -symmetry) and then its coordinates are mirror reflected ( $P$  symmetry), then the laws of physics do not change. In standard model of particle physics,  $CP$  symmetry is violated in the weak interactions. The source of this (small)  $CP$  violation is the mixing among different generations of quarks by Cabibbo-Kobayashi-Masakawa (CKM) matrix or by the neutrino mixing. However the amount of  $CP$  violation is very small due to these effects. There is also a possible source of  $CP$  violation coming from the so called  $\theta$ -term in QCD, arising from the instanton effects.

In ref [69] Altes *et al* discussed a possible source of spontaneous  $CP$  violation in standard model. This is due to the thermal effects the phase of Wilson line. They stressed that because quarks carry quantum number under each of the gauge group that constitute the standard model, one should not consider the effective potential for any single gauge group but that of the full gauge group  $SU(3) \times SU(2) \times U(1)$ . They generalized the calculation done by Weiss [72,73] and calculated the effective potential for the full gauge group. Since the eigenvalues are gauge invariant, they chose diagonal gauge for  $A_0$  and calculated the effective potential for the background constant field  $A_0$ . Note that this  $A_0$  is the gauge potential for the whole  $SU(2) \otimes SU(2) \otimes U(1)$  gauge group and includes the color, weak and hypercharge gauge fields. They find that the effective potential has long lived metastable minima. These minima are not  $CP$  self conjugate and as a result there is a spontaneous violation of  $CP$  symmetry.

Building on this work it was shown in [68] that during the electro weak phase transition in the early universe, the Higgs field forces the gauge potential either to be in one of the metastable vacua or to be zero. When these regions are juxtaposed together, a domain wall profile is obtained which interpolates between the true and the metastable vacua. Solving the Dirac equation in the Euclidean space, they find that the background profile localizes fermions but not the anti-fermions (and vice

versa). They then argued that the volume effects via sphaleron process then lead to a baryon asymmetry of the universe which is of the required magnitude. This is a generic feature of various models like standard model with fewer generations (which has no CKM type  $CP$  violation) and the Minimally Supersymmetric Standard Model.

In a separate work [74] it was found that such localized modes of fermions also exist in case of strong interaction alone. An important limitation of these works is that all the above studies are done at high temperature and hence perturbative analysis are used which are not trustworthy near the confinement-deconfinement transition. Another limitation was that they did not calculate the exact gauge field configuration and hence the discussion about the fermion localization was only qualitative. We take care of these limitations of the above studies by working with the effective potential for the Polyakov loop and extracting the constant background gauge field condensate from there [70]. In the following sections we present the details of our work.

## 3.2 Background Gauge Profile

We start by looking at the effective potential for the confinement-deconfinement transition (eq. 2.34). The cubic term in  $l(x)$  leads to the three degenerate vacua in the QGP phase. As a result interfaces are formed in between the three vacua. The profile of domain wall was first calculated in [64] by minimizing the total energy of the system. Fig. 3.1 shows the plot of  $|L(\vec{x})|$  for the interface between two different vacua (in the absence of quarks all the three interfaces have same profile for  $|L(\vec{x})|$ ). We mention that the surface tension  $\sigma$  of the  $Z(3)$  walls was estimated in refs. [75] for the above effective potential and it was found that  $\sigma = 0.34, 2.62$  and  $7 \text{ GeV}/\text{fm}^2$  for  $T = 200, 300$  and  $400 \text{ MeV}$  respectively. There have been Lattice studies of  $Z(3)$  wall tension. In ref. [76] the surface tension was found to be  $\sigma(T_c) = 0.17T_c^3$ . With  $T_c = 182 \text{ MeV}$  the  $T = 200 \text{ MeV}$  result for  $\sigma$  in ref. [75] is larger by almost factor 10 than the lattice result of [76]. However, the values of  $\sigma$  for larger temperatures,  $T = 300$  and  $400 \text{ MeV}$  are in reasonable agreement with the analytical estimates [77] (which give  $\sigma = \frac{4(N-1)\pi^2 T^3}{3\sqrt{3}g}$  for large temperatures).

The energy minimization program gives the full profile for  $L(\vec{x})$  which is then used for calculating  $A_0(\vec{x})$  as described in the next section.

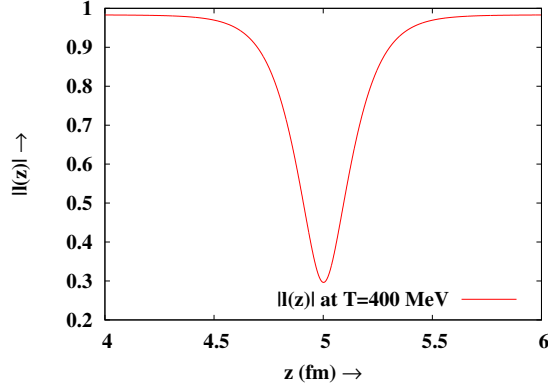


Figure 3.1: Variation of  $|L(\vec{x})|$  between different  $Z(3)$  vacua for  $T = 400$

### 3.2.1 Calculating $A_0$ Profile

We calculate the  $A_0$  profile from  $L(\vec{x})$  profile by inverting eq.(2.17). We choose  $A_0$  to be of the form

$$A_0 = \frac{2\pi T}{g} (a\lambda_3 + b\lambda_8), \quad (3.1)$$

where,  $g$  is the coupling constant and  $T$  is the temperature, while  $\lambda_3$  and  $\lambda_8$  are the diagonal Gell-Mann matrices. Coefficients  $a$  and  $b$  are the fields depending only on spatial coordinates<sup>1</sup>. The advantage of taking this gauge choice is that we are dealing with the eigenvalues of the matrices that are invariant under gauge transformation.

Substituting eq.(3.1) in eq. (2.17), we get

$$3L(x) = \exp(i\alpha) + \exp(i\beta) + \exp(i\gamma), \quad (3.2)$$

where,  $\alpha = 2\pi(a + b)$ ,  $\beta = 2\pi(-a + b)$  and  $\gamma = 2\pi(-2b)$ . Here  $a$  and  $b$  are rescaled like  $a \rightarrow a/2$  and  $b \rightarrow b/(2\sqrt{3})$ . On comparing the real and imaginary part of eq. (3.2), we get

$$\cos(\alpha) + \cos(\beta) + \cos(\gamma) = 3|L| \cos(\theta), \quad (3.3a)$$

$$\sin(\alpha) + \sin(\beta) + \sin(\gamma) = 3|L| \sin(\theta). \quad (3.3b)$$

In eq. (2.17),  $A_0$  appears as a phase, so any increment in the value of  $A_0$  by a factor of type  $2\pi n$  will result in same value of  $L(\vec{x})$ . Eq. (3.3), when solved for  $|L| = 1$  and

<sup>1</sup>In constructing the mean field theory, 2.34, we neglected the fluctuations.

$\theta = 0$ , give a set of ordered pairs  $(a, b)$  as the solutions. Since all these solutions reflect  $2\pi n$  ambiguity in  $A_0$ , we choose one ordered pair and set it as the initial condition.

Perhaps the most important step in solving the set of eq. (3.3) is to realize that the variation of  $A_0$  should be smooth and continuous across the domain wall. This is a crucial ingredient in the numerical scheme that we used to determine  $a, b$  and hence,  $A_0$ .  $A_0$  profile between  $L = 1$  and  $L = \exp(2\pi i/3)$  vacua was obtained by demanding the continuity of  $A_0$ . The initial point (for  $L = 1$  vacua) was chosen to be  $(a, b) = (-1.5, -1.0)$ . A small region was chosen near the new  $a, b$  and  $|L|$  was then calculated for all values in that region. Those values of  $a$  and  $b$  were selected for which the error between the calculated  $|L|$  and  $|L|$  obtained by energy minimization (figure (3.1)) was minimum. The process was then repeated for each value of  $z$  to obtain  $a, b$  values. Comparison between the calculated  $|L|$  profile and the one obtained by energy minimization is given in figure (3.2a). Figure (3.2b) shows the profile of parameters  $a$  and  $b$  across the domain wall. The calculated  $a, b$  were then used to calculate  $A_0$  using

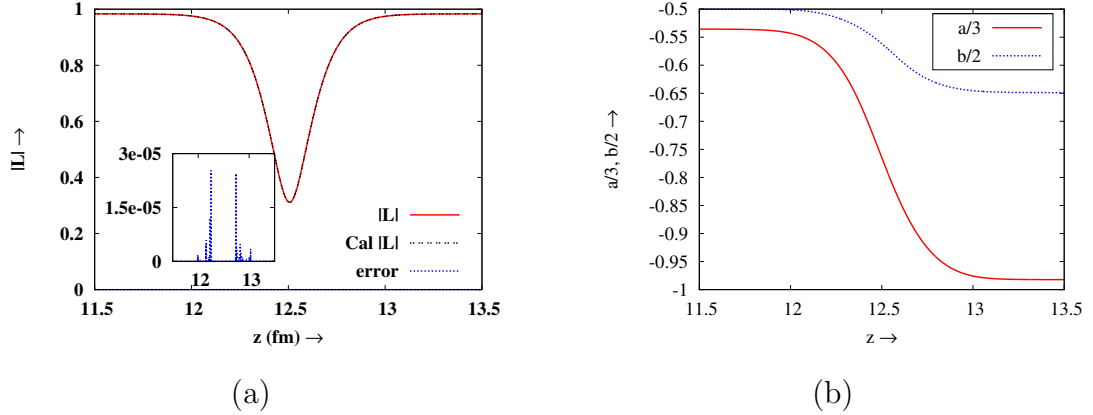


Figure 3.2: On left: Plot of calculated  $|L|$  and the one obtained from minimizing the energy. The inset figure shows the deviation between the two profiles. On right: Variation of  $a$  and  $b$  between the regions  $L(\vec{x}) = 1$  and  $L(\vec{x}) = e^{i2\pi/3}$ . Initial point is  $(-1.5, -1.0)$

eq (3.1). The  $A_0$  profile was fitted to the function  $A_0(x) = p \tanh(qx + r) + s$  using gnuplot. The calculated  $A_0$  profile, fitted  $A_0$  profile and their difference is plotted in figure (3.3).

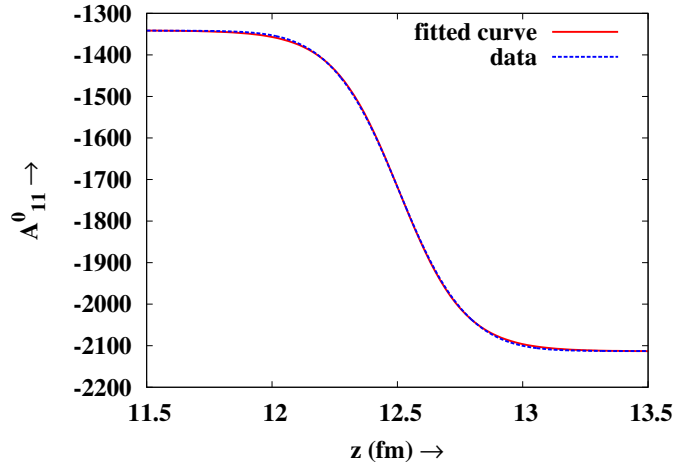


Figure 3.3: Plot of calculated  $A_0$  and the fitted profile ( $A_0(x) = p \tanh(qx + r) + s$ ). The parameters have values  $p = -378.27$ ,  $q = 7.95001$ ,  $r = -49.7141$ ,  $s = -1692.48$ . Only  $(1, 1)$  component of  $A_0$  is plotted. The other components also have similar fit.

### 3.2.2 Schematic Uncertainties

We now address the issue of the uncertainties in the determination of the  $A_0$  profile depending on the choice of the specific form of the effective potential. Other parameterization of the effective potential for the Polyakov loop have been given in the literature, e.g. in refs. [71, 78], and we will repeat the calculations of the previous section for the effective potential of the Polyakov loop as provided by Fukushima [71]. For spatially varying  $L$  configurations, we will continue to use the derivative terms as in Eq. 2.34 with general dimensional considerations (with suitable normalization of  $L$ ). The effective potential for ref. [71] has the following form

$$V[L]/T^4 = -2(d-1)e^{-\sigma a/T}|TrL|^2 - \ln[-|TrL|^4 + 8Re(TrL)^3 - 18|TrL|^2 + 27] \quad (3.4)$$

$\sigma = (425 \text{ MeV})^2$  is the string tension and  $2(d-1)e^{-\sigma a/T_d} = 0.5153$  with  $T_d = 270 \text{ MeV}$  is taken as the transition temperature by choosing the lattice spacing  $a = (272 \text{ MeV})^{-1}$ . Note that for consistency with the notations of ref. [71], we will use  $T_d$  and  $T_c$  interchangeably, both meaning the deconfinement transition temperature.  $L$  is the Polyakov loop but without the normalizing factor of  $N_c (= 3)$ . (Thus, we re-write the above effective potential in terms of the normalized Polyakov loop.

Henceforth by  $L$  even for the above equation we will mean this normalized Polyakov loop). It has been argued by Schaefer et al. [79] that the transition temperature has to be tuned depending on the number of quark flavors  $N_f$  (and also the value of the baryon-chemical potential). In ref. [79], the value of  $T_d = 270$  MeV corresponds to the pure SU(3) case with  $N_f = 0$ . In section 2.2.4 we have used the effective potential where the coefficient  $b_4$  is suitably normalized for the case of 3 flavors,  $N_f = 3$ . For the case of  $N_f = 3$ , the value of transition temperature from ref. [79] is  $T_d = 178$  MeV. Thus, we will use this value of  $T_d$  for the effective potential in Eq. (3.4).

The effective potential in Eq.(3.4) is of qualitatively different nature than the one given in Eq.(2.34). For small values of  $L$  the two forms will be similar as one can see by the expansion of the Logarithmic term in the above equation. However, for  $|L|$  approaching unity the two potentials are dramatically different.  $V[l]$  in Eq.(3.4) diverges at this limiting value thereby constraining  $|L|$  within value 1. There is no such constraint in Eq.(2.34). Even the shape of  $V[L]$  is very different away from the origin, especially near the three  $Z(3)$  vacua. It is thus reasonable to expect that the resulting profile of  $Z(3)$  wall and resulting  $A_0$  profile (using calculations of previous sections) for Eq.(3.4) may be quite different from the ones obtained in section 3.2.1 for Eq. (2.34).

With diverging  $V[L]$  at  $|L| = 1$  in Eq.(3.4), and due to its non-trivial shape near the  $Z(3)$  vacua, the application of the technique of ref. [64] for the determination of  $L$  profile between two  $Z(3)$  vacua is much more complicated here. Especially non-trivial is the choice of initial ansatz for the wall profile which is used for the energy minimization program. In ref. [64], the initial profile was taken to linearly interpolate between the two  $Z(3)$  vacua as a function of spatial coordinate  $z$ . This choice simply does not work for Eq.(3.4) due to the fact that  $V[L]$  diverges at  $|L| = 1$  and linear interpolation takes it outside this bound. For this we chose the initial trial profile to consist of two parts, one linearly decreasing (with  $z$ ) to  $L = 0$  along  $\theta = 0$  from the vacuum value and join this with the second part linearly increasing (with  $z$ ) along  $\theta = 2\pi/3$  to the second vacuum value. This keeps the initial profile within the allowed region of  $V[L]$  in Eq.(3.4).

Second complication arises with the algorithm of energy minimization itself. In ref. [64] correct  $L$  profile was obtained from the initial trial profile by fluctuating the

value of  $L$  at each lattice point and determining the acceptable fluctuation which lowers the energy (with suitable overshoot criterion etc. as described in detail in ref. [64]). However, with Eq.(3.4), fluctuations of  $L$  can take it out of the allowed region of  $V[L]$ . To handle this, we simply skip those fluctuations which take  $L$  outside the allowed region. With these modification in the procedure, we were able to determine the profile of the  $Z(3)$  wall and associated  $A_0$  profile. In section 3.2.1 we had calculated the profiles for temperature  $T = 400 \text{ MeV}$  (with  $T_c = 182 \text{ MeV}$  for the effective potential in Eq.(2.34)). For the sake of comparison with that case, for  $V[L]$  in Eq.(3.4) with  $T_c = 178 \text{ MeV}$  [79], we calculate the profiles for  $T = 391 \text{ MeV}$  which is close enough to the value  $T = 400 \text{ MeV}$ , and has the same value for  $T/T_c$ .

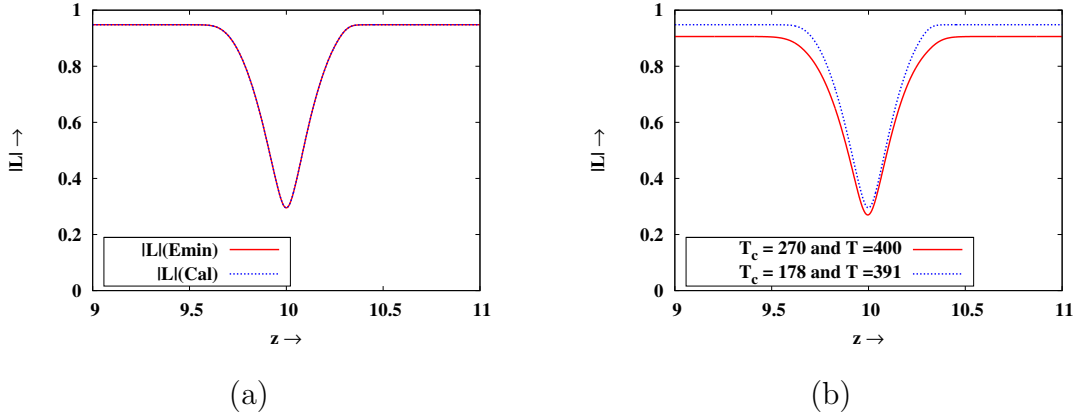


Figure 3.4: (a) Plot of the profile of  $|L|$  corresponding to the effective potential in Eq.(3.4). (b) Comparison of the profiles of  $|L|$  for different choices of  $T_d$  in Eq.(3.4).

Fig. 3.4a shows the wall profile of  $|L|$  for  $V[L]$  in Eq. (3.4) (again, with normalized  $L$ ). The profile is almost the same as the one shown in Fig. 3.2a. We mention here that for Fig. 3.4a we have used the same value of the coefficient of the first  $|TrL|^2$  term in Eq.(3.4) as with  $T_d = 270 \text{ MeV}$  (by suitably changing the values of string tension etc.). This is so that the shape of the barrier near the confining vacuum remains unaffected (which determines the first order nature of the transition). In any case, the overall features of the profile of the wall, such as its width and height, should depend more on the temperature scale rather than on the shape of the barrier for the confining vacuum. To check this, we also calculate the wall profile of  $|L|$  for Eq.(3.4),

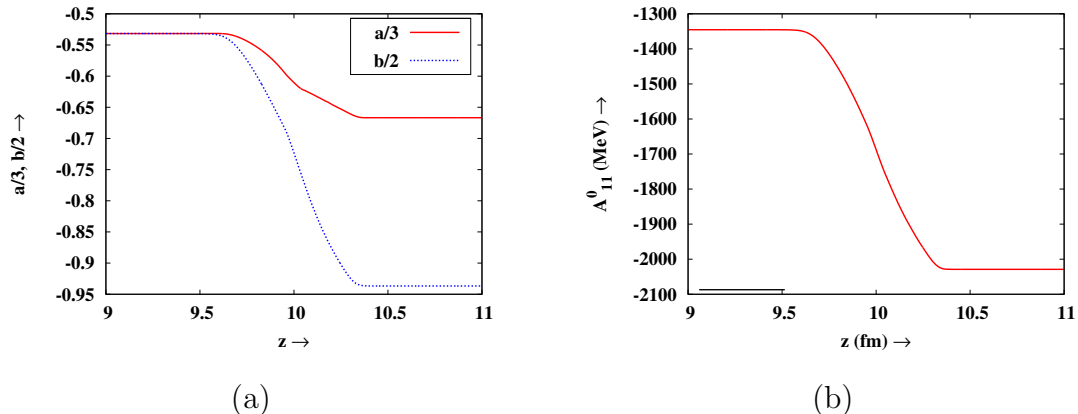


Figure 3.5: (a) Plot of calculated values of  $a$  and  $b$  for the  $|L|$  profile of Fig. 3.4a. (b) corresponding plot of  $A_0$ .

but now with the value of  $T_d = 270$  MeV and  $T = 400$  MeV. The comparison of the two profiles is shown in Fig. 3.4b. We see that the two profiles are very close to each other confirming above arguments.

We recalculate the plots of  $a$  and  $b$  for the case with  $T = 391$  MeV (with  $T_d = 178$  MeV). The resulting plots are shown in Fig. 3.5a which are seen to be very similar to those on Fig. 3.2b. Finally, the profile of  $A_{11}^0$  in Fig. 3.4b is also very close to the one in Fig. 3.3. Note that though overall all the plots in Figs.(3.4), (3.5) are very close to the corresponding plots in Figs. (3.2), (3.3), there is one clear difference. The profiles in Figs. (3.4), (3.5) have somewhat sharper variations from their asymptotic values compared to the case in Figs. (3.2), (3.3). This originates from the qualitatively different shapes of the two potentials in Eq. (2.34) and Eq.(3.4) near the region of  $Z(3)$  vacua, and in that sense characterizes the difference in the two potentials.

These results are quite remarkable. Even though the two effective potentials Eq.(2.34) and Eq.(3.4) (from refs. [54] and [71]) are of qualitatively different shapes, the resulting wall profile and  $A_0$  profile are almost the same. As we mentioned above, for small values of  $L$  the two effective potentials will have similar forms, which are fitted with the Lattice data. Our results thus point out that the profile of  $L$  (and consequently, the profile of  $A_0$ ) are primarily determined by the small  $L$  region of the effective potentials. This is likely to happen if the variations near the  $Z(3)$  vacua are primarily in the magnitude of  $L$  and not in its phase. The robustness of our

results against different choices of the effective potentials gives us confidence in the use of our procedure to calculate the reflection of quark and anti-quarks from the  $Z(3)$  interfaces. Since the  $A_0$  profiles of Fig. 3.3 and Fig 3.5 are almost the same, the resulting values of reflection coefficients for quarks/anti-quarks will also be very similar. In the rest of analysis in the paper, we will use the effective potential as given in Eq. (2.34).

### 3.3 Reflection of Quarks From $A_0$ Profile

We now use the  $A_0$  profile obtained by using the potential in eq. (2.34) to calculate the reflection of quarks. To calculate the reflection and transmission coefficient, we need the solutions of Dirac equation in Minkowski space. The  $A_0$  profile, calculated above, is in Euclidean space which *cannot* be used for solving Dirac equation in the Minkowskian space.

#### 3.3.1 Dirac Equation

We start with the Dirac eq. in 1 + 1 dimensional Euclidean space

$$[\gamma_e^0 \partial_0 \delta^{jk} + ig \gamma_e^0 A_0^{jk}(z) + \gamma_e^3 \partial_3 + m] \psi_k = 0, \quad (3.5)$$

where  $\gamma_e^0 \equiv \gamma^0$  and  $\gamma_e^3 \equiv i\gamma^3$  are Euclidean Dirac matrices. We now analytically continue the eq (3.5) to the Minkowski space to get

$$[i\gamma^0 \partial_0 \delta^{jk} + g\gamma^0 A_0^{jk}(z) + \gamma_e^3 \partial_3 + m] \psi_k = 0. \quad (3.6)$$

Note that the  $A_0$  in eq (3.6) is fundamentally different from the  $A_0$  in eq (3.5). However, it's the *same domain wall profile* (i.e same  $A_0$  dependence on  $z$ ) that appears in both the cases, which is what is needed for the calculation of reflection and transmission coefficients. For a plane wave solution ( $\psi(x)e^{-iEt}$ ), the eq (3.6) reduces to

$$[\gamma^0 \gamma^3 \partial_3 \delta^{jk} + \gamma^0 m \delta^{jk}] \psi_k(x) = (E - V_0(z)) \psi_k(x). \quad (3.7)$$

where  $V(z) = -gA_0^{jk}(z)$  is the potential as seen by the incoming fermion.

### 3.3.2 Numerical Technique

We do not have any analytic way to calculate the reflection and transmission coefficients for the continuously varying smooth potential, so we go for the numerical computation. Kalotas and Lee [80] have discussed a numerical recipe to solve Schrödinger eq. We take their cue and solve eq (3.7) by the same technique. We approximate the actual potential by  $n$  step potentials in series, each of equal width  $w$  as shown in figure (3.6). Let  $\psi_j$  be the wave-function for the  $j^{\text{th}}$  bin and the height of potential be

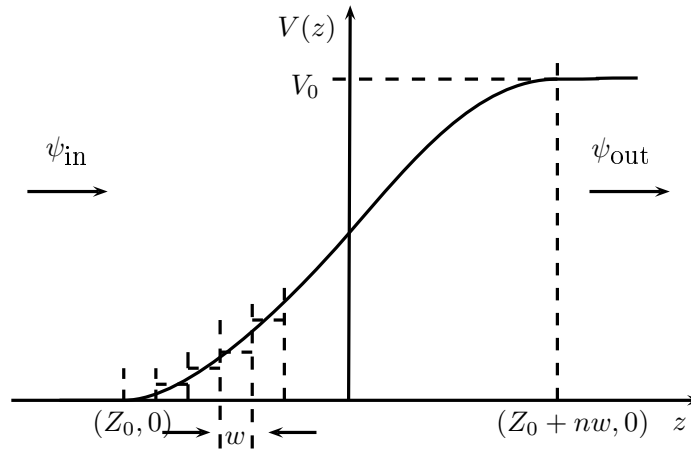


Figure 3.6: Potential ( $V(z)$ ) approximated by  $n$  step potentials, each of width  $w$ , in series.

$V_j$ . The height of the  $j^{\text{th}}$  step potential is taken to be the mean value of  $V(L + jw)$  and  $V(L + (j + 1)w)$ , i.e

$$V_j = \frac{[V(L + jw) + V(L + (j + 1)w)]}{2} \quad (3.8)$$

The incoming fermion wave-functions ( $\psi_j$ ) and outgoing fermion wave-functions ( $\psi_{j+1}$ ) at  $j^{\text{th}}$  site are

$$\psi_j(z) = A_j \begin{pmatrix} 1 \\ 0 \\ \frac{k_j}{E_j+m} \\ 0 \end{pmatrix} e^{ikz} + B_j \begin{pmatrix} 1 \\ 0 \\ \frac{-k_j}{E_j+m} \\ 0 \end{pmatrix} e^{-ik_j z}, \quad (3.9a)$$

$$\psi_{j+1}(z) = A_{j+1} \begin{pmatrix} 1 \\ 0 \\ \frac{k_{j+1}}{E_{j+1}+m} \\ 0 \end{pmatrix} e^{ik_{j+1}z} + B_{j+1} \begin{pmatrix} 1 \\ 0 \\ \frac{-k_{j+1}}{E_{j+1}+m} \\ 0 \end{pmatrix} e^{-ik_{j+1}z}, \quad (3.9b)$$

$$\text{where } k_j = \sqrt{E_j^2 - m^2}, \quad \text{and } E_j = E - V_j \quad (3.9c)$$

We now apply boundary conditions at  $j^{\text{th}}$  step i.e at  $z = L + jw$ . This gives us a set of two equations, which when written in matrix form look like

$$\begin{pmatrix} A_j \\ B_j \end{pmatrix} = M^{-1}(L + jw, k_j) \times M(L + jw, k_{j+1}) \begin{pmatrix} A_{j+1} \\ B_{j+1} \end{pmatrix} \quad (3.10a)$$

$$\text{where } M(L + jw, q) = \begin{pmatrix} e^{ik_q(L+jw)} & e^{-ik_q(L+jw)} \\ \frac{e^{ik_q(L+jw)} k_q}{E_q+m} & -\frac{e^{-ik_q(L+jw)} k_q}{E_q+m} \end{pmatrix} \quad (3.10b)$$

On iteration we obtain the relation

$$\begin{pmatrix} A_{\text{in}} \\ B_{\text{in}} \end{pmatrix} = M^{-1}(L, k_{\text{in}}) \times M(L, k_1) \times \dots \times M^{-1}(L + nw, k_n) \times M(L + nw, k_{\text{out}}) \begin{pmatrix} A_{\text{out}} \\ 0 \end{pmatrix} \quad (3.11)$$

The reflection and transmission coefficients are then given by

$$R \equiv \left| \frac{J_{\text{ref}}}{J_{\text{in}}} \right| = \left| \frac{B_{\text{in}}}{A_{\text{in}}} \right| \quad (3.12a)$$

$$T \equiv \left| \frac{J_{\text{trans}}}{J_{\text{in}}} \right| = \left| \frac{A_{\text{out}}}{A_{\text{in}}} \right| \times r \quad (3.12b)$$

$$\text{where } r = \left( \frac{k_{\text{out}}}{k_{\text{in}}} \right) \left( \frac{E + m}{E - V_{\text{max}} + m} \right). \quad (3.12c)$$

### 3.3.3 Results

We first calculated the reflection and transmission coefficients by assuming the  $A_0$  profile to be a step function rather than a smooth one. The analytic expressions

for the step potential are in standard text [81]. For anti-quarks the reflection and transmission coefficients are obtained by changing  $g \rightarrow -g$ , as anti-quarks are in  $\bar{3}$  representation of  $SU(3)$ . We have chosen the energies of the particles such that  $E > V + m$ , so as to avoid the Klein paradox regime. The results for different quarks and anti-quarks are given in table 3.1. It is clear that quarks have different reflection coefficients than their CP conjugates. Also, effect is significantly higher for the heavier quarks (for example charm quark).

	$u$	$d$	$s$	$c$
$E(\text{GeV})$	3.00	3.0	3.0	3.0
$m(\text{MeV})$	2.5	4.95	100	1270
$R_q$	$1.72527 \times 10^{-7}$	$6.76381 \times 10^{-7}$	0.00028303	0.140431
$R_{\bar{q}}$	$1.92498 \times 10^{-8}$	$7.54673 \times 10^{-8}$	0.0000314683	0.0064916

Table 3.1: Table for the reflection coefficients for various quarks. Reflection is higher for heavier quarks.

We then calculate the reflection coefficient for charm quark using the exact potential. The product of the matrices in eq (3.11) were calculated by a FORTRAN code and also by using Mathematica. Eq (3.12) were then used to calculate the reflection coefficient. At  $E = 3 \text{ GeV}$ , we get  $R = 0.00104992$  for  $c$  quark while for  $\bar{c}$  the result is  $R = 5.24229 \times 10^{-10}$ . As an additional check on the results (for the smooth profile), we shrank the profile and compared the reflection coefficient with the step potential result. The results are summarized in Table 3.2.

An important observation is the dependence of  $A_0$  profile on initial condition. If we start with  $(a', b') = (-a, b)$ , i.e with  $(1.5, -1)$ , then eq (3.1) tells us that  $A_0'^{11} = A_0^{22}$  and  $A_0'^{22} = A_0^{11}$ . In color space  $A_0$  is  $\text{diag}(A_0^{11}, A_0^{22}, A_0^{33})$ , and it acts on the color triplet  $(r, b, g)^T$ . So,  $A_0^{11}$  acting on  $(1, 0, 0)^T$  is same as  $A_0^{22}$  acting on  $(0, 1, 0)^T$  which is same as making different gauge choices in color space. Earlier in section (3.2.1), we had argued that different choices of  $(a, b)$  (for  $L(\vec{x}) = 1$ , say) were due to  $2\pi n$  ambiguity. Also note that since both  $\lambda_3$  and  $\lambda_8$  commute with all  $\lambda_p \in SU(3)$ , different ordered pairs  $(a, b)$  cannot be transformed into one another by a gauge transformation. Hence, it is surprising that profiles of  $A_0$  obtained by different initial condition are gauge

Shrinking Factor	Reflection Coeff
No shrinking	0.00104992
0.5	0.0169996
0.05	0.119157
0.005	0.123136
Step Potential	0.140431

Table 3.2: Table for the reflection coefficients when the profile is shrunk. Results approach the step potential as the profile gets narrower.

related to each other.

A possible reason for this to happen is that now we are looking at the spatial variation of the scalar potential and hence, global transformations do not apply. So, the gauge relation between various  $(a, b)$  values or, equivalently between corresponding  $A_0$  profiles, may well be the artifact of local transformations. The results above, however, conclusively show that there is a spontaneous  $CP$  violation due to the background profile.

### 3.4 Discussion

This  $CP$  violation will have interesting observable consequences for the Relativistic Heavy Ion Collision experiments at RHIC and at LHC. If QGP is formed in these experiments (and there are strong indications of that), then various  $Z(3)$  domains will inevitably be formed, leading to the formation of  $Z(3)$  walls. (We mention that the QGP strings [64] which also necessarily form during transition to QGP phase should also lead to spontaneous  $CP$  violation. Its effects on quark/anti-quarks scattering, or possible localization on the QGP strings needs to be explored). As these domain walls move/collapse, quarks/anti-quarks will get reflected/transmitted differently from these domain walls leading to the segregation of quarks and anti-quarks. The concentration of quarks (or anti-quarks, depending on the collapsing vacuum) will grow in different regions of the QGP. As the effects would be stronger for heavier quarks (Table 3.1), this should lead to enhancement of strange and charmed

baryons along with the suppression in the yield of corresponding mesons (such as  $J/\psi$ ).

Detailed exploration of the formation and evolution of  $Z(3)$  walls and QGP strings in the context of RHICE has been carried out in ref. [66,67]. These simulations show that in the typical region of QGP formed in RHICE, one expects several  $Z(3)$  domain walls to form, their numbers ranging from 1 to 4, 5. The walls may extend throughout the QGP region with size of order  $10 fm$ . There are closed domain walls formed with initial size of about  $5 - 8 fm$ . The velocities of these walls was also estimated in ref. [66,67] and were found to range from 0.5 to 0.8. For detailed discussion of the properties of  $Z(3)$  wall and QGP string networks expected in RHICE, see ref. [66,67]. These results about the sizes and numbers of  $Z(3)$  walls and QGP strings are very important. This is because one should realize that in a very large sized QGP region, as in the early Universe, for every domain wall connecting  $\theta = 0$  and  $\theta = 2\pi/3$  vacua, there will be one connecting  $\theta = 0$  and  $\theta = 4\pi/3$  vacua. These walls are conjugate of each other and the reflection of a quark from the first wall is identical to the reflection of an anti quark from the second wall. These two walls are strictly degenerate, even in the presence of explicit symmetry breaking effects from dynamical quarks. Thus, on the average there will not be any bias for quarks and anti-quarks as they scatter from a network of  $Z(3)$  walls.

This is, however, not true for a small QGP region as produced in RHICE. As the number of  $Z(3)$  walls produced in such a small region is of order one [66,67], there may be a net effect for the concentration of baryon number, or for anti-baryon, in each event. This can be revealed by event-by-event analysis. Even statistically, for a large number of events, one can calculate the variance of baryon number density, and spontaneous CP violation from  $Z(3)$  walls may be detected. For a given event also, segregation of baryons and anti-baryons will occur over large distances of order several fm as indicated by the typical wall size and separation [66,67].

This CP violation can also be very important in the context of early universe where it can have interesting implications for generation of baryon inhomogeneities. As collapsing domain walls preferentially sweep quarks (or anti-quarks), segregation of quarks and anti-quarks will occur. One can then discuss the formation of baryonic (or anti-baryonic) lumps. These baryon inhomogeneities can be of large magnitude,

with large separations in the context of certain low energy inflationary models [75], (but now with  $CP$  violation incorporated). This is the subject of chapter 4.

Another important consequence will be on the  $P_t$  spectra of hadrons. The quarks/anti-quarks with high momenta will undergo non-trivial scattering from these  $Z(3)$  walls. As  $Z(3)$  walls collapse, some get transmitted while others are reflected back. For  $Z(3)$  walls forming closed, collapsing, structures, the quarks suffer multiple reflections inside the wall, resulting in an increment in their transverse momenta. This process continues until the walls either melt away or collapse completely. So the final transverse momentum of some quarks may be reasonably enhanced before they escape. One can then use a specific model (such as Recombination/Coalescence model) to study the  $P_t$  spectra of final state hadrons, which should show an increase in the yield of hadrons at high  $P_t$ . This has been discussed in ref. [82], however, no account of  $CP$  violation was considered in that work. In the presence of  $CP$  violation, the modified  $P_T$  spectra will be different for quarks and for anti-quarks. We plan to carry out these analyses in a future work.

The most important limitation of our analysis is the absence of quark effects. Dynamical quarks will lead to lifting of degeneracy between different  $Z(3)$  vacua, making  $L = 1$  vacuum as the true vacuum as discussed in refs. [54, 57–59]. The one-loop corrections from dynamical quarks have also been discussed in refs. [83–86]. As we mentioned, recent lattice studies [65] have provided evidence for the existence of such metastable  $Z(3)$  vacua. Our analysis above of calculation of  $A_0$  profile and calculation of reflection coefficients for quarks and anti-quarks can be straightforwardly applied for this non-degenerate case. This is discussed in detail in chapter 5. Apart from affecting the numbers (for reflection coefficients), its most important effect will be on the evolution of  $Z(3)$  wall and QGP string network, (see ref. [66, 67] for a detailed simulation study of these aspects). However, for the case of RHICE, due to small length (and time) scales involved, the dynamics of  $Z(3)$  walls is likely to remain dominated by the surface tension effects with the difference in pressure between different vacua not playing dominant role for such length scales). Thus the above mentioned features of effects on hadron spectra due to  $CP$  violation may remain qualitatively true for RHICE.

However, for the universe the entire issue of formation and evolution of  $Z(3)$  walls

crucially depends on the importance of quark effects. Some discussion of this has been provided in [75]. In the next chapter, we will present our work [87] in which we discuss an interesting possibility arising out due to this spontaneous  $CP$  violation in context of early universe.

# Chapter 4

## Cosmological Implications of Spontaneous $CP$ Violation

In this chapter we focus our attention on the confinement-deconfinement transition in the early universe. In section 1.6.2 we discussed the thermal history of the universe and argued that Universe purportedly underwent the confinement-deconfinement transition just micro-seconds after the Big-Bang. It will then be interesting to study the interesting physics that might have happened in the QGP phase before that time, and the possible implications it can have on the subsequent cosmological evolution.

In section 4.1, we'll discuss one such interesting possibility as first discussed by Witten [88]. He argued that if the QCD phase transition is strongly first order, then there is a possibility of formation of dense cold objects with huge concentration of quarks in it called quark nuggets. These nuggets were proposed as the candidates of dark matter entirely within standard model. However, with lattice studies indicating that the confinement-deconfinement transition is essentially a crossover, this scenario lost it's appeal. It was then argued in [75], that it is still possible to form these nuggets via the  $Z(3)$  domains in early universe. The question of formation of these  $Z(3)$  domains in the early universe is itself a non trivial issue. This is the subject of section 4.2. This is specifically important in the context of early universe as the effect of dynamical quarks, which renders these domains meta stable thereby raising survival issues of these domains till late times, which cannot be possibly neglected in the case of early universe. It has been argued that it may be possible to ignore the effects of

quarks in context of certain low energy inflationary models and one can work with the pure gauge QCD [75]. In the subsequent sections we describe our work [87], where we discuss the possibility of formation of quark nuggets as well as anti-nuggets due to the spontaneous  $CP$  violation from QCD  $Z(3)$  domains. These nuggets can provide the dark matter for the universe entirely within the standard model. It is important to note that such compact baryonic objects formed much before the nucleosynthesis epoch are consistent with all observations.

## 4.1 Witten's Scenario

In this section we outline the scenario of quark nuggets formation as originally presented by Witten [88]. Witten's argument is based on the assumption that the quark hadron transition is first order.

As the temperature of the Universe falls just below the critical temperature, hadronic phase starts to appear in the QGP phase in the form of bubbles. The surface energy tries to reduce the size while the volume energy tends to increase the size. For the bubbles with radius larger than the value of a critical radius, the bubbles of the Hadronic phase do not disappear but start expanding. In the process, the latent heat gets expelled into the surrounding medium and it increases the temperature of the Universe back to  $T_c$ . Once Universe has attained  $T_c$ , the hadronic bubble stops expanding as its pressure is balanced by the QGP phase outside. At  $T_c$ , both the phases have equal pressure. As the universe expands, the hadronic bubbles expand. The universe still remain at  $T_c$  due to the latent heat getting expelled as the Hadronic bubble grows. Soon, the hadronic bubbles occupy a major fraction of the universe and they meet and percolate, merge and arrange together to form fewer, larger bubbles so as to minimize the surface area.

Soon the situation is reversed and the QGP phase occupies a minority region in space. The QGP at this stage is confined to the isolated and roughly spherical region in the Universe. Witten argued that at that time, the QGP bubbles can concentrate about 80–99% of the entire baryon content of the Universe. As the Universe expands further it tends to cool, but for it to remain at the critical temperature, heat must come from the QGP regions. This can happen by emission of particles like neutrinos,

that have a large mean free path or by the evaporation of the surface layers of bubbles. If the heat loss by neutrinos dominates, then the high temperature phase keeps on shrinking and thereby trapping the excess baryon into smaller and smaller volume.

It was argued in subsequent works [89–91] that if the concentration of baryon inside is greater than a critical value, then these nuggets can be stable and can survive till date. It is usually stated that the data on Nucleosynthesis and CMBR does not allow baryonic dark matter. This indeed holds true for baryons in the form of gas (e.g. hydrogen, helium). Observational constraints from nucleosynthesis and CMBR are very strong on such forms of baryonic matter and restrict it to less than 20% of all matter/radiation in the universe (excluding the dark energy). However, it is important to note that these constraints do not apply if baryons are in the form of heavy bodies, such as quark nuggets, MACHOS, etc., provided that such objects form before nucleosynthesis. There are separate strong observational constraints on MACHOS from gravitational microlensing observations.

#### **4.1.1 Why an Alternate Scenario?**

The interest in quark nuggets declined with results from lattice gauge theory showing that a first order quark-hadron transition is very unlikely. The transition, for the range of chemical potentials relevant for the early universe, is most likely a crossover. Witten’s scenario of formation of quark nuggets does not work in such a case. However, with most attempts of explaining the dark matter not meeting any success (such as supersymmetric dark matter candidates in view of LHC results), it is important to appreciate following points about quark nuggets as dark matter candidates. As we mentioned above, here one does not need any new species of particles, quarks do the job. Secondly, any scenario of forming quark nuggets will most naturally fit in the QGP phase of the universe, well above radiation decoupling and nucleosynthesis stages. Those baryons (quarks) which form (heavy) quark nuggets completely decouple from the processes happening at nucleosynthesis stage, and later on at the radiation decoupling stage. Thus, nucleosynthesis and CMBR constraints do not apply to the fraction of baryons in quark nuggets. Further, stability of these quark nuggets, especially strangelets, has been extensively discussed and it has been argued that strangelets with baryon number of several hundred to general quark nuggets with

baryon number of order up to  $10^{50}$  may be stable up to the present stage [89–91]. The only issue then remains is how to form these objects when quark-hadron transition is a cross-over. This issue was addressed in [75], where  $Z(3)$  interface provided the interface between different regions of the Universe. The alternate scenario as presented in [75] doesn't require any first order quark-hadron phase transition, or even a phase transition for that matter.

We would like to emphasize that even in the absence of a mechanism for the formation of quark nuggets, it is important to recognize that quark nuggets provide a viable dark matter candidate entirely within the Standard model. It then provides a strong motivation to search for mechanisms which can lead to formation of such objects in the early stages of the universe. Indeed, these exciting objects have fascinated cosmologists and even now there are attempts to detect these objects [92, 93].

## 4.2 $Z(3)$ Domains in Early Universe

In a standard scenario of defect formation in early universe, the symmetry is present at higher temperature (for example in the GUT theories) and it is broken as the temperature of the universe decreases, leading to the formation of defects in the low temperature phase of the theory. This is not true for the confinement-deconfinement phase transition. Here, the  $Z(3)$  symmetry is restored in the confined (low temperature) phase while it is spontaneously broken in the high temperature phase. To discuss the formation of  $Z(3)$  structures, one would require a situation where the universe undergoes the transition from the hadronic (confined/low temperature) phase to the QGP (deconfined/high temperature) phase. Kibble mechanism [63] can then be invoked to study the formation of these defects. Inflationary cosmology meets this requirement perfectly well and the defect formation occurs naturally in this framework.

Our discussion is confined to the paradigm of inflationary cosmology and follows closely the chain of arguments presented in ref. [75]. Before inflation, the universe was at a very high temperature ( $T \gg T_c$ ) and quarks and gluons were deconfined. During inflation, the temperature of the universe decreases exponentially to zero due to the rapid expansion. As a result  $Z(3)$  interfaces disappear as the temperature

drops below the critical temperature  $T_c$  (if universe is in equilibrium during inflation) or as the energy density drops below  $\Lambda_{QCD}$  due to expansion (in a standard out of equilibrium scenario). There are situations (warm inflationary models [94]) where the temperature of the universe remains quite high during the inflation period. However, in such models the decay of inflaton field is very non-trivial [95]. As inflation dilutes away particles, at any instant there are new thermally generated particles available. In such a scenario it is unclear how these  $Z(3)$  domains evolve. Situation is clearer in standard inflationary scenario. Before inflation,  $l(x)$  initially was in one of the  $Z(3)$  vacua ( $l(x) \neq 0$ ). As  $T \rightarrow 0$  during inflation, the potential (eq. (2.34)) changes its shape and becomes a paraboloid with a unique minimum at  $l(x) = 0$ . So,  $l(x)$  will start to roll down from  $l(x) \neq 0$  to  $l(x) = 0$ . Let  $t_{inf}$  be the inflation time scale and  $t_{roll}$  be the roll down time of  $l(x)$  to the minimum of the potential. The following situations are possible:-

1.  $t_{inf} > t_{roll}$ :- Then  $l(x)$  will roll down to the minimum of the potential during the inflation and restore the  $Z(3)$  symmetry. This symmetry will be spontaneously broken as the universe reheats above  $T_c$  towards the end stages of inflation. Various  $Z(3)$  domains and interfaces will then arise during this spontaneous symmetry breaking transition via the standard Kibble mechanism [63]. The typical sizes of the domains will be decided by the correlation length (which would be the Hubble size of the universe) at the time of formation of these structures during reheating. As one expects the energy density stored in  $l(x)$  to be of the order of  $\Lambda_{QCD}$ ,  $t_{roll} \sim (\Lambda_{QCD})^{-1} \sim 1 \text{ fm}$ . So  $t_{inf} > 1 \text{ fm}$ , which sets the inflation energy scale to about  $10^9 \text{ GeV}$ . This is possible in certain low energy inflation models [96–98]. We discuss this scenario in detail later in this section.
2.  $t_{inf} \leq t_{roll}$ :-If the inflation time scale is much shorter than about  $\Lambda_{QCD}^{-1}$ , then the  $l(x)$  will not have time to roll down to the minimum of the potential. Even though we do not understand the dynamics of  $l(x)$  in such non-equilibrium conditions, it's natural to assume that the potential energy of  $l(x)$  will be greatly reduced during inflation. With matter completely diluted away, the only relevant scales for this potential energy can be only be  $\Lambda_{QCD}$ , or quark masses.

After inflation, the universe starts reheating and eventually the temperature is higher than critical temperature for confinement-deconfined transition. At this stage, the universe is in deconfined state and as a result a network of  $Z(N)$  interfaces is formed. The exact details of the formation of these networks itself makes a engrossing study and is not very clear. However, one may expect it to depend on the details of reheating itself. For example, whether universe slowly reheats above the  $T_c$  or whether it quenches to a temperature above  $T_c$  may be one of the important factors in determining the network of these interfaces. In any case, it seems reasonable to assume that the energy density of the matter which is produced by the decay of inflaton field will be much higher than the potential energy  $l(x)$  which could survive during the inflationary stage. In other words, the evolution of  $l(x)$  during reheating stage, and consequently, the network of  $Z(3)$  walls formed, should be determined solely by the decay product of inflation field and with no or almost zero contribution coming from the pre-existing Polyakov loop condensate. Therefore, in this case as well, one expects  $Z(3)$  domain wall formation according to the Kibble mechanism, with typical sizes of the order of relevant correlation length at an appropriate stage during reheating.

Hence for a generic case the formation of  $Z(3)$  domains after inflation is by standard Kibble mechanism . For  $T \gg \Lambda_{QCD}$ , the energy scale for these walls is set by the temperature of the universe. The tension of the  $Z(3)$  interface and associated string [64] is set by the QCD parameters and the temperature. As a result the dynamics, of the tension forces at the least, should be decided by the background plasma for temperatures far above the QCD scale. However, in presence of quarks, there is an explicit breaking of  $Z(3)$  symmetry. Two of the vacua, with  $l(x) = z, z^2$ , become metastable leading to a pressure difference between the true vacuum and the metastable vacua [69,99]. This leads to a preferential shrinking of metastable vacua. As the collapse of these regions can be very fast (simulations indicate  $v_w \sim 1$  [66,67]), they are unlikely to survive until late times, say until QCD scale, to play any significant role in the context of the universe. However, there is a possibility that when effects of quarks scattering from the walls is taken into account their collapse may be slower due to the friction experienced by domain wall. For large friction the walls

may even remain almost frozen in the plasma. For example, it has been discussed in the literature that dynamics of light cosmic strings can be dominated by friction which strongly affects the coarsening of string network [100, 101]. It is very much plausible that the dynamics of these  $Z(3)$  walls is friction dominated. This is because of the  $l(x)$  profile across the interface. As quark energy depends on  $l(x)$ , we expect a significant change in quark energy while crossing the wall. As a result it is energetically unfavorable for the quarks to cross the wall. This can lead to significant friction in wall motion.

Even if the dynamics of the domain walls is not friction dominated, it is still possible for these  $Z(3)$  domains to survive until the QCD scale, in certain low energy inflationary models [96–98]. In these models the reheating temperature can be quite low ( $\sim 1 \text{ TeV}$ ). As discussed above, in these models, the inflation time scale is larger than the time needed by the  $l(x)$  field to roll down to the bottom of the potential. After inflation, the temperature of the universe increases slowly (in comparison to the Hubble expansion) from a very low value to the reheating temperature, in the process crossing the critical temperature for quark-hadron transition. As a result, the  $Z(3)$  symmetry is spontaneously broken and  $Z(3)$  interfaces are formed. Although the details depends on the reheating mechanism but it's clear that at the time of formation the size of these structures cannot be larger than the  $\Lambda_{QCD}^{-1}$ , as these structures cannot form below  $T_c$  which is of the order of QCD scale. Another important point is the pressure difference between the true vacuum and metastable vacuum which will crucially affect the formation and evolution of these domains. For example, there may be a bias in formation of these domains as temperature crosses  $T_c$  due to this pressure difference. However, we assume that such bias would be completely washed out by the thermal fluctuations and the continued reheating. We also assume that the pressure difference between the metastable  $Z(3)$  vacua and the true vacuum resulting from the explicit symmetry breaking term is small near  $T_c$  (see also, ref. [57–59]). In essence, we can use the effective potential given in eq. (2.34) for the rest of the discussion and ignore the effects of explicit symmetry breaking due to quarks.

In such a case, the dynamics is dictated by the surface tension and pressure difference is sub-dominant. This also suppresses the decay of metastable vacuum to true vacuum. The domain wall network then undergoes coarsening leading to a few

domain walls within the horizon volume. Detailed simulation of the formation and evolution of these  $Z(3)$  walls is discussed in ref [66,67]. Even though the simulations are done in context of relativistic heavy ion collision experiments, the basic physics doesn't change much and the evolution of these  $Z(3)$  domains, once they are formed, can be understood quite well in these simulations. In context of the universe it is important that, during reheating, the temperature should remain near  $T_c$  for large enough time so that significant coarsening can occur while the pressure difference remains negligible. If sufficient time is spent near  $T_c$  one may get almost horizon size walls at the final reheat temperature. If the pressure difference becomes significant in the early stages, then resulting domains will be smaller due to insufficient coarsening. As temperature reaches large values during the end stages of reheating, pressure difference will become important and wall dynamics should depend on expansion rate of the universe and the wall velocity through the plasma. However as we discussed previously, large friction due to quark scattering can lead to almost frozen walls (or negligible wall velocities) and may help in retaining large sizes up-to the stage of quark-hadron transition. Such large frozen (or very slowly moving) walls may lead to stretching of the domain due to the expansion of the universe and then one can even get domain sizes of order of a fraction of the horizon size at QCD scale.

### 4.3 Nuggets Anti-Nuggets Formation

In this section we discuss how these collapsing  $Z(3)$  structures lead to the segregation of baryon number and can lead to the formation of quark nuggets. After the domain walls have formed (as we discussed in the previous section), the closed domains start to collapse. As discussed in section 3.2, there is a profile of  $l(x)$  which implies that there is a background  $A_0$  condensate profile. This  $A_0$  will interact with quarks and anti-quarks in a different manner. In other words, it will have different reflection and transmission coefficients for the quarks and their CP conjugates leading to a spontaneous violation of CP symmetry. This will lead to the concentration of quarks (or anti-quarks) within the collapsing domain, thereby resulting in the segregation of baryons and anti-baryons in the early universe. These collapsing, baryon (anti-baryon) rich regions can form quark (anti-quark) nuggets if the baryon concentration is quite high in these

regions. It is important to note that as these  $Z(3)$  walls are expected to be formed irrespective of the order of the phase transition, the formation of quark nuggets is via a very different mechanism than the originally proposed one [88]. In context of  $Z(3)$  walls the baryon inhomogeneity generation was discussed in [75] however there was no CP violation in their discussion as they deal with only  $l(x)$  profile and not the gauge field.

### 4.3.1 Baryon Anti-Baryon Segregation

While studying the baryon transport across the domain wall, we assume constant temperature. A major simplification that happens due to above assumption is that one can take the height of the potential to be constant. This also makes it possible for us to ignore the effects coming from the reheating due to decreasing surface area as the wall collapses. In other words, we assume that the thermal equilibrium is maintained as the quarks and anti-quarks are reflected from the domain wall. We also assume that the collapse of the domain walls is very fast. This allows us to ignore the expansion of the universe as domain walls will then collapse in the time smaller than the Hubble time. In our calculations we take the wall velocity to be the sound velocity,  $v_w = 1/\sqrt{3}$ . These velocities could be larger if the friction is sub-dominant in comparison to the surface tension of the wall. To study the change in the number densities inside and outside the collapsing region we assume that the baryons homogenize instantaneously as the baryon transport occurs across the wall. We can then work with only the number density inside and outside the domain wall and ignore the diffusion of baryons.

Let  $V$  be the total volume of the observable universe. Since we are ignoring the expansion of the universe, this is fixed. In this volume suppose there are  $N_d$  number of collapsing domains.  $V_i = 4\pi/3R(t)^3N_d$  ( $R(t)$  being the size of domain) be the volume contained within the domain walls and  $V_o = V - V_i$  be the volume outside the collapsing regions. The radius of the domain is given by the expression

$$R(t) = \frac{r_H}{N_d^{1/3}} - v_w(t - t_0), \quad (4.1)$$

where  $r_H$  is the horizon size at the initial time  $t_0 \simeq 30 \left( \frac{150}{T(\text{MeV})} \right)^2$  (in the units of micro seconds). If  $n_i$  and  $n_o$  are the number densities of baryons in the regions

inside and outside the domain walls, then the total number of baryons in each region is  $N_i = n_i V_i$  and  $N_o = n_o V_o$ . The equations for studying quark number density concentration inside and outside the domain wall can then be written as

$$\dot{n}_i = \left( -\frac{2}{3}v_w T_w n_i + \frac{v_o^{rel} n_o T_- - v_i^{rel} n_i T_+}{6} \right) \frac{S}{V_i} - n_i \frac{\dot{V}_i}{V_i} \quad (4.2)$$

$$\dot{n}_o = \left( -\frac{2}{3}v_w T_w n_i - \frac{v_o^{rel} n_o T_- - v_i^{rel} n_i T_+}{6} \right) \frac{S}{V_i} + n_o \frac{\dot{V}_i}{V_o}, \quad (4.3)$$

where  $S$  is the surface area of the collapsing wall.  $T_w$  is the transmission coefficient for the quarks inside the domain and moving parallel to the wall. The relative velocity for such quarks with respect to the wall is  $v_w$  and they constitute  $4/6$  of the total number of the inside quarks.  $T_-$  ( $T_+$ ) is the transmission coefficient calculated for the quarks that are moving from outside (inside) of the wall towards the inside (outside) with the relative velocity  $v_o^{rel}$  ( $v_i^{rel}$ ) with respect to the wall. Each contributes towards  $1/6$  of the corresponding number densities. Eq. (4.1), (4.2) and (4.3) are then solved simultaneously to get the evolution of the baryon densities inside the collapsing domain.

As the wall collapse, it leaves behind a profile of baryon density. Consider a spherical shell of thickness  $dR$ , at a distance  $R$  from the center of the domain wall. Then if  $\rho(R)$  is the baryon density, then total number of baryons in the shell is given by  $dN_i = 4\pi R^2 \rho(R) dR$ . Using eq (4.1) we get,

$$\rho(R) = -\frac{\dot{N}_i}{4\pi v_w R^2}. \quad (4.4)$$

Eq. (4.1) and (4.4) are solved simultaneously to get the density profile. It is important to note that during last stages of the collapse of domain wall, it is possible that the baryon concentration becomes so large that chemical potential in the region is comparable to the temperature. This will alter the transmission probability of the baryons across the domain wall. We are neglecting any such effects that may arise during the evolution.

As we discussed in section 4.3.1, the domain wall is selective in the transmission of baryons and anti-baryons due to its CP odd nature. This will lead to the baryon anti-baryon segregation. As a result we get baryon rich and anti-baryon rich regions that can form nuggets and anti-nuggets if there is sufficient concentration of baryons

or anti baryons. In addition, the domain wall is also sensitive to the color of quark as it has different reflection and transmission coefficient for different colors. Eq (4.1) to (4.4) need to be solved for each color which will result in the color specific baryon concentration. This in itself is not surprising as in the QGP phase, the degrees of freedom are color degree of freedom and the requirement to have colorless objects in QGP would be an artificial one.

## 4.4 Results

To calculate the  $A_0$  profile, we followed the procedure outlined in section 3.2.1. Figure (4.1) shows the background  $A_0$  profile between  $l = 1$  and  $l = z^2$ , calculated using the profile given in fig. (3.1) for  $T = 400 \text{ MeV}$ .

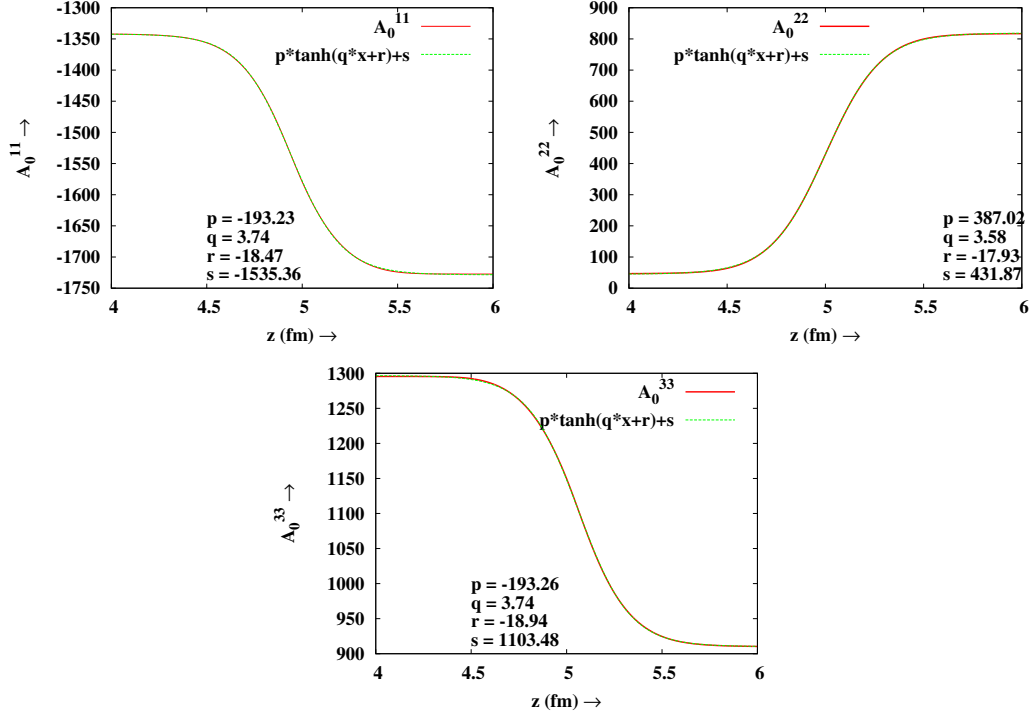


Figure 4.1: The background  $A_0$  profile calculated from the  $l(x)$  profile. The profile is fitted to a tanh curve.

We will discuss the concentration of charm quarks. Their number density at  $T \simeq 400 \text{ MeV}$  is still significant and with large reflection coefficients, they lead to

large baryon/anti baryon concentrations. Up and down quarks are ultra-relativistic and have very small reflection coefficients. The case of strange quark is an important one. We will comment on that case at the end of this section. For charm quark at  $T = 400 \text{ MeV}$ , the thermal velocity  $v_p$  is less than the sound velocity  $v_s$ . As we are assuming the wall velocity  $v_w$  to be same as  $v_s$ , the particles moving from outside towards the wall are unable to catch up. This means that  $T_+$  is identically zero. For the particles moving towards the wall, the energy (in the rest frame of the wall) is much larger than the potential so most of them pass through ( $T_-$  is close to unity). Only the particles moving parallel to the wall can get concentrated. The potential as seen by the incoming fermion is  $V(z) = -gA_0(z)$ . The value of  $g$  is chosen such that  $N/g^2 = 0.8$ . Since  $g$  is positive for quarks, the background  $A_0$  profile dictates that red, green and anti-blue quarks are concentrated in the collapsing regions with  $l = z^2$ . (Note, in Fig. 4.1,  $A_0^{22}$  has opposite sign compared to  $A_0^{11}$  and  $A_0^{33}$ . Thus, while red and green quarks experience a potential barrier leading to significant reflection, the blue quark sees a potential well. It is the blue anti-quark which experiences a potential barrier and undergoes significant reflection.) Table (4.1) lists the values of  $T_w$  for charm quark for smooth profile. It clearly indicates that two color species of quarks and one color species of anti-quark are not transmitted. These transmission

	$r$	$b$	$g$
$c$	0.0	0.936623	0.0
$\bar{c}$	0.997471	0.0	0.99903

Table 4.1: Table for the transmission coefficients for charm quarks and anti-quarks, moving parallel to the wall, from the  $l = z^2$  wall.

coefficients were then used to solve eq. 4.2 and 4.3 simultaneously. This gives us the evolution of number densities inside and outside the domain wall for each color. Fig. 4.2(a) and 4.2(b) show the evolution of number densities for charm quark and anti-quark inside the collapsing domain wall at  $T = 400 \text{ MeV}$  for the case of step potential approximation. The result is for  $N_d = 10$ . It is clear that the number of quarks contained in the domain wall is several orders of magnitude higher than the number of anti-quarks. The number densities of quarks and anti-quarks are shown

in fig 4.3(a) and 4.3(b). Looking at fig. (4.2a) and fig (4.3a) we note that the number densities are not much different for the smooth and step potential. This might seem surprising. However a look at fig. (4.2b) and fig (4.3b) clearly shows that the number density of anti-red (and other corresponding) quarks, that are not getting concentrated, is much less for the smooth profile than the step potential. So, the number densities in fig (4.2a) and (4.3a) have same order of magnitude but not same numbers.

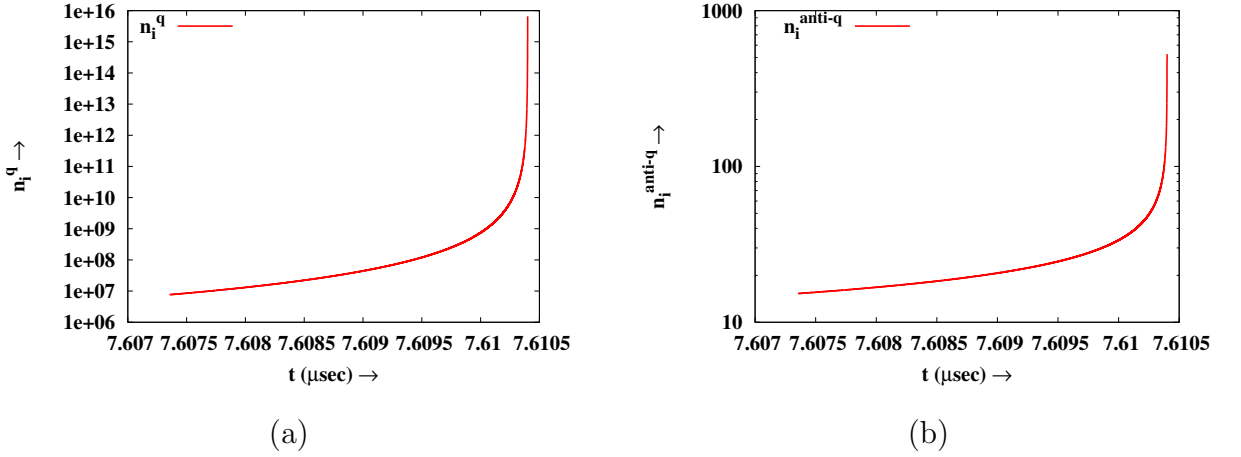


Figure 4.2: Number density evolution with step function profile: (a)For Red, green and anti-blue charm quark. (b)For anti-red, anti-green and blue charm quark.

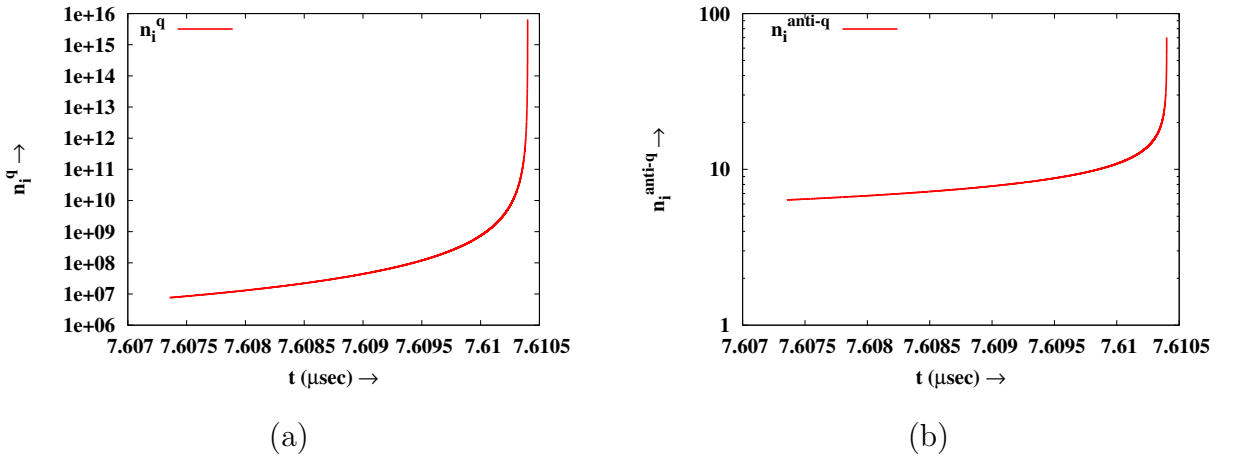


Figure 4.3: Number density evolution with smooth profile: (a)For Red, green and anti-blue charm quark. (b)For anti-red, anti-green and blue charm quark.

Fig.4.4 shows the density profile of red charm quark. As the majority of anti-quarks are completely transmitted, they do not leave any density profile behind. Fig.(4.2) and (4.3) give the number density of quarks in units of the background quark/anti-quark number density  $n_0$ , as a function of the size of the collapsing domain wall. At  $T = 400$  MeV,  $n_0 \simeq O(1)/fm^3$  for each type of quark. This gives the net baryon number trapped inside the domain wall to be of order  $10^{52}$  when domain wall collapses to a size of order one meter. This is with the optimistic assumption that all the baryons get trapped inside the wall while anti-quarks leave the wall virtually unreflected. This may not be a reasonable assumption, especially in view of the assumption of thermal equilibrium and homogeneous baryon distribution inside the wall. In the most conservative scenario, the net baryon number inside the domain wall should remain trapped. Net baryon number to entropy ratio being of order  $10^{-10}$ , it is safe to say that at least net baryon number of order  $10^{42}$  can be trapped inside collapsing domain walls. These *quark nuggets* may then survive until present and provide dark matter. In this case (fig. 4.3a), we had a concentration of baryons. This concentration is due to the wall between  $l(x) = 1$  and  $l(x) = z^2$  vacua. There would also be a wall between  $l(x) = 1$  and  $l(x) = z$  vacua, which will be the conjugate of the wall between  $l(x) = 1$  and  $l(x) = z^2$ . In this domain, it will be the anti-baryons which will get concentrated. As a result we will have a net segregation of baryons and anti baryons. Though, note that for the concentration of anti-quarks, the above type of conservative estimate of  $10^{42}$  baryon number may not be applicable.

An important point is the choice of initial conditions for calculating  $A_0$ . We will now discuss the effect of this choice of initial conditions on the baryon segregation. As we discussed in section 3.3.3, the ambiguity in the initial condition and hence in determining  $A_0$  is reasonable as we are extracting information about a colored object ( $A_0$ ) starting from a colorless variable  $L(x)$ . Thus there is no reason to expect unique solution for  $A_0$  starting from a given  $L(x)$  profile. This is reflected in the various sets  $(a, b)$  that are available for each of the  $Z(3)$  vacua. It appears that choosing a different sets  $(a, b)$  amounts to selecting domain wall profiles which carries different color information for the scattering of a fixed color (say red) quark. In the present context that would simply mean that if for a specific choice of  $(a, b)$ , on color (say red) is being concentrated inside the collapsing domain, another color (say blue) will be

concentrated in the region for a different choice of  $(a, b)$ . Nonetheless there would be concentration of quarks (or anti-quarks, as the case may be) and the number densities will also be same.

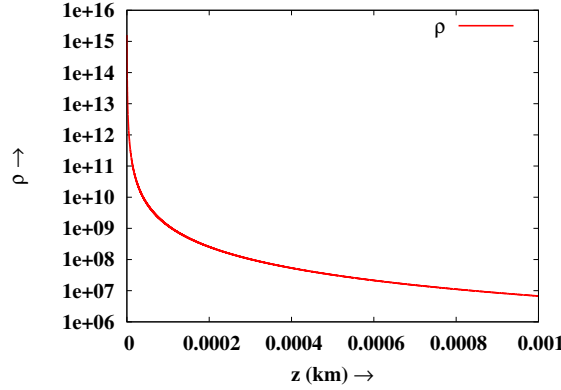


Figure 4.4: Evolution of baryon density profile

In his original proposal, Witten [88] discussed the formation of strangelets. We have not discussed concentration of strange quarks. This is due to the fact that strange quarks are in Klein regime at these temperature i.e. reflection coefficients are greater than unity. As Klein paradox is understood in terms of particle anti-particle pair production, it seems likely that we will have even larger concentration of strange quarks (or anti-strange-quarks) because the pair produced species will also contribute to the number density inside the collapsing volume. However, there is a conceptual complication in doing the quantitative estimation of the number densities. In pair production, there is a back-reaction on the background field. The pair production is at the cost of the energy of the background field, which decreases as more and more particle are pair produced. This is difficult to implement in the present case as the background configuration is a topological configuration and it is not clear how to decrease the magnitude of  $A_0$  here (affecting the magnitude of  $l(x)$ ) while maintaining the topological property of the wall configuration. Nonetheless, it is clear that the concentration of strange quarks/anti-quarks of at least same order as above will be expected in our model, naturally leading to the formation of strangelets. This is one of the strengths of our model that it can naturally lead to formation of strangeness rich quark nuggets. As we mentioned in the introduction, stability of strangelets has

been discussed extensively in the literature and for a wide range of quark numbers the strangelets could be stable. From our discussion of the formation of  $Z(3)$  walls it is clear the formation of small  $Z(3)$  walls is almost unavoidable in the QGP phase. Thus formation of small strangelets will happen very naturally in our model. As we have discussed above, under certain optimistic conditions, even very large strangelets are possible within our model.

## 4.5 Discussions and Conclusions

We have addressed the issue of viability of quark nuggets as dark matter candidates by showing an alternate mechanism for the formation of these objects in the QGP phase of the early universe. Here the nature, or even the existence of quark-hadron phase transition is completely irrelevant. Quarks and anti-quarks are reflected by collapsing  $Z(3)$  walls. This leads to concentration of baryon number in localized regions, forming quark nuggets, exactly as in the original scenario of Witten. This possibility was discussed by some of us in an earlier paper [75] where an effective constituent quark mass was introduced as a function of the Polyakov loop order parameter. Here we have extended that analysis by recognizing that the  $A_0$  field associated with  $l(x)$  leads to spontaneous CP violation leading to different scattering of quarks and anti-quarks from a given  $Z(3)$  wall. Thus one gets quark nuggets as well as anti quark nuggets in this scenario. Such nuggets and anti nuggets have been discussed in recent publications [102] in context of a soft radio background. It would be interesting to explore if these nuggets and anti- nuggets discussed here can play a role in such phenomenon. Importantly, these nuggets and anti-nuggets provide a natural candidate, entirely within the standard model, for dark matter of the universe. Note that as the CP violation here is resulting from a specific domain wall configuration in a given region, overall there will not be any net concentration of baryons or anti-baryons. It is tempting to speculate that with the use of CP violating  $\theta$  term in the QCD Lagrangian, can one get a net concentration of anti-baryons over anti-baryons? If that could be achieved then one can attempt to explain baryogenesis also in this model where excess anti-baryons remain trapped in anti-quark nuggets while compensating baryon number accounts for the visible matter in the universe.

# Chapter 5

## Effect of Quarks

In chapter 2, 3 and 4 we confined our discussion to the pure glue theory. However, the correct theory of strong interactions involves quarks. So for the full understanding of the confinement-deconfinement transition, one need to include the effects of quarks. In this chapter, we'll discuss the effect of dynamical quarks on the spontaneous  $CP$  violation in quark scattering from  $Z(3)$  interface [103].

In section 5.1, we discuss  $Z(N)$  symmetry in presence of dynamical quarks and see that  $Z(N)$  symmetry is violated in presence of quarks. In section 5.1.1, we discuss the effective potential with the effects of dynamical quarks included. We use that effective potential to discuss the scattering of quarks from the  $Z(3)$  interfaces in the subsequent sections. In section 5.2 we obtain the background profile using the effective potential discussed in section 5.1.1. We show that the  $l(x)$  profile is asymmetrical while the background  $A_0$  profile obtained is symmetrical. We then calculate the reflection of quarks, in section 5.3, from the  $Z(3)$  interfaces using the domain walls obtained in section 5.2. We end this chapter with a discussion of the possible implications in section 5.4.

### 5.1 $Z(N)$ Symmetry and Dynamical Quarks

The Polyakov loop acts as the order parameter for the quark hadron phase transition in the infinite quark mass limit. In the case of dynamical quarks this is not an order parameter any more, merely an indicator of the transition. This is due to the fact

that quarks do not respect  $Z(N)$  symmetry as can be seen by the following argument.

When we write the partition function the boundary conditions can be deduced by looking at the thermal Green's function for fermions, which is defined as

$$G(x, y; \tau, 0) = Z^{-1} \text{Tr} \left( e^{-\beta H} \hat{T} [\psi(x, \tau) \psi(y, 0)] \right) \quad (5.1a)$$

$$\text{where } \hat{T} [\psi(x, \tau_1) \psi(y, \tau_2)] = \psi(x, \tau_1) \psi(y, \tau_2) \theta(\tau_1 - \tau_2) - \psi(x, \tau_1) \psi(y, \tau_2) \theta(\tau_2 - \tau_1) \quad (5.1b)$$

is the time ordering operator. Then using the cyclic property of the trace, it can be shown that  $\psi(x, \beta) = -\psi(x, 0)$ . Under  $Z(N)$  transformations, the fermionic fields transform as

$$\psi(x, 0) \longrightarrow \psi'(x, 0) = U^\dagger(x, 0) \psi(x, 0) \quad (5.2a)$$

$$\psi(x, \beta) \longrightarrow \psi'(x, \beta) = Z U^\dagger(x, 0) \psi(x, \beta). \quad (5.2b)$$

It is clear from the above equations that the  $Z(N)$  transformed fields do not respect the anti-periodic boundary conditions for fermions. As a result, fermions do not respect the  $Z(N)$  symmetry. Hence the symmetry is lost in presence of the fermions and it may not be possible to argue for the existence of the  $Z(N)$  vacua in presence of dynamical quarks.

### 5.1.1 Effective potential with Dynamical Quarks

It was argued in [56, 104, 105] that the dynamical quarks act like a “background magnetic field” and break the  $Z(N)$  symmetry explicitly. This leads to the lifting of degeneracy of the ground state with two of the vacua having complex values of Polyakov becoming metastable while the real valued vacua being the true vacua. In the high temperature limit, the pressure difference between the true and the metastable vacua was calculated analytically in [99].

For the effective mean field theory given by eq. 2.34, the explicit breaking term can be added by considering a linear term in  $l(x)$

$$V(l) = \left( -b_1 \frac{(l + l^*)}{2} - b_2 |l|^2 + b_3 (l^3 + (l^*)^3) + |l|^4 \right) b_4 T^4. \quad (5.3)$$

A detailed discussion of the effect of  $b_1$  can be found in [106]. Here we present some of the important points related to the effect of the incorporation of linear term.

For  $b_1 = 0$ , the effective potential turns into that of the pure gauge case and gives a first order phase transition. For very small values of  $b_1$ , the first order phase transition persists and it vanishes for  $b_1 = 0.026$ . For  $b_1 > 0.026$ , there is no true phase transition. It was found that the crossover from the confined to the deconfined regime is rather sharp due to the effect of dynamical quarks. There are other studies [104, 107, 108] that suggest that the explicit breaking of the  $Z(3)$  symmetry due to the dynamical quarks can be very important in determining the critical end point of the deconfining phase transition.

## 5.2 Profile of $Z(3)$ Interfaces with Dynamical Quarks

The explicit symmetry breaking arising from quark effects will have important effects on the structure of  $Z(3)$  walls. For non-degenerate vacua, even planar  $Z(3)$  interfaces do not remain static, and move away from the region with the unique true vacuum. Thus, while for the degenerate vacua case every closed domain wall collapses, for the non-degenerate case this is not true any more. A closed wall enclosing the true vacuum may expand if it is large enough so that the surface energy contribution does not dominate.

The absence of time independent solutions of the field equations for  $Z(3)$  walls leads to complications in the implementation of the techniques of ref. [64] for determination of  $l(x)$  profile for the domain wall which were based on the algorithm of energy minimization. In ref. [64], correct  $l(x)$  profile was obtained from an initial trial profile by fluctuating the value of  $l(x)$  at each lattice point and determining the acceptable fluctuation which lowers the energy (with suitable overshoot criterion etc. as described in detail in ref. [64]). For the case without explicit symmetry breaking, a trial initial configuration of  $l(x)$  with appropriate fixed boundary conditions (corresponding to the two  $Z(3)$  vacua under consideration) yielded correct profile of  $l(x)$  for the wall within relatively few iterations. However, with explicit symmetry breaking, this simple procedure fails as energy can always be lowered by shifting the wall towards to metastable vacua (thus expanding the region with true vacuum).

From the computational point of view, one of the major change due to the inclusion of  $b_1$  term is the the scaling. Without  $b_1$  all the vacua are degenerate, so  $|l(x)| \rightarrow 1$

in all the vacua. However, that is not the case with the potential given by Eq. (5.3). This leads to the  $b_1$  dependence of the scaling. We normalize the potential in such a manner that  $|l(x)| \rightarrow 1$  in the true vacuum. As we mentioned above, the energy splitting between vacua itself amounts to a pressure difference between the two vacua. Thus the program tries to minimize the energy by moving the domain wall in one direction till it goes completely out of the lattice, in the process it changes the boundary values too if they are not held fixed. If we fix the boundary value in the far left and far right region of lattice, the program minimizes the energy by not only moving the profile in the intermediate region but also by re-adjusting the values of  $|l(x)|$  on the two sides. The effect is most pronounced for the large  $b_1$ . This statement becomes clearer if we look at the Fig. 5.1. It shows the initial and the final profile of  $l(x)$  between  $l = 1$  and  $l = z$  vacua for  $b_1 = 0.645$  at  $T = 400 \text{ MeV}$ . The asymmetry is pretty clear in the boundary conditions of the initial trial configuration itself. Note the central region in the final configuration (solid curve). There is a sharp variation of  $|l(x)|$  in a small region and on either side of it the  $|l(x)|$  values are same (but different from actual boundary values) leading to a stable configuration in the middle. Since the domain wall is characterized by the sharp variation of the field in a small spatial region, we fit the profile such that it meets the correct boundary values while keeping the variation as given by the energy minimization program. This is shown by the dotted curve in the left figure. Though this procedure of *smoothing* the domain wall profile near its edges is somewhat ad hoc, it will not affect our results much as the scattering of quarks and antiquarks are primarily decided by the height and width of the sharply varying profile of  $l(x)$ . On comparing with Fig. (3.1) (for  $b_1 = 0$  case), we note that explicit breaking of  $Z(3)$  symmetry leads to asymmetric profiles of  $l(x)$ . This immediately suggests that there will be a difference between the scattering of a quark coming from the right and the scattering of the one coming from left.

The  $A_0$  profile corresponding to the  $l(x)$  profile was calculated in section 3.2.1 (ref. [70]), where we also discussed various conceptual issues related to the ambiguities in the extraction of a colored quantity  $A_0$  from color singlet  $l(x)$ . Here also we choose Polyakov gauge (diagonal gauge) for  $A_0$ . We have carried out this calculation for the profiles of  $l(x)$  obtained from the energy minimization program for  $b_1 \neq 0$ . The calculated  $a, b$  were then used to calculate  $A_0$  using Eq. (3.1). The  $A_0$  profile thus

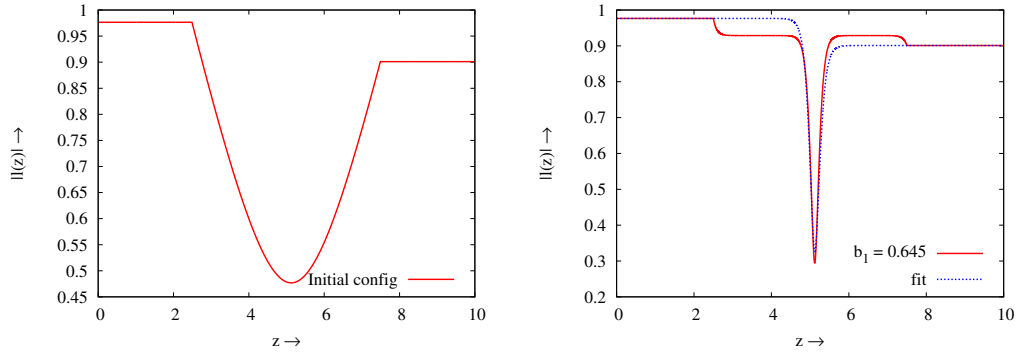


Figure 5.1: Plot of  $|l(x)|$  obtained from energy minimization for  $b_1 = 0.645$  (solid curve). On the left is the initial trial configuration. The final configuration is on right.

obtained is reasonably well fitted to the function  $A_0(x) = p \tanh(qx + r) + s$  using gnuplot. The calculated  $A_0$  profile and fitted  $A_0$  profile are plotted in figure (5.2).

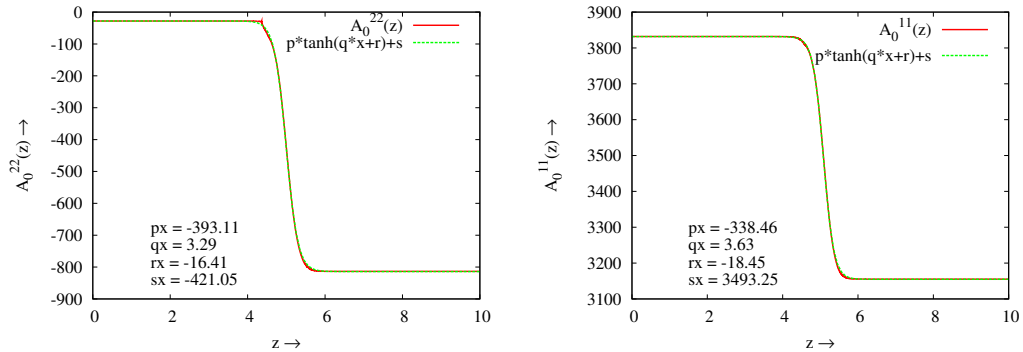


Figure 5.2: Plot of calculated  $A_0$  and the fitted profile ( $A_0(x) = p \tanh(qx + r) + s$ ) for  $b_1 = 0.03$  and  $0.645$ .

We note that the fit to tanh profile is almost perfect just as was the case for  $b_1 = 0$  case in Fig. 3.3. We thus conclude that the scattering of a quark coming from left with such an  $A_0$  profile (in the Dirac equation) will be the same as the scattering of an antiquark coming from right (with same kinetic energy). Thus a collapsing domain wall with  $l = 1$  inside and  $l = z$  outside will give same reflection coefficients (hence resulting concentration) for quarks inside as a collapsing domain wall with  $l = z$  inside and  $l = 1$  outside will give for antiquarks (assuming zero baryon chemical

potential). This is interesting in view of the asymmetric profiles of  $l(x)$  in Fig. 5.1 for  $b_1 \neq 0$  cases. Though still there will be important differences from the  $b_1 = 0$  case as now a sufficiently large closed domain wall with true vacuum ( $l = 1$ ) inside will expand instead of collapsing, leading to concentration of quarks or antiquarks in a shell like region. We will discuss these possibilities later in section 5.4.

It may also be noted that we have shown  $A_0^{11}$  for  $b_1 = 0.645$  and  $A_0^{22}$  for  $b_1 = 0.03$ . This is for the reason that both the profiles are similar in the shape and size. It has to do with the choice of initial  $(a, b)$  values while calculating  $A_0$ . This essentially means that we should compare the reflection of red quark in  $b_1 = 0.645$  case with the reflection of green quark in  $b_1 = 0.03$  case. One may use hit and trial method to find a specific choice of  $(a, b)$  in the case of  $b_1 = 0.03$  such that  $A_0^{11}$  obtained has the same spatial variation as the one for  $b_1 = 0.645$  (see the discussion before the fig. ??).

As we mentioned, it is interesting to note that asymmetry of  $l(x)$  is not reflected in the background gauge configuration. The effect of non-zero  $b_1$  is reflected in the  $A_0$  profile not in terms of the change in shape but in terms of the height of the potential getting reduced. For  $b_1 = 0.645$ , the height of  $A_0$  is almost 100 MeV less than the height of  $A_0$  in  $b_1 = 0.03$  case. However, this decrease in the height will not give any asymmetry in the reflection of quarks and anti-quarks from the  $A_0$ , neither will it change the amount of reflection in a drastic fashion. We will now consider another possibility which allows for asymmetry in concentration of quarks and antiquarks for the  $b_1 \neq 0$  case.

For this we recall the discussion of quark/antiquark scattering due to  $l$  dependent effective mass, as discussed in ref. [75]. The basic idea proposed in ref. [75] was that as  $l(x)$  is the order parameter for the quark-hadron transition, physical properties such as effective mass of the quarks should be determined in terms of  $l(x)$ . This also looks natural from the expected correlation between the chiral condensate and the Polyakov loop. Lattice results indicate that the chiral phase transition and the deconfinement phase transition may be coupled, i.e as the Polyakov loop becomes non zero across  $T_c$ , the chiral order parameter attains a vanishingly small value. Thus, if there is spatial variation in the value of  $l(x)$  in the QGP phase then effective mass of the quark traversing that region should also vary (say, due to spatially varying chiral condensate). For regions where  $l(x) = 0$ , quarks should acquire constituent

mass as appropriate for the confining phase. To model the dependence of effective quark mass on  $l(x)$  we could use the color dielectric model of ref. [109] identifying  $l(x)$  with the color dielectric field  $\chi$  in ref. [109]. Effective mass of the quark was modeled in [109] to be inversely proportional to  $\chi$ . This leads to divergent quark mass in the confining phase consistent with the notion of confinement. However, we know that the divergence of quark energy in the confining phase should be a volume divergence (effectively the length of string connecting the quark to the boundary of the volume).  $1/l(x)$  dependence will not have this feature, hence we do not follow this choice. For the sake of simplicity, and for order of magnitude estimates at this stage, we will model the quark mass dependence on  $l(x)$  in the following manner.

$$m(x) = m_q + m_0(l_0 - |l(x)|) \quad (5.4)$$

Here  $l(x)$  represents the profile of the  $Z(3)$  domain wall, and  $l_0$  is the vacuum value of  $|l(x)|$  (for the true vacuum) appropriate for the temperature under consideration.  $m_q$  is the current quark mass of the quark as appropriate for the QGP phase with  $|l(x)| = l_0$ , with  $m_u \simeq m_d = 10$  MeV and  $m_s \simeq 140$  MeV.  $m_0$  characterizes the constituent mass contribution for the quark. We will take  $m_0 = 300$  MeV. Note that here  $m(x)$  remains finite even in the confining phase with  $l(x) = 0$ . As mentioned above, this is reasonable since we are dealing with a situation where  $l(x)$  differs from  $l_0$  only in a region of thickness of order  $1fm$  (thickness of domain wall).

The space dependent part of  $m(x)$  in Eq.(5.4) is taken as a potential term in the Dirac equation for the propagation of quarks and antiquarks. As we see from Fig.(5.1),  $l(x)$  varies across a  $Z(3)$  interface, acquiring small magnitude in the center of the wall. A quark passing through this interface, therefore, experiences a nonzero potential barrier leading to non-zero reflection coefficient for the quark. Important thing here is that due to asymmetric profile of  $l$  (Fig.(5.1)), the effective mass of quarks/antiquarks will have different values on the two sides of the domain wall. This effect, when combined with the scattering from the background  $A_0$  configuration, will lead to asymmetry in the scattering of quarks from one side and that of antiquarks from the other side of the domain wall.

One may be concerned here whether combining the scattering from  $A_0$  configuration with the scattering due to  $l$  dependent effective mass amounts to double

counting in the sense that both effects originate from the same  $l(x)$  profile. For this we note that there are indeed two different effects at play here due to the existence of  $Z(3)$  walls. First effect arises from the existence of three different phases of QGP characterized by spontaneous breaking of  $Z(3)$  symmetry. In the absence of explicit symmetry breaking one will expect that physics should be identical for these three phases. Thus, even  $l$  dependent effective mass of quarks should have the same value in these three phases, as indeed is the case from Eq. (5.4) due to same value of  $|l|$  in the three  $Z(3)$  phases. However, with explicit symmetry breaking, there is no physical argument to say that physics should be the same for the three  $Z(3)$  vacua, as the two vacua ( $l = z$  and  $l = z^2$ ) become metastable. As  $|l|$  in these two vacua has smaller magnitude, effective mass of quarks may actually be larger in these two phases of QGP. As explained for Eq.(5.4), we can think of this  $|l|$  dependent mass in terms of chiral condensate whose value will depend on  $l(x)$ . (We mention that  $l(x)$  dependent quark mass by itself is a non-trivial implication of our proposal and it will have many other interesting implications on propagation of quarks/antiquarks in QGP in the presence of these  $Z(3)$  domains.) Next we come to the presence of background gauge field. This arises from spatial variation of  $l(x)$  leading to color electric field from which quarks and antiquarks scatter in different manner. This color electric field is entirely localized at the boundary of  $Z(3)$  domains (where  $l(x)$  has spatial variation), and vanishes in the interiors of the  $Z(3)$  domains. It couples differently to quarks/antiquarks of different color charges. Hence, this effect is entirely different from the effect of effective mass which has different values in the interiors of the two domains, irrespective of the color charges of quarks and antiquarks (even though for the scattering purposes, both effects lead to non-trivial potential at the location of the  $Z(3)$  wall).

### 5.3 Reflection and Transmission Coefficients with explicit symmetry breaking

We now calculate the reflection and transmission coefficient for quarks and antiquarks subject to the above two effects. One is CP violating, arising from the background

gauge field  $A_0$  (Eq.(3.1)), and the other is CP preserving, arising from the space dependent effective mass of quarks/antiquarks (Eq.(5.4)). We recall the steps for calculation from [70]. To calculate the reflection and transmission coefficient, we need the solutions of Dirac equation in the Minkowski space but the  $A_0$  profile is calculated in Euclidean space. We start with the Dirac equation in the Euclidean space, with the spatial dependence of  $A_0$  calculated from  $Z(3)$  wall profile as mentioned above, and with space dependent mass term as given in Eq.(9).

$$[\gamma_e^0 \partial_0 \delta^{jk} - g \gamma_e^0 A_0^{jk}(z) + (i \gamma_e^3 \partial_3 + m(x)) \delta^{jk}] \psi_k = 0, \quad (5.5)$$

where  $\gamma_e^0 \equiv i \gamma^0$  and  $\gamma_e^3 \equiv \gamma^3$  are the Euclidean Dirac matrices.  $\partial_0$  denotes  $\partial/\partial\tau$  with  $\tau = it$  being the Euclidean time.  $j, k$  denote color indices.  $m(x)$  is the effective mass as given in Eq.(9). We now analytically continue the Eq. (5.5) to the Minkowski space to get

$$[i \gamma^0 \partial_0 \delta^{jk} + g \gamma^0 A_0^{jk}(z) + (i \gamma^3 \partial_3 + m(x)) \delta^{jk}] \psi_k = 0. \quad (5.6)$$

where now  $\partial_0$  denotes  $\partial/\partial t$  in the Minkowski space.

Eq.(5.6) is used to calculate the reflection and transmission coefficients. The results for charm quark and anti-quark (with  $E = 3.0 \text{ GeV}$  taken as example for each case) are given in table 5.1. As we mentioned, the important quantity for us is to calculate the reflection coefficient of (say) quarks coming from the left of the wall and compare it with the reflection coefficient of antiquarks (with the same kinetic energy) coming from the right of the wall. Any (possible) difference in these two reflection coefficients directly relates to the expected concentration of quarks and antiquarks by a domain wall of one kind and its opposite wall (interpolating between the two  $Z(3)$  vacua in reverse order). Table 5.1 shows clear difference in these two reflection coefficients.

## 5.4 Discussion

In this work we have extended our earlier studies of CP violating scattering of quarks/antiquarks from  $Z(3)$  walls [70, 87, 110], by including the effects of explicit breaking of  $Z(3)$  symmetry which is expected to arise due to dynamical quarks. The resulting profile of  $l(x)$  between the true vacuum and a metastable vacuum is no more

	$b_1 = 0.03$	0.126	0.645
Left $R_q$	$1.65437 \times 10^{-6}$	$4.40706 \times 10^{-6}$	$1.43314 \times 10^{-10}$
Right $R_q$	0.00003366	0.0141752	0.00394808
Left $R_{aq}$	$2.25671 \times 10^{-6}$	$1.85367 \times 10^{-7}$	$2.07835 \times 10^{-7}$
Right $R_{aq}$	0.000376883	0.0820803	0.073885

Table 5.1: Table for the reflection coefficients for charm quark and antiquark for smooth profiles of  $A_0$  and  $m(x)$ .

symmetric in this case which leads to new effects. We study scattering of quarks and antiquarks from the background  $A_0$  field associated with the profile of  $l(x)$  while also incorporating the effect of spatially varying effective mass of quarks and antiquarks in the respective  $Z(3)$  domains. The combined effect of the scattering shows interesting behavior leading to left-right asymmetry in scattering of quarks (from left) and antiquarks (from right). This will lead to important differences in resulting concentrations of quarks and antiquarks in cosmology as well as in RHICE. For example, in the early universe, a network of domain walls will arise with varying sizes and interpolating between different  $Z(3)$  vacua. For all domain walls of a given size interpolating between given two vacua in a given order, there will be roughly same number of walls with similar size but interpolating between the same two  $Z(3)$  vacua in the reverse order. (Though explicit symmetry breaking may also produce difference between formation of such walls, introducing further richness in the effects of explicit symmetry breaking). In the absence of explicit symmetry breaking, if first type of walls give certain concentration of (say) quarks, then the other set of walls will give similar concentration of antiquarks. This is, however, not the case when explicit symmetry breaking effects are incorporated. In view of results from table 5.1, the two sets of walls will lead to very different concentrations of quarks and antiquarks (especially if the value of  $b_1$  is large). Though for each domain wall (say interpolating between  $l = 1$  and  $l = z$ , there is always the *conjugate* wall (interpolating between  $l = 1$  and  $l = z^2$ ) which will lead to same scattering between quarks and antiquarks. Final effect of our results will then appear as two different magnitudes for the concentrations of quarks and antiquarks, even if one takes all domain walls of the same size. This is

very different from the case without explicit symmetry breaking where domain walls of same size will lead to quark and antiquark inhomogeneities of same magnitude (for same kinetic energies of quarks and antiquarks). This difference will be particularly dramatic for RHICE where number of domain walls is of order one for each event [67]. Thus even for same type of events, one may get very different concentration of baryons or antibaryons in different events leading to very large event-by-event fluctuations.

Situation is even more interesting when we consider the effect that with explicit symmetry breaking certain closed domain walls may expand, those with true vacuum inside (and with sufficiently larger size so that volume energy difference dominates over the surface energy contribution [66]). This can lead to concentration of quarks and antiquarks in a shell like structure. For cosmology very large expanding domain walls may trap shells of baryons/antibaryons if enclosed by a collapsing *antiwall* configuration. Such shells can form in RHICE also and will have important observations signatures.

# Chapter 6

## Summary

We are finally ready to summarize this thesis. In this thesis, we have considered non-trivial scattering of quarks and anti-quarks from background gauge fields associated with the  $Z(3)$  walls. These  $Z(3)$  walls appear as the topological defects in the Quark Gluon Plasma (QGP) phase of QCD at high temperature. After providing a brief introduction to the QCD phase diagram and the Relativistic Heavy Ion Collisions (RHIC) experiments, that are being conducted to study this QGP phase in detail, we discussed the confinement-deconfinement transition in a bit detail in chapter 2. The confinement-deconfinement transition has an associated order parameter (in the infinite quark mass limit) which is the thermal expectation value of the Polyakov loop, which is defined as

$$l(x) = \text{Tr} \left\{ \mathbf{P} \left[ \exp \left( ig \int_0^\beta d\tau A_0(x) \right) \right] \right\}. \quad (6.1)$$

where,  $A_0(\vec{x}, \tau) = A_0^a(\vec{x}, \tau) T^a$ , ( $a = 1, \dots, N$ ) are the gauge fields and  $T^a$  are the generators of  $SU(N)$  in the fundamental representation.  $\mathbf{P}$  denotes the path ordering in the Euclidean time  $\tau$ ,  $\beta = T^{-1}$  and  $g$  is the gauge coupling. It relates to the change in the free energy of the system when a static test quark is put in a pure gluonic system ( $\langle l(x) \rangle \propto e^{-\beta F}$ ). In the confined (hadron) phase the energy required to add a color charge (quark) is infinite hence  $l(x)$  is zero, while in the deconfined phase only a finite amount of energy is required and as a result  $l(x)$  is finite.

Under the action of  $Z(3)$ , which is the center of  $SU(N)$ ,  $l(x) \rightarrow z l(x)$ , where  $z$  is an element of  $Z(3)$  ( $z = 1, e^{2\pi i/3}, e^{4\pi i/3}$ ). In the confined phase,  $l(x) = 0$ , so it's

invariant under the action of  $Z(3)$  but this is not the case in the deconfined phase. As a result there are 3 distinct ground states in the deconfined phase, connected by  $Z(3)$  rotations. Thus  $Z(3)$  is not the symmetry of the order parameter, it's spontaneously broken in the deconfined phase. Using the symmetry arguments, an effective potentials that capture these properties was constructed by Pisarski, which we outlined in section 2.2.4. One of the most interesting consequence of spontaneous symmetry breaking is the formation of topological defects. The type of topological defects formed depends upon the topology of the set of values order parameter is allowed to take in the ground state (vacuum manifold). We provided some discussion on the formation of topological defects via Kibble mechanism and presented some examples of topological defects from condensed matter systems. In case of the Polyakov loop the vacuum manifold is a set of discrete values hence this system has domain walls as the topological defects. These are the domain walls between different  $Z(3)$  vacua.

The discussion in chapter 3 was based on our work [1]. We calculated the detailed profile of  $A_0$  using the profile of  $l(x)$  between different  $Z(3)$  vacua and calculated the reflection and transmission coefficients for the pure gauge case. The profile of  $l(x)$  was calculated by minimizing the energy of a trial configuration with appropriate boundary conditions. To calculate  $A_0$  from  $l(x)$ , we inverted eq (6.1). Working in the diagonal gauge we determined the profile of  $A_0$  and used it to calculate the reflection and transmission coefficients for quarks and anti-quarks. It was found that the  $CP$  violating effect was stronger for heavier quarks. We repeated this calculation of  $A_0$  profile for another choice of effective potential of the Polyakov loop as provided by Fukushima to address the issue of the model dependence of the background gauge field. We found that even though the two effective potentials are of qualitatively different shapes, with polynomial type effective potential and logarithmic effective potential, the resulting  $l(x)$  profile of the wall and the associated  $A_0$  profile were very similar. This gives us confidence that our conclusions arising from the calculations of scattering of quarks and antiquarks from  $Z(3)$  walls are not crucially dependent on the specific choice of the effective potential. This  $CP$  violation was first demonstrated by Altes et al. However, the entire discussion was in the Euclidean formalism and detailed gauge field profile associated with the  $Z(3)$  interfaces was not determined.

Our universe has undergone through various phase transition during it's evolution.

The QCD phase transition occurred just few micro seconds after the big bang. The implications of this CP violation in context the Universe was the subject of study of the work presented in chapter 4. One important difference for the formation of  $Z(3)$  walls compared to the formation of other topological defects in the early universe arises from the fact that here symmetry is broken in the high temperature phase, and is restored as the universe cools while expanding. Standard mechanism of formation of defects (the Kibble mechanism) leads to the formation of defects during the transition to the symmetry broken phase. An appropriate scenario for the formation of these  $Z(3)$  domains in early universe can be most naturally discussed in the framework of Inflationary cosmology. During inflation, universe cools rapidly and temperature drops below the critical temperature for confinement-deconfined transition. After inflation, universe reheats and the temperature rises above the hadron-quark transition temperature. The  $Z(3)$  symmetry will then break spontaneously, and  $Z(3)$  walls and associated QGP string will form via the standard Kibble mechanism. However in presence of quarks, there is an explicit breaking of  $Z(3)$  symmetry with  $l(x) = z, z^2$ , becoming metastable. This results in a pressure difference between the true vacuum and the metastable vacua. This leads to a preferential shrinking of metastable vacua due to which these domains are unlikely to survive until late times. However it is possible to argue that in certain low energy inflationary models, these  $Z(3)$  domains can survive until the QCD scale. Another possibility is that when effects of quarks scattering from the walls is taken into account their collapse may be slower due to the friction experienced by domain wall. For large friction, the walls may even remain almost frozen in the plasma. With inclusion of some friction in the dynamics of domain walls in the low scale inflationary models, it is then possible for the walls to survive until QCD transition. It may then be possible to ignore the effect of explicit symmetry breaking.

With the above mentioned optimistic scenario, we studied the effects of such large domain walls in the universe, near the QCD phase transition epoch. We showed that due to this CP violation there is a baryon-antibaryon segregation that can lead to the formation of quark nuggets in early universe. The formation of quark nuggets was first proposed by Witten [88]. He proposed that if the universe underwent a (strong) first order QCD phase transition, then localized regions of high temperature phase,

trapped between expanding hadronic bubbles, will shrink, in the process trapping the baryons inside them. He also argued that resulting quark nuggets may be stable and survive up-to the present epoch. With lattice QCD calculations ruling out the first order phase transition, the interest in the quark nuggets died away. However the  $Z(3)$  walls exist in the QGP phase as topological defects, forming irrespective of the order of the quark-hadron phase transition, even if it is a cross-over. Hence, the formation of quark nuggets in our model is via a very different mechanism than the originally proposed one and works independent of the order of the quark-hadron transition.

We calculated the evolution of baryon density within a collapsing domain by studying the baryon transport across the  $Z(3)$  wall [87]. We found that at  $T = 400 \text{ MeV}$ , the baryon concentration inside the domain wall to be of the order of  $10^{52}$  when the domain wall size is roughly one meter. This is the upper limit where we do not consider any anti-quark to be present inside. Net baryon number to entropy ratio is about  $10^{-10}$ , hence it is safe to say that at least net baryon number of order  $10^{42}$  can be trapped inside collapsing domain walls. These quark nuggets may survive till now and may provide the dark matter candidates within the standard model. There were many investigations discussing the issues of stability of such objects. It was generally considered that quark nuggets (strangelets) having density above nuclear density, with baryon number ranging from few Thousand to  $\sim 10^{50}$  (sizes varying from fm to meters) may provide required dark matter. Such a candidate for dark matter will be extremely appealing as it does not require any physics beyond standard model.

In chapter 5 we extend our first work [70] by incorporating the effects of quarks in the effective potential [?]. The presence of quarks lifts the degeneracy of different  $Z(3)$  vacua with the two vacua ( $l(x) = z, z^2$ ) becoming metastable.  $Z(3)$  interfaces are no more solutions of time independent field equations as they move away from the region with the unique true vacuum. However, this does not mean that these domains do not survive as the topological structures. As the resulting profile of  $l(x)$  between the true vacuum and a metastable vacuum is no more symmetric it raises interesting possibilities for the generation of quark and antiquark inhomogeneities as a network of collapsing domain walls is considered, with different walls interpolating between different sets of  $Z(3)$  vacua. The effect of quarks is accounted for by adding a linear term in the Pisarski potential, which breaks the  $Z(3)$  symmetry explicitly.

The coefficient of the linear term measures the extent of symmetry breaking.

On calculating the  $l(x)$  profile for the effective potential with the linear term, we found that explicit breaking of  $Z(3)$  symmetry leads to asymmetric profiles of  $l(x)$ . As expected, the extent of asymmetry depended on the extent of symmetry breaking i.e. on the coefficient of the linear term. We obtained the  $A_0$  profile from the asymmetric  $l(x)$  profile. We find that even though the profile of  $l(x)$  is asymmetric in this case (under reflection  $x \rightarrow -x$ ) quark-antiquark scattering from the gauge field configuration associated with it does not show any difference from the symmetric case when explicit  $Z(3)$  symmetry breaking is absent. The only difference is in the height of the potential which depends on the extent of symmetry breaking. Changing the coefficient of linear term by a factor of 20 produced a change of roughly 15% in the height of the potential. In short, the scattering of a quark from left on the wall is identical to the scattering of an antiquark from the right, as was the case in  $A_0$  profile obtained for the case with symmetric  $l(x)$  profile. To incorporate the effect of asymmetry, we modeled the dependence of effective quark mass on the magnitude of the Polyakov loop order parameter  $l(x)$ . Spatially varying profile of  $l(x)$  leads to spatially varying effective mass, which behaves as potential in the Dirac equation for quarks/antiquarks leading to non-trivial scattering. Both these effects lead to asymmetry in the scattering of quarks from one side and that of antiquarks from the other side of the domain wall. We find that the reflection coefficient of a quark coming from the left is roughly thousand times smaller than that of an anti-quark coming from the right (for the charm quark). We discuss the implications of these asymmetric reflection and transmission coefficients in context of early universe and also in the case of relativistic heavy ion collisions (like generation of event by event fluctuations in the heavy ion collisions due to  $Z(3)$  domains).

# Bibliography

- [1] M. Gell-Mann, Phys. Rev. **92**, 833 (1953).
- [2] T. Nakano and K. Nishijima, Prog. Theor. Phys. **10**, 581 (1953).
- [3] M. Gell-Mann, CTSL-20.
- [4] Y. Ne'eman, Nucl. Phys. **26**, 222 (1961).
- [5] J. Prentki,
- [6] M. Gell-Mann, Phys. Lett. **8**, 214 (1964).
- [7] G. Zweig, CERN-TH-401.
- [8] G. Zweig, Developments in the Quark Theory of Hadrons, Volume 1. Edited by D. Lichtenberg and S. Rosen. pp. 22-101
- [9] O. W. Greenberg, Phys. Rev. Lett. **13**, 598 (1964).
- [10] M. Y. Han and Y. Nambu, Phys. Rev. **139**, B1006 (1965).
- [11] D. J. Gross and F. Wilczek, Phys. Rev. Lett. **30**, 1343 (1973).
- [12] H. D. Politzer, Phys. Rev. Lett. **30**, 1346 (1973).
- [13] K. Johnson, Acta Phys. Polon. B **6**, 865 (1975).
- [14] J. Cleymans, R. V. Gavai and E. Suhonen, Phys. Rept. **130**, 217 (1986).
- [15] K. Fukushima and T. Hatsuda, Rept. Prog. Phys. **74**, 014001 (2011)  
[arXiv:1005.4814 [hep-ph]].
- [16] M. Fukugita, M. Okawa and A. Ukawa, Nucl. Phys. B **337**, 181 (1990).

- [17] Y. Aoki, G. Endrodi, Z. Fodor, S. D. Katz and K. K. Szabo, *Nature* **443**, 675 (2006) [hep-lat/0611014].
- [18] C. DeTar and U. M. Heller, *Eur. Phys. J. A* **41**, 405 (2009) [arXiv:0905.2949 [hep-lat]].
- [19] K. Rajagopal and F. Wilczek, In \*Shifman, M. (ed.): At the frontier of particle physics, vol. 3\* 2061-2151 [hep-ph/0011333].
- [20] L. McLerran and R. D. Pisarski, *Nucl. Phys. A* **796**, 83 (2007) [arXiv:0706.2191 [hep-ph]].
- [21] A. Andronic, D. Blaschke, P. Braun-Munzinger, J. Cleymans, K. Fukushima, L. D. McLerran, H. Oeschler and R. D. Pisarski *et al.*, *Nucl. Phys. A* **837**, 65 (2010) [arXiv:0911.4806 [hep-ph]].
- [22] T. Peitzmann, *Pramana* **60**, 651 (2003) [nucl-ex/0201003].
- [23] G. Agakichiev *et al.* [CERES Collaboration], *Phys. Rev. Lett.* **75**, 1272 (1995).
- [24] A. Toia [PHENIX Collaboration], *Nucl. Phys. A* **774**, 743 (2006) [nucl-ex/0510006].
- [25] J. Rafelski and B. Muller, *Phys. Rev. Lett.* **48**, 1066 (1982) [Erratum-ibid. **56**, 2334 (1986)].
- [26] P. Koch, B. Muller and J. Rafelski, *Phys. Rept.* **142**, 167 (1986).
- [27] F. Antinori *et al.* [NA57 Collaboration], *J. Phys. G* **32**, 427 (2006) [nucl-ex/0601021].
- [28] B. I. Abelev *et al.* [STAR Collaboration], *Phys. Rev. C* **77**, 044908 (2008) [arXiv:0705.2511 [nucl-ex]].
- [29] A. R. Timmins [STAR Collaboration], *J. Phys. G* **36**, 064006 (2009) [arXiv:0812.4080 [nucl-ex]].
- [30] T. Matsui and H. Satz, *Phys. Lett. B* **178**, 416 (1986).
- [31] M. C. Abreu *et al.* [NA50 Collaboration], *Phys. Lett. B* **410**, 337 (1997).

- [32] B. Alessandro *et al.* [NA50 Collaboration], Eur. Phys. J. C **39**, 335 (2005) [hep-ex/0412036].
- [33] A. Adare *et al.* [PHENIX Collaboration], Phys. Rev. Lett. **98**, 232301 (2007) [nucl-ex/0611020].
- [34] A. Adare *et al.* [PHENIX Collaboration], Phys. Rev. C **84**, 054912 (2011) [arXiv:1103.6269 [nucl-ex]].
- [35] B. Abelev *et al.* [ALICE Collaboration], Phys. Rev. Lett. **109**, 072301 (2012) [arXiv:1202.1383 [hep-ex]].
- [36] P. Braun-Munzinger and J. Stachel, Phys. Lett. B **490**, 196 (2000) [nucl-th/0007059].
- [37] R. L. Thews, M. Schroedter and J. Rafelski, Phys. Rev. C **63**, 054905 (2001) [hep-ph/0007323].
- [38] A. Andronic, P. Braun-Munzinger, K. Redlich and J. Stachel, Phys. Lett. B **652**, 259 (2007) [nucl-th/0701079 [NUCL-TH]].
- [39] X. Zhao and R. Rapp, Phys. Lett. B **664**, 253 (2008) [arXiv:0712.2407 [hep-ph]].
- [40] K. H. Ackermann *et al.* [STAR Collaboration], Phys. Rev. Lett. **86**, 402 (2001) [nucl-ex/0009011].
- [41] D. A. Teaney, arXiv:0905.2433 [nucl-th].
- [42] K. Adcox *et al.* [PHENIX Collaboration], Phys. Rev. Lett. **88**, 022301 (2002) [nucl-ex/0109003].
- [43] C. Adler *et al.* [STAR Collaboration], Phys. Rev. Lett. **89**, 202301 (2002) [nucl-ex/0206011].
- [44] G. Aad *et al.* [ATLAS Collaboration], Phys. Rev. Lett. **105**, 252303 (2010) [arXiv:1011.6182 [hep-ex]].
- [45] E. W. Kolb and M. S. Turner, “The Early Universe,” Front. Phys. **69**, 1 (1990).

- [46] S. Dodelson, “Modern cosmology,” Amsterdam, Netherlands: Academic Pr. (2003) 440 p
- [47] M. Kardar, “Statistical Physics of Fields,” Cambridge University Press (2007)
- [48] N. D. Mermin, Rev. Mod. Phys. **51**, 591 (1979).
- [49] L. D. McLerran and B. Svetitsky, Phys. Rev. D **24**, 450 (1981).
- [50] T. Celik, J. Engels and H. Satz, Phys. Lett. B **129**, 323 (1983).
- [51] F. Karsch and E. Laermann, Phys. Rev. D **50**, 6954 (1994) [hep-lat/9406008].
- [52] T. Umeda, S. Ejiri, S. Aoki, T. Hatsuda, K. Kanaya, Y. Maezawa and H. Ohno, Phys. Rev. D **79**, 051501 (2009) [arXiv:0809.2842 [hep-lat]].
- [53] F. Karsch and E. Laermann, In \*Hwa, R.C. (ed.) et al.: Quark gluon plasma\* 1-59 [hep-lat/0305025].
- [54] R. D. Pisarski, Phys. Rev. D **62**, 111501 (2000) [hep-ph/0006205].
- [55] R. D. Pisarski, hep-ph/0203271.
- [56] T. Banks and A. Ukawa, Nucl. Phys. B **225**, 145 (1983).
- [57] A. Dumitru and R. D. Pisarski, Phys. Lett. B **504**, 282 (2001) [hep-ph/0010083].
- [58] A. Dumitru and R. D. Pisarski, Nucl. Phys. A **698**, 444 (2002) [hep-ph/0102020].
- [59] A. Dumitru and R. D. Pisarski, Phys. Rev. D **66**, 096003 (2002) [hep-ph/0204223].
- [60] G. Boyd, J. Engels, F. Karsch, E. Laermann, C. Legeland, M. Lutgemeier and B. Petersson, Nucl. Phys. B **469**, 419 (1996) [hep-lat/9602007].
- [61] M. Okamoto *et al.* [CP-PACS Collaboration], Phys. Rev. D **60**, 094510 (1999) [hep-lat/9905005].
- [62] A. Dumitru, Y. Hatta, J. Lenaghan, K. Orginos and R. D. Pisarski, Phys. Rev. D **70**, 034511 (2004) [hep-th/0311223].

- [63] T. W. B. Kibble, *J. Phys. A* **9**, 1387 (1976).
- [64] B. Layek, A. P. Mishra and A. M. Srivastava, *Phys. Rev. D* **71**, 074015 (2005) [hep-ph/0502250].
- [65] M. Deka, S. Digal and A. P. Mishra, *Phys. Rev. D* **85**, 114505 (2012) [arXiv:1009.0739 [hep-lat]].
- [66] U. S. Gupta, R. K. Mohapatra, A. M. Srivastava and V. K. Tiwari, *Phys. Rev. D* **86**, 125016 (2012) [arXiv:1111.5402 [hep-ph]].
- [67] U. S. Gupta, R. K. Mohapatra, A. M. Srivastava and V. K. Tiwari, *Phys. Rev. D* **82**, 074020 (2010) [arXiv:1007.5001 [hep-ph]].
- [68] C. P. Korthals Altes and N. J. Watson, *Phys. Rev. Lett.* **75**, 2799 (1995) [hep-ph/9411304].
- [69] C. P. Korthals Altes, K. M. Lee and R. D. Pisarski, *Phys. Rev. Lett.* **73**, 1754 (1994) [hep-ph/9406264].
- [70] A. Atreya, A. M. Srivastava and A. Sarkar, *Phys. Rev. D* **85**, 014009 (2012) [arXiv:1111.3027 [hep-ph]].
- [71] K. Fukushima, *Phys. Lett. B* **591**, 277 (2004) [hep-ph/0310121].
- [72] N. Weiss, *Phys. Rev. D* **24**, 475 (1981).
- [73] N. Weiss, *Phys. Rev. D* **25**, 2667 (1982).
- [74] C. P. Korthals Altes, In \*Dallas 1992, Proceedings, High energy physics, vol. 2\* 1443-1447
- [75] B. Layek, A. P. Mishra, A. M. Srivastava and V. K. Tiwari, *Phys. Rev. D* **73**, 103514 (2006) [hep-ph/0512367].
- [76] K. Kajantie, L. Karkkainen and K. Rummukainen, *Nucl. Phys. B* **357**, 693 (1991).
- [77] T. Bhattacharya, A. Gocksch, C. Korthals Altes and R. D. Pisarski, *Phys. Rev. Lett.* **66**, 998 (1991).

- [78] S. Roessner, C. Ratti and W. Weise, Phys. Rev. D **75**, 034007 (2007) [hep-ph/0609281].
- [79] B. J. Schaefer, J. M. Pawłowski and J. Wambach, Phys. Rev. D **76**, 074023 (2007) [arXiv:0704.3234 [hep-ph]].
- [80] T. M. Kalotas and A. R. Lee Am. J. Phys. **59**, 48 (1991).
- [81] C. Itzykson and J. B. Zuber, New York, Usa: McGraw-hill (1980) 705 P.(International Series In Pure and Applied Physics)
- [82] A. P. Mishra, A. M. Srivastava and V. K. Tiwari, Indian J. Phys. **85**, 1161 (2011).
- [83] M. Ciminale, R. Gatto, N. D. Ippolito, G. Nardulli and M. Ruggieri, Phys. Rev. D **77**, 054023 (2008) [arXiv:0711.3397 [hep-ph]].
- [84] W. j. Fu, Z. Zhang and Y. x. Liu, Phys. Rev. D **77**, 014006 (2008) [arXiv:0711.0154 [hep-ph]].
- [85] P. Costa, M. C. Ruivo, C. A. de Sousa, H. Hansen and W. M. Alberico, Phys. Rev. D **79**, 116003 (2009) [arXiv:0807.2134 [hep-ph]].
- [86] G. Marko and Z. Szep, Phys. Rev. D **82**, 065021 (2010) [arXiv:1006.0212 [hep-ph]].
- [87] A. Atreya, A. Sarkar and A. M. Srivastava, Phys. Rev. D **90**, 045010 (2014) [arXiv:1405.6492 [hep-ph]].
- [88] E. Witten, Phys. Rev. D **30**, 272 (1984).
- [89] P. Bhattacharjee, J. e. Alam, B. Sinha and S. Raha, Phys. Rev. D **48**, 4630 (1993).
- [90] G. Lugones and J. E. Horvath, Phys. Rev. D **69**, 063509 (2004) [astro-ph/0310082].
- [91] A. Bhattacharyya, S. Banerjee, S. K. Ghosh, S. Raha, B. Sinha and H. Toki, Pramana **60**, 909 (2002).

- [92] P. W. Gorham, Phys. Rev. D **86**, 123005 (2012) [arXiv:1208.3697 [astro-ph.CO]].
- [93] P. Astone, M. Bassan, E. Coccia, S. D'Antonio, V. Fafone, G. Giordano, A. Marini and Y. Minenkov *et al.*, arXiv:1306.5164 [astro-ph.HE].
- [94] A. Berera, Phys. Rev. Lett. **75**, 3218 (1995) [astro-ph/9509049].
- [95] J. Yokoyama and A. D. Linde, Phys. Rev. D **60**, 083509 (1999) [hep-ph/9809409].
- [96] L. Knox and M. S. Turner, Phys. Rev. Lett. **70**, 371 (1993) [astro-ph/9209006].
- [97] E. J. Copeland, D. Lyth, A. Rajantie and M. Trodden, Phys. Rev. D **64**, 043506 (2001) [hep-ph/0103231].
- [98] B. J. W. van Tent, J. Smit and A. Tranberg, JCAP **0407**, 003 (2004) [hep-ph/0404128].
- [99] V. Dixit and M. C. Ogilvie, Phys. Lett. B **269**, 353 (1991).
- [100] E. Chudnovsky and A. Vilenkin, Phys. Rev. Lett. **61**, 1043 (1988).
- [101] C. J. A. P. Martins and E. P. S. Shellard, Phys. Rev. D **53**, 575 (1996) [hep-ph/9507335].
- [102] K. Lawson and A. R. Zhitnitsky, Phys. Lett. B **724**, 17 (2013) [arXiv:1210.2400 [astro-ph.CO]].
- [103] A. Atreya, P. Bagchi, A. Das and A. M. Srivastava, Phys. Rev. D **90**, 12, 125016 (2014)
- [104] F. Green and F. Karsch, Nucl. Phys. B **238**, 297 (1984).
- [105] O. Kaczmarek, F. Karsch, E. Laermann and M. Lutgemeier, Phys. Rev. D **62**, 034021 (2000) [hep-lat/9908010].
- [106] A. Dumitru, D. Roder and J. Ruppert, Phys. Rev. D **70**, 074001 (2004) [hep-ph/0311119].

- [107] P. N. Meisinger and M. C. Ogilvie, Phys. Rev. D **52**, 3024 (1995) [hep-lat/9502003].
- [108] C. Alexandrou, A. Borici, A. Feo, P. de Forcrand, A. Galli, F. Jegerlehner and T. Takaishi, Phys. Rev. D **60**, 034504 (1999) [hep-lat/9811028].
- [109] S. C. Phatak, Phys. Rev. C **58**, 2383 (1998) [nucl-th/9805009].
- [110] A. Atreya, P. Bagchi and A. M. Srivastava, Phys. Rev. C **90**, 3, 034912 (2014)